Analysis of moonlight data taken with H.E.S.S.

Bachelorarbeit aus der Physik

Vorgelegt von

Christian Elflein

09.04.2021

Erlangen Centre for Astroparticle Physics

Friedrich-Alexander-Universität Erlangen-Nürnberg

Betreuer: Prof. Dr. Stefan Funk

Gutachter: Prof. Dr. Christopher van Eldik

Abstract

The High Energy Stereoscopic System (H.E.S.S.), located in Namibia, is an array of five IACTs, which are a special type of Cherenkov telescope. It detects gamma-rays coming from different sources in the universe via the Imaging Atmospheric Cherenkov Technique. Most of the time H.E.S.S. observes astronomical targets during dark moonless nights because of the very faint Cherenkov radiation that is detected. By finding the correct telescope configuration so that measurements during moonlight are possible, additional observation time can be gained. This also benefits the monitoring of known flaring active galactic nuclei and transient sources like gamma-ray bursts.

This study is about analyzing data taken with H.E.S.S coming from observations during weak to moderate moonlight and comparing it with data taken during dark moonless nights. For this PKS 2155-304, which is one of the brightest blazars in the southern hemisphere, is used as the gamma-ray source. It is shown that in most cases the moon with a fraction up to 40 % does not have a significant impact on the trigger rates and camera image parameters. If the pixel/trigger threshold of the telescopes does not change, these parameters gathered from both dark observations and moon observations are directly comparable for the current moonlight settings. Probably no change in the current analysis procedure for dark data has to be made for the camera image parameters coming from data taken during nights with relatively weak moonlight.

Kurzfassung

Das High Energy Stereoscopic System (H.E.S.S.), welches sich in Namibia befindet, ist ein System aus fünf IACTs, welche ein spezieller Typ von Cherenkov Teleskop sind. Es detektiert Gammastrahlung, die von verschiedenen Quellen im Universum kommt, mit Hilfe der Imaging Atmospheric Cherenkov Technik. Die meiste Zeit beobachtet H.E.S.S. astronomische Ziele während dunklen, mondlosen Nächten, da die zu detektierende Cherenkov Strahlung sehr schwach ist. Durch Finden von passenden Teleskopeinstellungen, so dass Messungen bei Mond möglich sind, lässt sich zusätzliche Beobachtungszeit gewinnen. Ebenso lassen sich dadurch aufleuchtende aktive Galaxienkerne und schnell vergängliche Quellen wie zum Beispiel Gammablitze besser überwachen.

Diese Studie analysiert mit H.E.S.S. aufgenommene Daten, die von Nächten mit Mond am Himmel kommen und vergleicht sie mit Daten, die während dunklen und mondlosen Nächten erhalten worden sind. Für das wird PKS 2155-304, welcher einer der hellsten Blazare in der südlichen Hemisphere ist, als Gammastrahlungsquelle verwendet. Es wird gezeigt, dass in den meisten Fällen ein Mond, der einen Mondanteil von weniger als 40 % hat, keinen signifikanten Einfluss auf die Trigger Raten und die Parameter von den Kamerabildern hat. Wenn die Pixel-/Triggerschwelle nicht geändert wird, sind die Parameter, die aus den Mondlichtdaten und dunklen Daten entnommen sind vergleichbar für die derzeitigen Mondlicheinstellungen. Wahrscheinlich muss keine Änderung des derzeitiges Analyseverfahren von dunklen Daten für die Parameter der Kamerabilder, die von Nächten mit relativ schwachem Mondlicht stammen, vorgenommen werden.

Contents

1 Gamma astronomy with H.E.S.S.

In the following the necessary information for understanding this study will be explained. First a brief description of gamma-rays, their production processes and their sources is given. After that the mechanism and instruments that are responsible for the detection of this type of radiation are explained. Lastly before going into the analysis of moonlight data it is explained why and how the moon plays an important role in observations of gamma-rays.

1.1 VHE gamma-rays

1.1.1 What are gamma-rays?

Gamma-rays (γ-rays) are photons that have an energy higher than about 0.5 MeV and thus they represent a specific part of the electromagnetic spectrum. So far their energy range already exceeds eight orders of magnitude since photons that have energies above 50 TeV already have been detected. Additionally the gamma-ray energy domain is subdivided into even more energy subdomains which have to be mentioned. Photons with an energy up to 100 GeV are contained in the so called high-energy gamma ray domain and these gamma rays can be efficiently explored by space-based instruments. Above this limit the energy range is called very-high-energy (VHE) and ground-based instruments like H.E.S.S. [1] are mostly used for the detection of this type of gamma-rays [2].

1.1.2 Production of gamma-rays

For the production of gamma-rays there are two different types of processes, which are called leptonic and hadronic.

The main leptonic interaction which produces VHE gamma-rays is Inverse Compton scattering (IC). In contrast to the widely known Compton scattering this process describes VHE electrons transferring their energy to low energy photons from the environment of stars but also from synchrotron radiation which occurs when electrons go through magnetic fields. These interactions result in VHE photons. On the other hand the main hadronic process for producing gamma-rays is the decay of neutral pions. These are produced by other hadronic interactions and eventually decay into two photons [3]. Both processes are illustrated in figure 1.

1.1.3 Sources of gamma-rays

The sources of VHE gamma-rays, which are divided into galactic and extragalactic sources, are described in the following. First it is looked at some galactic sources:

- Supernova remnants (SNR): This type of galactic gamma-ray source occurs when the fusion reactions in the core of a star stop happening which results in collapsing of it

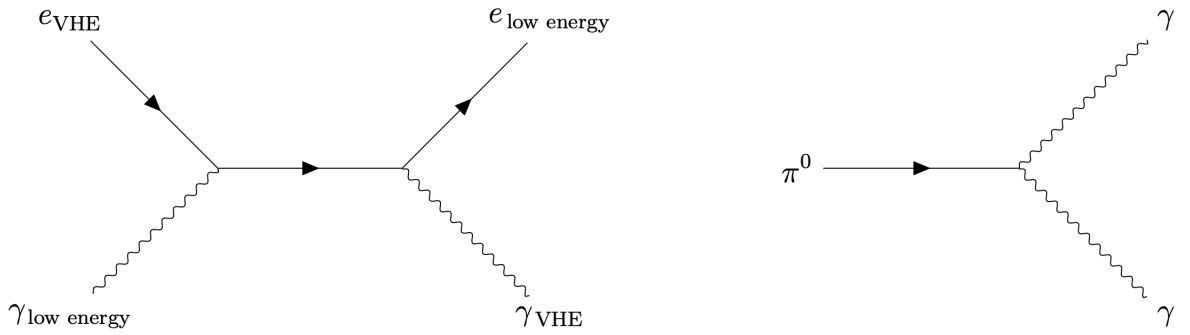

Figure 1: Illustration of the two main processes for the production of gamma-rays. Left: Inverse Compton scattering (leptonic channel). Right: Decay of the neutral pion π^0 into two photons (hadronic channel).

through the gravitational force. The emission of VHE gamma-rays in SNR happens through high energy protons interacting with target material or through electrons. Primary particles which start the emission can have energies up to hundreds of TeV.

- Pulsars and pulsar-wind nebulae (PWN): A PWN which is another type of galactic source is a rotating neutron star that stays within the system. Here gamma-rays can be emitted through the nebula and the pulsar in the center of this structure.

Compact objects, binary systems, stellar clusters and stellar winds are other galactic sources for γ-radiation. On the other hand examples for extragalactic sources are:

- Active galactic nuclei (AGN): An AGN consists of a super-massive black hole having an accretion disk which powers this type of source.

- Gamma-ray bursts (GRB): GRBs are randomly and non predictably occurring sources of gamma-rays that have a short time of activity making their detection rather challenging.

Besides AGNs and GRBs starburst galaxies and galaxy clusters are also extragalactic sources which are able to emit γ-rays [3].

1.2 The imaging atmospheric Cherenkov technique

1.2.1 Instruments for detecting VHE gamma-rays

At lower energies ($< 50\,\text{GeV}$) gamma-rays are not able to reach the Earth's surface and thus they cannot be detected by terrestrial instruments. Hence spaced-based instruments are used for detecting gamma-rays in this energy range. At higher energies ground-based instruments are the better choice. A further distinction of the latter has to be made since there are two types of ground-based detectors that are used for gamma-astronomy, water

Cherenkov detectors and Imaging Atmospheric Cherenkov Telescopes (IACTs). Since the data in the following analysis is taken with H.E.S.S., a system of IACTs, only the procedure of detecting gamma-rays with this kind of instrument is explained in this chapter [4].

1.2.2 Air showers and their detection

Gamma-rays from outer space can be detected through the imaging atmospheric Cherenkov technique (figure 2) which is the detection of secondary particles from a so called air shower created by the primary particle interacting with the atmosphere. If gamma-rays enter the atmosphere the air shower is called electromagnetic and in case of cosmic rays a high energy hadron is the primary particle and thus the shower is called hadronic. Additionally in such a shower through the decay of a neutral pion the production of photons can happen which results in a electromagnetic sub shower. For the electromagnetic air showers caused by gamma-rays there are two main processes that are involved in the creation, pair production and bremsstrahlung. Pair production can occur if the energy of a photon is at least twice the mass of an electron/positron at rest. Through deflection by the Coulomb field of a nucleus a charged particle gets accelerated which results in emission of bremsstrahlung. When the incoming primary particle interacts with atmospheric nuclei it can produce an electron-positron pair. These particles can radiate bremsstrahlung and the outcoming photons can produce electron-positron pairs again and so on. Thus a cascade of particles is created which corresponds to the previously mentioned electromagnetic air shower. Due to the production of new particles and ionisation newly created particles have less and less energy. If the energy of a particle is below a specific critical energy there is no possibility to produce new particles anymore. Within both types of showers there are charged particles with high energy having a velocity higher than the speed of light in vacuum and therefore they emit Cherenkov light on a cone. With n and β being the refraction index of the medium and the velocity in units of the speed of light in vacuum, the angle Θ_C between the path of the charged particle and the Cherenkov light front is given by $\cos(\Theta_C) = (\beta \cdot n)^{-1}$. When the produced Cherenkov light arrives at the surface of the Earth suitable instruments like H.E.S.S. placed within the light pool are able to detect the signal [5].

1.3 The High Energy Stereoscopic System (H.E.S.S.)

The High Energy Stereoscopic System describes a system of five IACTs located in the Khomas highlands in Namibia (figure 3). With these telescopes it is possible to detect the very faint Cherenkov radiation from air showers via reflection of the down going light off the mirrors onto a camera. An illustration of that process can be found in figure 2. The four smaller telescopes which are called CT1-4 have a diameter of 12 m with a total mirror area of 108 m^2 and they have been working since 2003 [6]. The sensitivity of these telescopes goes from about 100 GeV up to about 100 TeV. The fifth telescope of H.E.S.S. which is located in the middle of the other IACTs and started detecting in the year 2012 is referred to as CT5 and has a diameter of 28 m. The total mirror area of 614 m^2 results in a lower total threshold of H.E.S.S. of about 30 GeV [1].

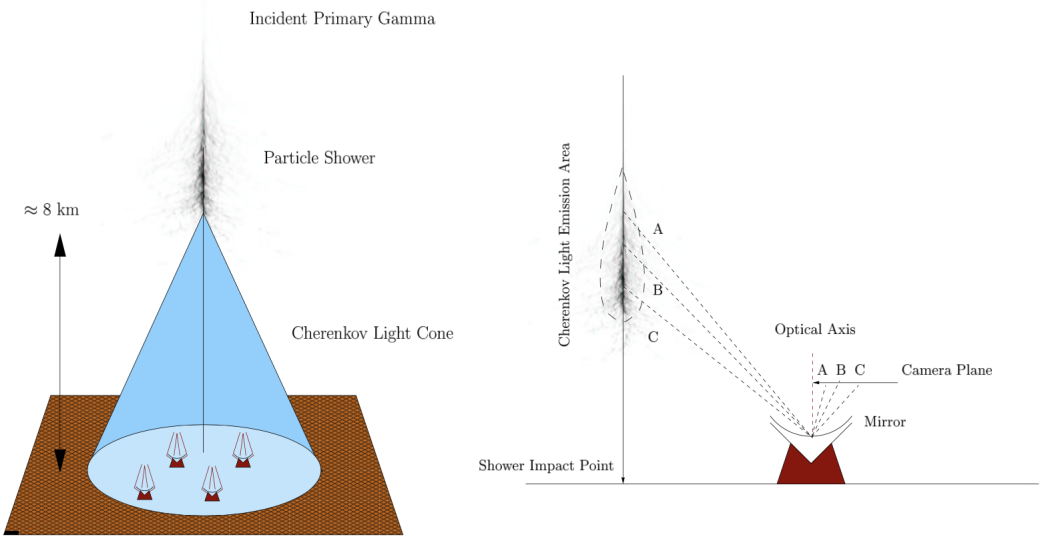

Figure 2: Illustration of the imaging Cherenkov technique. Left: Schematic of an air shower; from primary particle going down till Cherenkov radiation hitting the ground. Right: Cherenkov radiation hitting the mirror of a telescope with follow-up reflection onto camera. [5]

1.3.1 The cameras of H.E.S.S.

The cameras of all H.E.S.S. telescopes are for capturing Cherenkov radiation coming from air showers. They mainly consist of photomultiplier tubes (PMTs), which are referred to as pixels, but electronics for other tasks like signal digitization or triggering are also included into the body of the cameras. Of course one has to distinguish between the camera of the small and the big telescopes when looking at the hardware. The cameras of the 12 m telescopes have a diameter of about 1.6 m, consist of 960 PMTs and have a field of view of 5°. On the other hand the camera of CT5 has 2048 photomultiplier tubes and a field of view of 3.2° [6]. It should be mentioned that the cameras of all telescopes received an upgrade. Every component of the cameras of CT1-4 besides the PMTs with their supplies were replaced in 2015/2016 [1] and the electronics of the CT5 camera received a "FlashCam" upgrade in the end of 2019 [7].

1.3.2 The trigger system of H.E.S.S.

After the reflection of the Cherenkov light into the pixels of a camera specific requirements have to be fulfilled for the events to be read out. This procedure is part of the local trigger that is in every individual telescope camera. Overall a certain number of photoelectrons in a certain number of pixels within a sector has to exceed a threshold. In case of CT1-4 the number of photoelectrons that have to be exceeded in a single PMT is called pixel threshold. If a specific number of pixels (usually 2–4 pixels) within a sector fulfills this condition the second requirement called sector threshold is met.

The background light which does not come from the air shower has a huge impact on

Figure 3: Photo of the H.E.S.S. site in Namibia [6]

these criteria because of additional photons. To reduce that increase there is an additional requirement of multiple telescope triggering within a short time period that has to be fulfilled. Responsible for this is the central trigger system (CTS) which is connected to all H.E.S.S. telescopes. The CTS is located in the control building of H.E.S.S. but also has interface modules in each telescope. Looking at CT1-4 it checks if coincidence is present in at least two IACTs and if this is the case that information will be passed to the single telescopes resulting in the read-out of the images. In the end that criterion results in camera images with less influence from the night sky background[8]. CT5 can also be used in monoscopic mode in which it does not need to be in coincidence with one of the small telescopes [9]. In general an array trigger rate or a single-telescope trigger rate is a description for the number of camera images that is read out within a second.

The array configuration of an observation depends on the telescopes that measure in coincidence. If all five telescopes take part the run is called “hybrid”. On the other hand a “stereo” run uses only the small telescopes for measuring air showers. The last possible configuration is called “mono” and is a description for using only CT5 and no other telescope besides that.

1.3.3 Event reconstruction via Hillas parameters

The reconstruction of air showers consists of two parts: image cleaning and the Hillas parameters.

First the images that are taken with the cameras are cleaned so that the background light is filtered out as much as possible. Thus pixels with mostly Cherenkov light are left and

these are used for the event reconstruction. The images in this study are cleaned with the help of two thresholds of 4 and 7 photoelectrons. Every pixel has to be above the lower threshold and has to have a pixel next to it above the higher threshold. This selection also works the other way around. The remaining pixels are arranged in an elliptical shape. An example image of a gamma-ray ellipse can be seen in figure 4. After the initial cleaning with the two thresholds the three rows around the ellipse are included for the analysis in this study [10].

The Hillas parameters are used to describe the elliptical shape on the camera image that comes from an air shower initiated by a photon but also the geometry of the shower itself. Also with these parameters one can separate events coming from a gamma-ray shower from background events like hadronic showers. There are a lot of Hillas parameters but in this study only a few parameters will be investigated:

- Hillas size: the summarized number of photoelectrons in all pixels
- Hillas length: the r.m.s. length of the Hillas ellipse
- Hillas width: the r.m.s. width of the Hillas ellipse

Additionally it will be looked at the number of pixels per individually taken image [11].

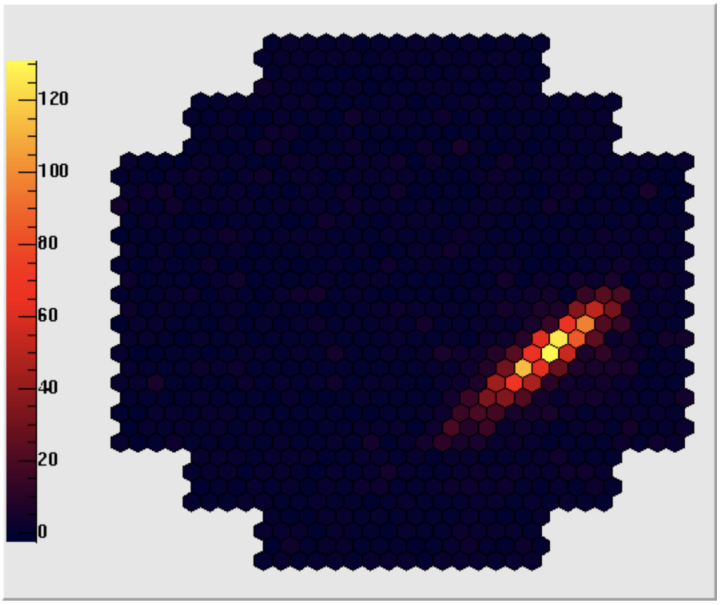

Figure 4: Uncleaned camera image with a Hillas ellipse caused by gamma-ray air shower [6]

1.4 The moon and its impact on H.E.S.S. observations

Most of the time IATCs observe targets during dark moonless nights. For H.E.S.S. darkness/dark time depends on the altitude of the sun and the moon. At the end of of

January 2020 the required sun altitude for observations was changed from −18° to −16°. For the moon it is required that its upper edge is below horizon, but the requested altitude of it is a bit lower, because of possible refraction of moonlight.

Moonlight which is part of the night sky background (NSB) light can be dangerous for the PMTs of the telescopes, since they age quickly if too much light goes into the tubes so a bright environment is not optimal. Also too much moonlight can result in high trigger rates. The duty cycle of IACTs is less than 18 % if observations only take place during moonless nights and that does not include the time that is lost because of additional problems like bad weather or moon. Extending observations into twilight and moonlight results in an increased duty cycle. There are two main things that profit from that increase of observation time. The first one is the general data that can be gathered through regular observations with an IACT. Detecting air showers during nights with moon increases the amount of that taken data. On the other hand the detection of transient γ-ray sources like gamma-ray bursts is an important reason for observations with moonlight. As explained in a previous section GRBs are very short living and randomly appearing phenomena and the moon can prevent any kind of detection of that source during that time period. Since additional light from the moon goes into the PMTs, the data that is taken during such nights is different than for an observation without moon. Therefore it is important to compare these two types of data and check the quality of the moonlight data [12].

The NSB rate is rate of NSB photons which go into the pixels [13]. The absolute value is not important for this study, since the focus lies on comparing the different data and thus the different NSB rates. The rates are calculated for every pixel and afterwards all values are averaged to get the mean NSB rate of the corresponding telescope.

The current moonlight settings of H.E.S.S. are as follows:

- Moon fraction of less than 40 %
- Minimal angle of separation between moon and target: 45°
- Maximal angle of separation between moon and target: 145°

As previously mention too much NSB light can be problematic for the cameras of the telescopes. Certain combinations of moon parameters can cause high NSB rates with the moon fraction being on of those parameters. A low moon fraction is required so that the NSB rate cannot be too high. Regarding the angle of separation, it should be looked at the theory of atmospheric scattering. There are different types of scattering of electromagnetic radiation in the atmosphere and these depend on the ratio between the wavelength of the scattered light and the size of the scattering center. Rayleigh scattering happens if light scatters off small particles like atoms or molecules. If it scatters off bigger particles, e.g. pollen or dust, the process is known as Mie scattering. For Rayleigh scattering the directional aspect of the intensity is described by $1 + \cos(\theta)^2$, with θ being the scattering angle. For Mie scattering another function that depends on the angle is attached to the previously mentioned one. So for the whole atmosphere the intensity depends approximately on $\cos(\theta)^2$. This shows that angles of separation between target and moon near 0° and 180° are not optimal, because the intensity of scattered moonlight is

as very high. On the other hand, if the angle of separation goes towards 90°, the intensity of scattered moonlight is as low as possible and this is preferred for measurements. This shows why the specific limits of 45° and 145° for the angle of separation were chosen for the moonlight settings [14].

After explaining the impact of the moon on H.E.S.S. observations it is important to talk about different run types that are used. The default observation, which mostly happens during dark moonless nights is called "ObservationRun" (OR). But there are also some ORs during which the moon is above horizon and these types of runs are also important for this study. The other run type is the so called "MoonlightObservationRun" (MOR) and as the name suggests it is focused on observations with the moon being up. It should be mentioned that there are also MORs without moon but these are mostly test runs and they are excluded from the following analysis. During ORs and MORs with moon the NSB rate is usually higher, which comes from the additional moonlight. Summarized it will be looked at data from ORs with moon, ORs without moon and MORs with moon. Also the terms "dark" run and "moonlight" run are important in this study. The first term describes only ORs without moon and the latter one refers to ORs and MORs with moon. The separation into all the different run types is visualized in table 1.

	Dark runs	Moonlight runs
OR	CT1-4: 5.5 p.e. in 2 pixels in a sector CT5: 69 p.e. within a 9-pixel sum	CT1-4: 5.5 p.e. in 2 pixels in a sector CT5: 69 p.e. within a 9-pixel sum
MOR	MOR without moon are mostly test runs	CT1-4: 5.5/6.5 p.e. in 2 pixels in a sector CT5: 104 p.e. within a 9-pixel sum

Table 1: Separation into different run types and corresponding trigger thresholds

The separation into dark and moonlight runs will be especially important in the second part of the analysis, which is about the camera image parameters.

2 Analysis of triggering behavior

In this first analysis the array trigger rates and single-telescope trigger rates are discussed. Before that it is looked at the selection of the target and the corresponding runs, which also refers to the analysis of the camera image parameters in the next chapter. After the zenith angle correction the part about the array and single-telescope trigger rates follows and in the end it is looked at the definition of H.E.S.S. dark time.

2.1 Selection of target and corresponding runs

PKS 2155-304 is one of the brightest blazars in the Southern Hemisphere and the source used for this study. It is a well-known target of H.E.S.S because it has been monitored since 2002 and had two exceptional flares in 2006 [15]. This and the selection of this target through the following process shows that it is a suitable source for the analysis of moonlight data.

Firstly it is important to discuss the selection process that results in this chosen target and its corresponding runs. For this one looks at all runs that happened within the time frame between 01.01.2019 and 10.11.2020. In January of 2019 the moonlight observations with H.E.S.S. started and the later date describes the time around the analysis of data regarding this study started. This time period gives 5771 runs in total which will be used for the further choices to make. Additionally it has to be mentioned that ORs without moon and MORs with moon are the two most important run types here. Nevertheless ORs with moon are included in the selection process and the analysis to investigate more moonlight data. Since the following chapters are about comparing dark runs with moonlight runs, a target with a specific number of fitting runs for this has to be found. The selection is mainly about getting moonlight runs (OR without moon and MOR with moon) because there are way less runs of this type in comparison to dark runs. So one searches for the target with the most moonlight runs that also has the same number (or more) of dark runs. At first some criteria have to be fulfilled before further investigation:

- The moon having an altitude above 3° at the start or the end of the run or during the whole run
- The run being a MoonlightObservationRun taken after 15.05.2019 or
- The run being an ObservationRun taken after 07.07.2020

At these dates the settings got changed to the ones used for this study and thus the earlier runs have to be filtered. All these conditions that are taken into account result in having 144 moonlight runs. After this all targets are sorted into a list regarding their number of moonlight runs. Table 2 lists five targets with the largest numbers of relevant runs. The sources without either ORs with moon or MORs with moon are filtered because it is important to look at both types of moonlight runs. Next it should be looked at the number of MORs since this is the most important run type regarding this study. There one can see that PKS 2155-304 has the most MORs and considering the fact that this

target is very bright shows that this source is very suitable for the following study.
One OR with moon and three MORs with moon have to be excluded for the further analysis. The OR failed to start and for the latter ones the separation angle between the source and the moon in the run is less than 45° which is not allowed for MORs and thus these runs cannot be used. Normally a MOR with such a low angle is not possible but these runs are from November of 2019 and at this time the moon parameters were checked manually. Since the NSB rates, the moon fraction and altitude in these nights were acceptable for MORs the observations happened although the angle of separation was too small in terms of moonlight criteria.

Target	Dark runs	Moonlight runs	
	OR w/out moon	OR w/ moon	MOR w/ moon
eHWC J2019+368	80	17	4
DWF19 NGC 6744	0	0	21
SN 1987A	103	15	0
PKS 2155-304	99	3	9
DWF19 NGC 6101	0	0	12

Table 2: Targets with most moonlight runs and the corresponding number of runs

Finally this whole selection results in having 2 ORs with moon and 6 MORs with moon, plus 8 ORs without moon. All these runs can be found in table 3 with the corresponding run configurations and moon parameters for the moonlight runs.

It should be mentioned that MOR 155280 happened on the 30th of October in 2019 which is before FlashCam has been stable. Because of this it will only be looked at the trigger rates of this run to see if there are maybe some major differences to run 155278 which happened in the same night. Also since this run is the only mono run it cannot be directly compared to any other run and thus it will not be further analyzed after that comparison.

2.2 Zenith angle correction

Before looking at the trigger rates of the different runs that were chosen in the last section the zenith angle correction has to be explained. The zenith angle θ is the angle between the zenith and an observed target. H.E.S.S. usually detects air showers with a zenith angle between 0° and about 30°. Measuring with higher zenith angles is also possible but only for another type of run that does not occur in this study. The distance between the beginning of the shower and the impact point at the ground changes with the zenith angle. Regarding this the shower has to pass less or more matter on its way. For an angle of 0° the distance and therefore the impact of the atmosphere on the shower is as small as possible. With an increasing zenith angle the length of the atmosphere for the passing particles extends and thus the shower gets more and more affected. For an unbiased comparison of the data regarding the zenith angle the trigger rates have to be corrected.

Run number	Run type	Array config.	Moon fraction	Moon altitude [°]	Angle of separation [°]	Pixel threshold of CT1-4
153899	MOR	stereo	0.40	8.5 ↑	137.9	5.5
154391	MOR	stereo	0.31	40.4 ↓	66.6	6.5
155278	MOR	stereo	0.09	13.2 ↓	72.1	5.5
155280	MOR	mono	0.09	11.5 ↓	72.0	-
161518	OR	stereo	-	-	-	5.5
162008	OR	stereo	-	-	-	5.5
162068	OR	stereo	-	-	-	5.5
162494	OR	hybrid	-	-	-	5.5
162495	OR	hybrid	-	-	-	5.5
162521	OR	hybrid	-	-	-	5.5
162548	OR	hybrid	-	-	-	5.5
162578	OR	hybrid	-	-	-	5.5
162658	MOR	hybrid	0.37	12.2 ↓	68.6	6.5
162659	MOR	hybrid	0.37	6.0 ↓	68.3	6.5
163256	OR	hybrid	0.22	22.5 ↓	60.5	5.5
163257	OR	hybrid	0.22	12.6 ↓	60.1	5.5

Table 3: List of the runs used in this study with corresponding run configuration and moon parameters

The correction function

$$\text{Corrected trigger rates} = \frac{\text{Observed trigger rates}}{\text{Correction function}} \tag{1}$$

differs for array trigger rates and single-telescope trigger rates. For array rates a default cosine function applies as correction function which is a simplification and probably only correct to 0th order. On the other hand for single-telescope rates a more accurate and data-based correction function [16]

$$a \cdot (1 + b \cdot (1 - \cos(\theta))^2) \tag{2}$$

is used with a being 1 and b being a parameter[1] that is different for every telescope and can be found in table 4.

	CT1	CT2	CT3	CT4	CT5
b	−2.1858	−2.0553	−2.1540	−2.1093	−0.6482

Table 4: Values of parameter b in the correction function of single-telescope trigger rates

Additionally figure 5 shows the evaluated correction functions for array rates and for single-telescope rates for CT1 and CT5. One can see that for small zenith angles the

[1]Private communication A. Yusafzai

correction function and therefore the single-telescope trigger rate does not significantly change in comparison to the correction function of the array trigger rate. Overall the single-telescope trigger rate for CT5 has the slowest change for increasing zenith angle. Another important thing that should be mentioned is that the trigger rates for the small telescopes are negative for zenith angles above 70° which is not physically meaningful because trigger rates cannot be negative. That behavior most likely occurs because the correction function is data-based and only data with zenith angles between 1° and 80° were used to determine these functions. The reason for the correction function being negative before the used limit of 80° can come from the fact that less data is present for high zenith angles since H.E.S.S. usually does not observe under these conditions. The small number of data points between 70° and 80° would not impact the correction function too much and thus it already gets negative for a smaller angle. Since the correction functions are based on zenith angles in a limited range the zenith angles of the runs in this study also have to be in this interval.

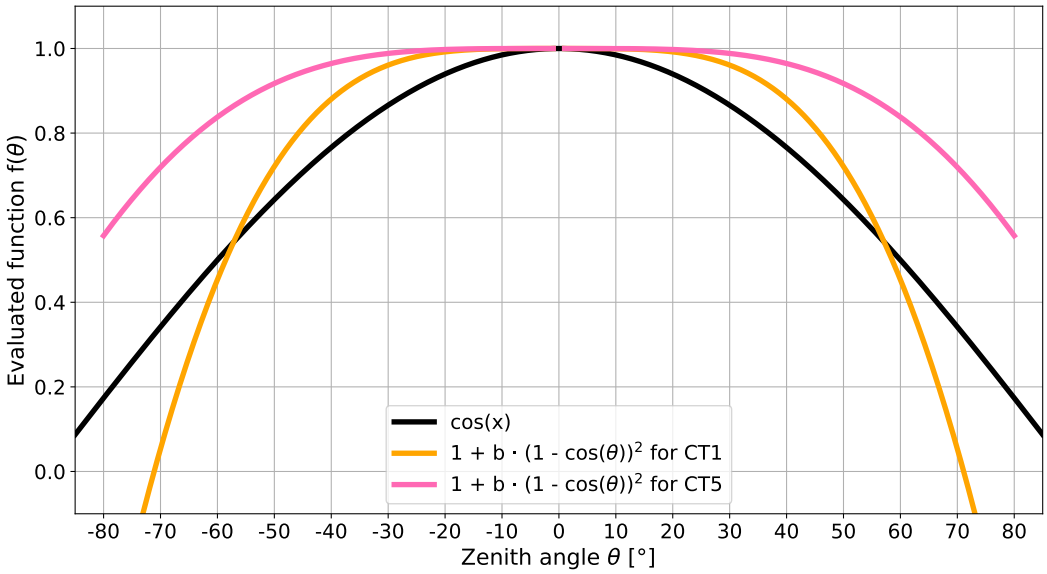

Figure 5: Functions for the correction of the array trigger rates and single-telescope trigger rates the zenith angle

All trigger rates that are looked at in this chapter are already zenith-angle corrected.

2.3 Array trigger rates

At first one looks at the array trigger rates of the dark and moonlight runs. All runs are separated regarding their array configuration. In this section the legend includes the run type and the number for all runs. Additionally the moon fraction, angle of separation and the moon altitude and movement is given for moonlight runs.

There are two things that should be mentioned before going into the analysis of the trigger rates. The first one is the upper limit for these. There is not a hard limit for the trigger rates but they should preferably be lower than 10 kHz to protect the hardware of the

cameras. The other important thing is a limit for the relative standard deviation/coefficient of variation of the trigger rates. This parameter is the ratio of mean and standard deviation and it describes how much the rates fluctuate. For this there is also no hard limit but one can say that rates with a relative standard deviation of less than 20.0 are considered acceptable for further analyzes.

Figure 6 shows the array trigger rates of all stereo runs. Except for MOR 155278 all array rates are fairly constant. There is no significant difference between the array rates of the dark and moonlight runs and all rates are around 250 Hz - 500 Hz with the exception of MOR 155278. At the beginning of that run the array rate is roughly constant with some visible fluctuations at around 300 Hz. After about 3 min the rate steeply increases from that value and varies around ~1500 Hz until the end of the run.

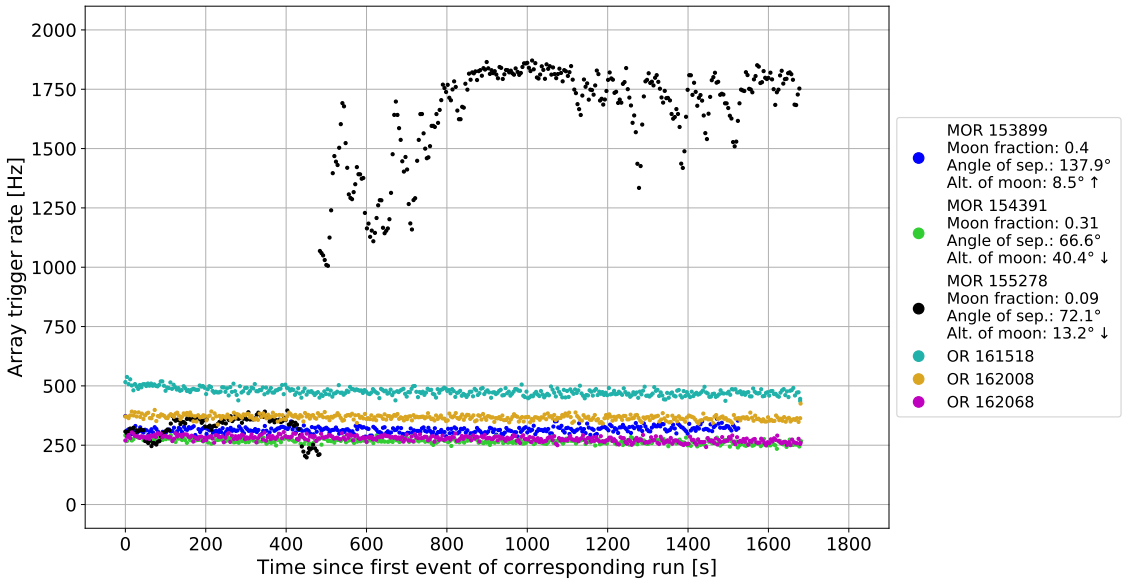

Figure 6: Array trigger rates for stereo configuration

In table 5 it is shown that the coefficient of variation is below 5.0 for all runs besides for 155278. The heavy fluctuations of its array rate can also be seen in the relative standard deviation of 49.6. The second part of this trigger rate shows a course that is usually caused by Cherenkov radiation that is scattered off clouds before it hits the mirrors. Also there are a few things like the low moon fraction of 0.09 and the angle of separation, which is near 90°, that make it unlikely for the moon to be the reason for this varying trigger rate. Also in comparison to the other two MOR, the moon parameters of run 155278 are way more optimal. The last thing that implies that the fluctuations rather come from scattering off clouds than from the moonlight is the NSB rate[2]. For this run it is about 63 MHz which is low compared to the rate of other MORs (around 200 MHz). Also the rate of run 155278 is lower than for the three ORs without moon which shows that the moonlight has a minimal impact and is most likely not the reason for the varying array trigger rates. It should also be mentioned that trigger rate of run 154391 is the lowest which comes from the higher pixel threshold of 6.5 p.e. in comparison to the threshold of

5.5 p.e. for all the other runs.

Run number	Mean [Hz]	Standard deviation σ [Hz]	Coefficient of variation σ/μ	Moon fraction	NSB rate CT1-4 [MHz]
153899	315.0	13.2	4.2	0.40	193.22
154391	267.5	10.2	3.8	0.31	213.68
155278	1266.8	628.3	49.6	0.09	63.82
161518	475.5	15.4	3.2	-	100.22
162008	367.2	10.9	3.0	-	70.44
162068	277.5	11.6	4.2	-	77.32

Table 5: Statistical parameters for the array trigger rates (stereo configuration)

The array trigger rates of the hybrid runs are shown in figure 7. As one can see all array trigger rates are fairly constant with small increases or decreases for some runs if one looks at the total run time. For example for OR 1629494 the trigger rate starts at about 3 kHz and constantly increases up to 3.1 kHz. Another important thing to mention is the difference of the rate of the MORs in comparison to the other rates. The two MORs (162658, 162659) have a relatively low array rate of about 1 kHz but for all other runs the rate is above 1.75 kHz. This comes from the fact that the pixel threshold of CT5 for MORs is 50 % larger than for ORs which results in more photoelectrons that are needed. This is the same situation as with the different pixel thresholds for the stereo runs. Because of the increased pixel thresholds the mean shifts to higher values. Also the rates of these two runs look quite similar which comes from the fact that one run started about half an hour after the other one. Thus the observations took place under almost the same conditions.

Looking at the statistical parameters in table 6 it can be seen that the relative standard deviation is below 2.5 for every run. For the two MORs with the low trigger rate the moon fraction is very high with regards to the moonlight settings of H.E.S.S. and near the chosen limit of 40 %. Also the altitude of the moon is less than 15° for both runs and the separation of target and moon goes towards 90° which is optimal for observations with the moon. The NSB rate of these runs is way higher than for ORs which comes from the additional moonlight but nevertheless no impact of the moon is visible. This shows that the random coincidences caused by moonlight are minimal. This is also the case for the two ORs with moon. Another point that has to be made is that the constant trigger rates of all runs could imply that in general the background light is filtered efficiently if all five telescopes take part in an observation. Especially for hybrid runs it is interesting to see the single-telescope trigger rates because both types of telescopes take part in this kind of run. The last interesting thing about all these trigger rates is the variation of the mean value. Except for the MORs all rates vary between 1.75 kHz and 3.25 kHz which should not be the case since the target location, the observation area in the sky and the settings of the telescopes does not change. Therefore another factor has to be responsible for this. The variability of the source but also the density of the atmosphere could be reasons for that. If the density is higher the particles lose more energy and the end of the air shower happens earlier which results in less energy of the Cherenkov radiation. This could change

[2]All NSB rates in this study were received via private communication with A. Yusafzai

the number of photoelectrons that are registered and thus the trigger rate. Of course there could be a lot of other reasons that cause the differences in these mean trigger rates.

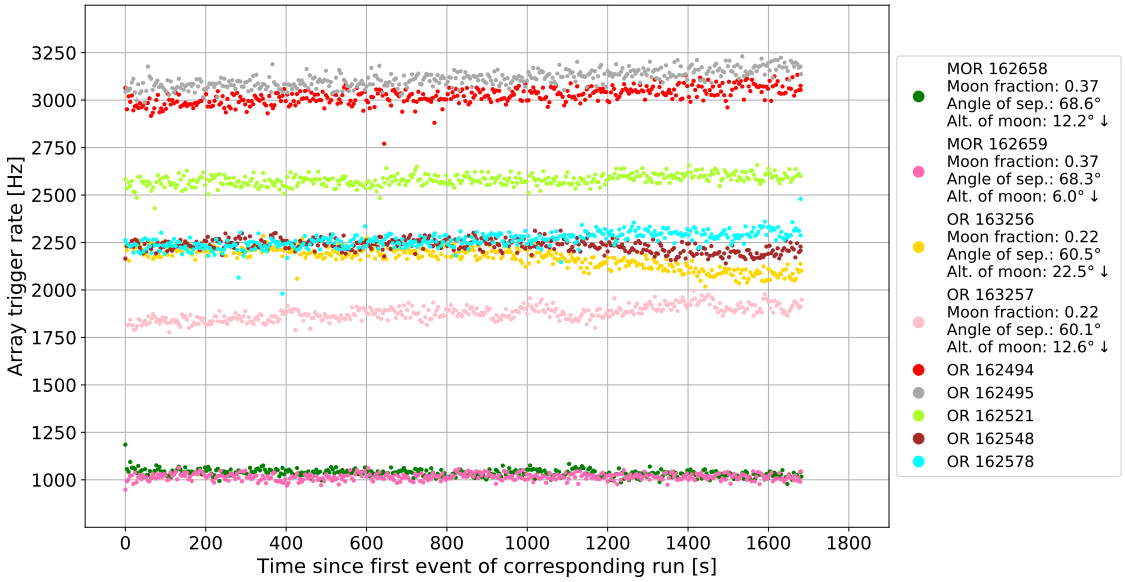

Figure 7: Array trigger rates for hybrid configuration

Run number	Mean μ [Hz]	Standard deviation σ [Hz]	Coefficient of variation σ/μ	Moon fraction	NSB rate CT1-4 [MHz]	NSB rate CT5 [MHz]
162658	1035.2	19.2	1.9	0.37	183.93	607.43
162659	1015.7	17.4	1.7	0.37	130.82	410.18
163256	2170.1	53.2	2.4	0.22	189.89	595.63
163257	1878.9	40.3	2.1	0.22	162.87	499.07
162494	3022.8	42.6	1.4	-	90.10	278.58
162495	3114.4	43.7	1.4	-	91.70	273.37
162521	2580.5	29.4	1.1	-	95.83	296.71
162548	2232.2	31.5	1.4	-	81.69	251.42
162578	2263.7	41.4	1.8	-	75.96	232.47

Table 6: Statistical parameters for the array trigger rates (hybrid configuration)

The only mono run that was selected is run 155280 and can be seen in figure 8. The array rate of this run fluctuates around a mean value of 1615.6 Hz with a relative standard deviation of 12.2. Like mentioned before this observation happened before FlasCam was stable and therefore this run cannot be directly compared to other runs with one exception. Also the data of this run should not be used for the further analysis. The rate of this run looks like the second part of the rate of MOR 155278 and that is because that run started detecting about 8 minutes before the mono run. Hence the present conditions on that observation day are similar which can be seen in the trigger rates. Thus the same reasoning for the fluctuations of the array trigger rate applies to this run. The interesting

thing is that the coefficient of variation is way lower for the mono run. This shows that the constant part at the start of run 155278 caused the high relative standard deviation of almost 50.0 and it heavily impacts the statistics in general.

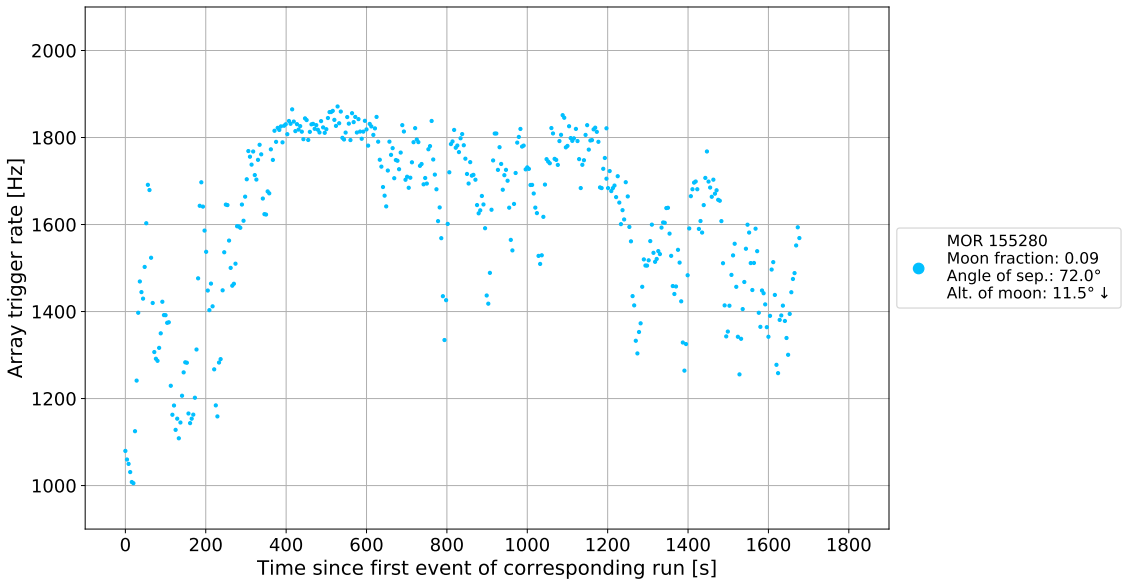

Figure 8: Array trigger rates for mono configuration

Overall looking at all array rates some conclusions can be drawn. There is no visible change of the array trigger rates caused by the moon and thus the number of random coincidences should be minimal. All array rates are fairly constant with the exception of the two runs that show fluctuating rates which is caused by scattering of the Cherenkov light off clouds. Also some mono runs have to happen to see how CT5 alone handles additional NSB light coming from the moon.

2.4 Single-telescope trigger rates

After analyzing the array trigger rates and not seeing a clear impact of the moon the single-telescope trigger rates are investigated. It is important to check if the moon individually affects any of the five telescopes. Therefore the single-telescope rate of every run is analyzed separately. Since the small telescopes show quite similar rates it is only looked at CT2 and CT5 in this section. For a better viewing of the CT2 trigger rates they are further divided. Like in the previous section the legend includes the run type and the number for all runs, plus the moon fraction and angle of separation. Lastly for moonlight runs the moon altitude and movement is given. The trigger rates for the telescopes that are not looked at can be found in the Appendix.

In figure 9 the single-telescope trigger rates of a few runs in which CT2 takes part in are shown. As one can see the trigger rates of all these runs are fairly constant with a varying mean value between about 450 Hz and 1000 Hz. The low trigger rate of the three MORs comes from the higher pixel threshold of 6.5 photoelectrons. The fluctuating mean value can have a lot of reasons (atmosphere, variability of source) like for the array rates of

the hybrid runs. Light pollution can also be responsible for a higher rate since additional light would result in more photoelectrons overall and thus the trigger requirement can be fulfilled earlier. This way one gets more images and the trigger rate would be higher.

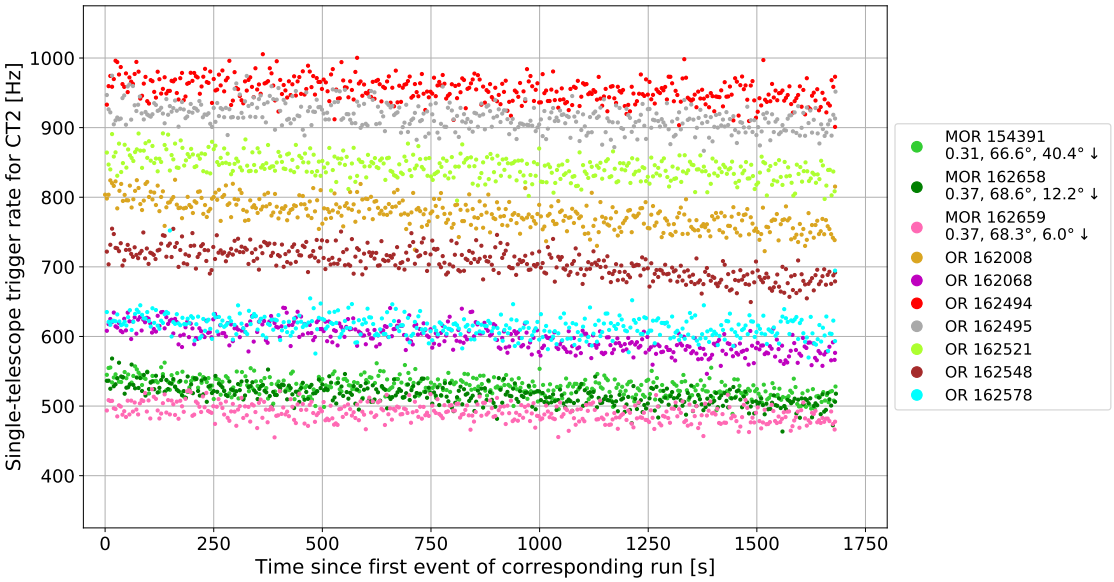

Figure 9: Single-telescope trigger rates for CT2 (part 1)

Table 7 shows that the relative standard deviation is below 6.0 or every run. So the rates of these runs do not show heavy fluctuations and the moon does not have a visible impact. Out of all these runs MOR 154391 has the highest NSB rate and a relatively high moon fraction of 31 %.

Run number	Mean μ [Hz]	Standard deviation σ [Hz]	Coefficient of variation σ/μ	Moon fraction	NSB rate [MHz]
154391	526.3	28.8	5.5	0.31	211.34
162658	514.9	28.1	5.5	0.37	194.81
162659	489.9	22.2	4.5	0.37	138.68
162008	776.6	19.9	2.6	-	74.35
162068	597.4	30.3	5.1	-	81.73
162494	951.8	44.3	4.7	-	95.11
162495	914.0	35.3	3.9	-	96.65
162521	841.6	41.5	4.9	-	101.44
162548	704.5	39.1	5.6	-	86.33
162578	613.6	24.7	4.0	-	80.34

Table 7: Statistical parameters for the single-telescope trigger rates of CT2 (part 1)

Nevertheless no variation in the single-telescope rate is visible and the coefficient of variation is only 5.5. Comparing the runs with moon and these without moon shows that the NSB rates are significantly higher because of the moon being up. Overall the

relative standard deviation is lower for the runs without moon and thus less fluctuations are present in these single-telescope trigger rates.

Looking at the trigger rates of the remaining runs (figure 10) it is clear that these show a non-constant course. The most important run to look at within all of these is run 153899 since these single-telescope trigger rates show an exponential behavior. The trigger rate starts at about 700 Hz and increases up to about 3100 Hz at the end of the run. It should be mentioned that for CT1 the rates even go up to around 27 kHz. MOR 155278 shows a mostly constant course with some minor fluctuations. For the one OR without moon the trigger rates quickly get lower after the run starts till they reach a constant mean value. This is also the case for the two ORs with moon but these rates decrease more slowly in comparison.

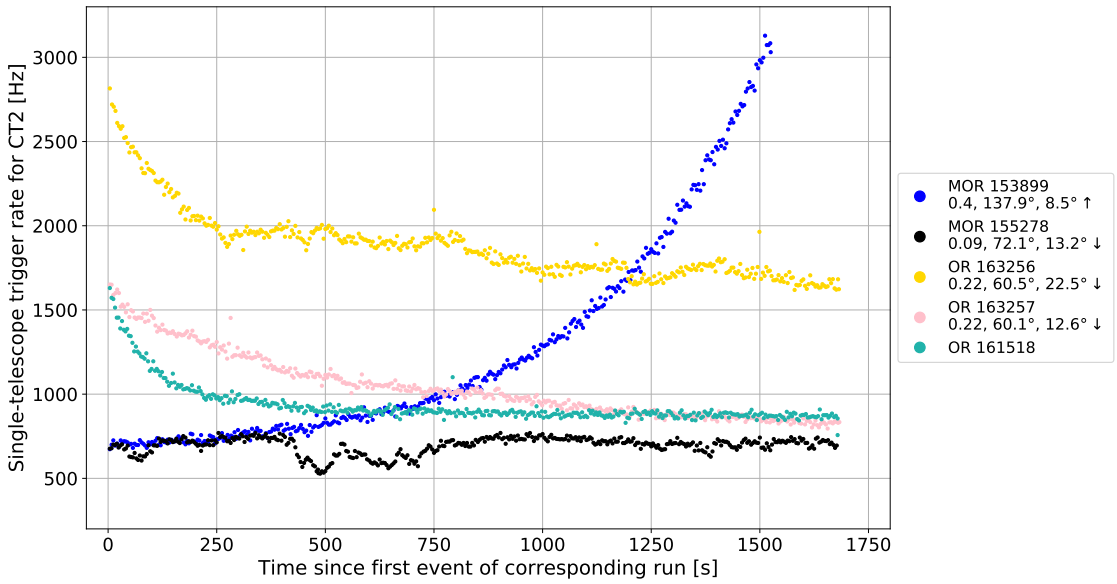

Figure 10: Single-telescope trigger rates for CT2 (part 2)

In table 8 the statistics can be found. The relative standard deviation of the trigger rate of all these runs goes from 8.8 up to 50.0 showing heavy fluctuations. MOR 153899 does have a very high coefficient of variation which comes from the exponential course of the trigger rates. The moon seems to be the reason for the increase, since both the moon and the trigger rate is rising. Also the moon has a very high moon fraction of about 40% and the angle of separation is 137.9° which is near the limit of the moonlight settings. Interestingly the NSB rate of this run is lower than for MOR 154391 which was one of the runs that showed constant single-telescope trigger rates. This implies that other factors besides the moon play a role for the exponentially increasing rates. Also since trigger rates should be below 10 kHz optimally this run shows that runs with the moon being up can cause problems for the cameras of H.E.S.S. telescopes in specific cases. At the start of run 161518 the moon is just above the horizon which causes the higher trigger rates. With the setting moon the rates sharply decrease after starting the run until they reach a constant value of about 800 Hz after about 8 min. The coefficient of variation for this run is 13.9 but it probably would be way lower without the decreasing rates in the beginning. For run 155278 the same reasoning as for the fluctuations of the array rates

apply which is scattering of Cherenkov light off clouds. In comparison the array rates the single-telescope rates only have a relative standard deviation of 8.8 which also can be seen in the less present fluctuations. Also for this case the NSB rate is very low with around 64 MHz which disproves the moon as reason for the varying rates. The two ORs with moon show the same behavior since one was taken right after the other. The trigger rate of OR 163256 starts at about 2900 Hz and goes down to about 1600 Hz. The rate of OR 163257 on the other hand starts at about 1600 Hz and goes down to about 900 Hz. Also the coefficient of variation for this run is 19.2 and higher than for the previous run. As one can see the moon has an impact on the trigger rates of these runs because the rates slowly decrease with the altitude of the moon except for the beginning of run 163256 where there is a sharp decrease. This also shows a potential high single-telescope rate that could have occurred if the run would have started earlier. The higher mean value of OR 163256 most likely comes from the higher moon altitude and the higher NSB rate. The moon fraction and the angle of separation is almost identical and thus these parameters cannot be the reasons.

Run number	Mean [Hz]	Standard deviation σ [Hz]	Coefficient of variation σ/μ	Moon fraction	NSB rate [MHz]
153899	1263.5	638.0	50.5	0.40	188.68
155278	693.0	61.1	8.8	0.09	63.44
163256	1875.4	226.6	12.1	0.22	200.64
163257	1042.2	200.3	19.2	0.22	171.78
161518	932.6	129.3	13.9	-	106.06

Table 8: Statistical parameters for the single-telescope trigger rates of CT2 (part 2)

Lastly the single-telescope rates of CT5 are presented. These trigger rates can be found in figure 11 and show mostly constant behavior besides for MOR 155280. This is the only mono run and it was discussed in the previous section so it is not analyzed in the following.

Table 9 shows that for every run the relative standard deviation is 5.5 or less. It is also important to mention that the rates of MOR 162658 and MOR 162659 are constant which is not the case for the single-telescope rates of these runs in CT2. Therefore in these cases CT5 filters the incoming NSB light better. This also could imply that the hardware of CT5 is more suitable for moonlight runs. Regarding this it is even more important to do observations with the big telescope alone to see if this it that is really the case. The mean value of the single-telescope trigger rates of the the ORs with and without moon vary like the array rates. Like explained in the previous section these differences can be caused by a lot of things (atmosphere, light pollution, ...). The trigger rates or MOR 162658 and MOR 162659 are lower than all of the other rates, which comes from the higher trigger threshold.

All in all it can be said that the moon can affect the single-telescope trigger rates. For all the viewed runs it is only the case for the small telescopes but there is the possibility that the moon could impact the CT5 rates visibly as well. Because of the few runs that

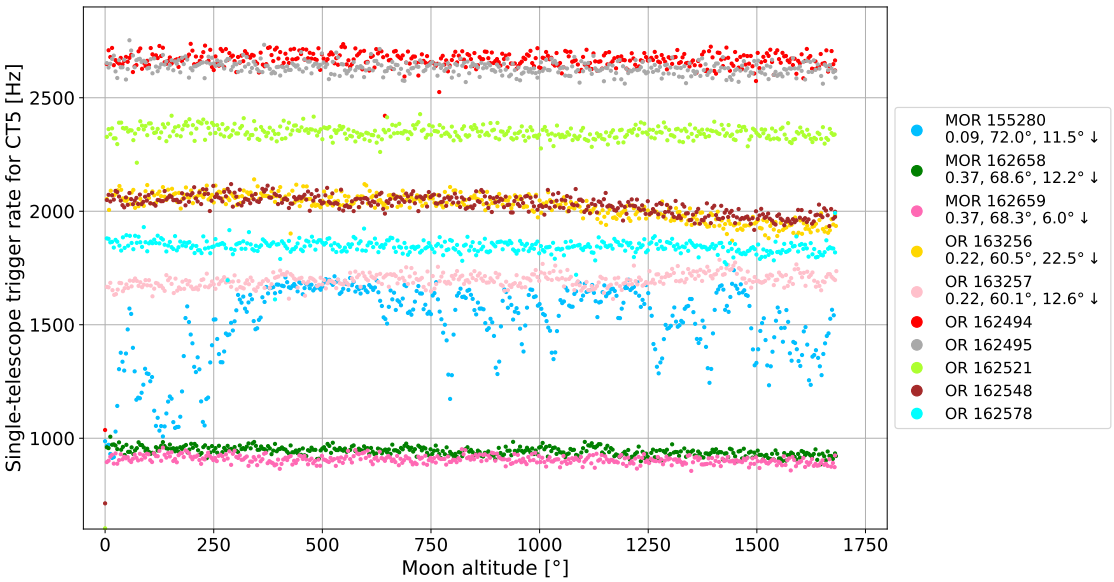

Figure 11: Single-telescope trigger rates for CT5

Run number	Mean [Hz]	Standard deviation σ [Hz]	Coefficient of variation σ/μ	Moon fraction	NSB rate [MHz]
162658	940.7	39.2	4.2	0.37	607.43
162659	904.1	45.0	5.0	0.37	410.18
163256	2017.2	110.7	5.5	0.22	595.63
163257	1692.5	87.2	5.2	0.22	499.07
162494	2663.5	85.7	3.2	-	278.58
162495	2626.9	121.4	4.6	-	273.37
162521	2343.0	89.1	3.8	-	296.71
162548	2027.1	75.2	3.7	-	251.42
162578	1840.1	89.1	4.8	-	232.47

Table 9: Statistical parameters for the single-telescope trigger rates of CT5

have changing trigger rates due to the moon it is needed to look at the settings of the telescopes and possibly change these for ORs and MORs with moon. Occuring trigger rates of 27 kHz are way too high for the H.E.S.S. cameras and could damage them. Although for the single-telescope rates the moon has an impact the array trigger rates are not visibly affected. This is an important point that shows that the multiple telescope triggering efficiently filters the random coincidences caused by the moon.

2.5 Defining H.E.S.S. dark time w.r.t. the moon

In the last few months of 2020 there were reports of steeply rising/dropping single-telescope trigger rates in the cameras of the small telescopes during observation nights with the moon being around the horizon. Because of this the start/stop altitude of dark observations was changed from −0.83° to −2° to ensure safety for the individual telescopes. Later

on it was discovered that a bug in the system caused the runs to start earlier or end later. Nevertheless it has to be looked at the runs with moon near the horizon to see how the rates are impacted. Theoretically scattered moonlight should only be seen in the single-telescope rates and the random coincidences should be minimal which results in a non-significant affection of the array trigger rates in these specific runs. This study looks at the array trigger rates and the single-telescopes rates of runs with moon just below horizon. Furthermore it checks how the moon fraction and the moon altitude affects these and if it is safe to go back to −0.83° as start/stop elevation.

Run selection

Firstly it is important to talk about the selection process for the runs that are chosen for this study. For this all runs that happen from 01 January 2020 until the beginning of December 2020 are included. Additionally the runs have to fulfill some criteria:

- The run has to be an ObservationRun with a duration of more than 30 s
- The moon has to be below an altitude of 1° at the start and stop of the run
- The moon has to have an altitude between −5° and −0.8° at either the start or the stop of the run
- Three runs are excluded because of corrupted trigger files

In the end after filtering the run list with all of these conditions 106 runs are left and looked at in the following. In figure 12 these chosen runs are visualized and separated into runs with rising moon and runs with setting moon.

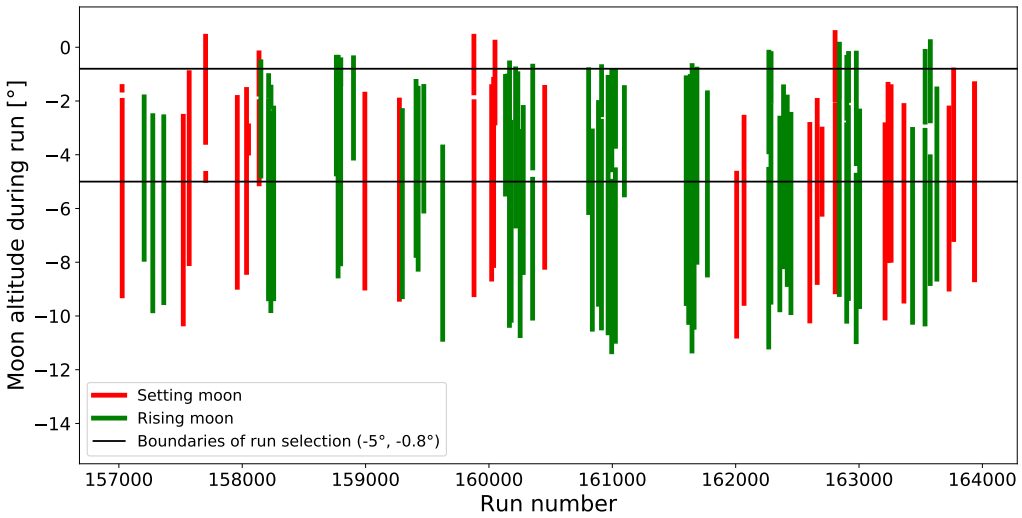

Figure 12: Visualization of all runs with the moon just below horizon that fulfill specific criteria

The array trigger rates and single-telescope trigger rates are also separated regarding the moon movement but also regarding the mean moon fraction during the run.

Also before going into the analysis of all the trigger rates it should be said that the legend in this section contains the run number, the mean moon fraction and the angle of separation. Additionally the name of the observed target is given. Another thing that should be mentioned is that for calculations in the analysis the of the trigger rates the middle of the moon is used and thus the moon is below the horizon if it has an altitude of about −0.26°. In the following this altitude is displayed next to all the trigger rates to visualize how much the moon elevation affects the trigger rates.

Array trigger rates

After selecting all runs it should be looked at the array trigger rates. Since for most runs the moon does not have an impact on the trigger rates in the following the runs with the highest moon fractions are looked at. The array trigger rates of the rest of the runs can be found in the Appendix.

In figure 13 all selected runs with a rising moon having a mean fraction between 80 % and 100 % can be seen. The array rates of all runs are fairly constant and there is no visible increase when the moon is around the horizon. Even for run 162481 the rates do not change significantly although more than half of the moon is above 0°. Nevertheless it can be seen that the rate of this run slightly increases after the moon moves above the horizon so an impact of it on the rates is visible. But overall there is no increase of the trigger rates that could cause problems for the cameras.

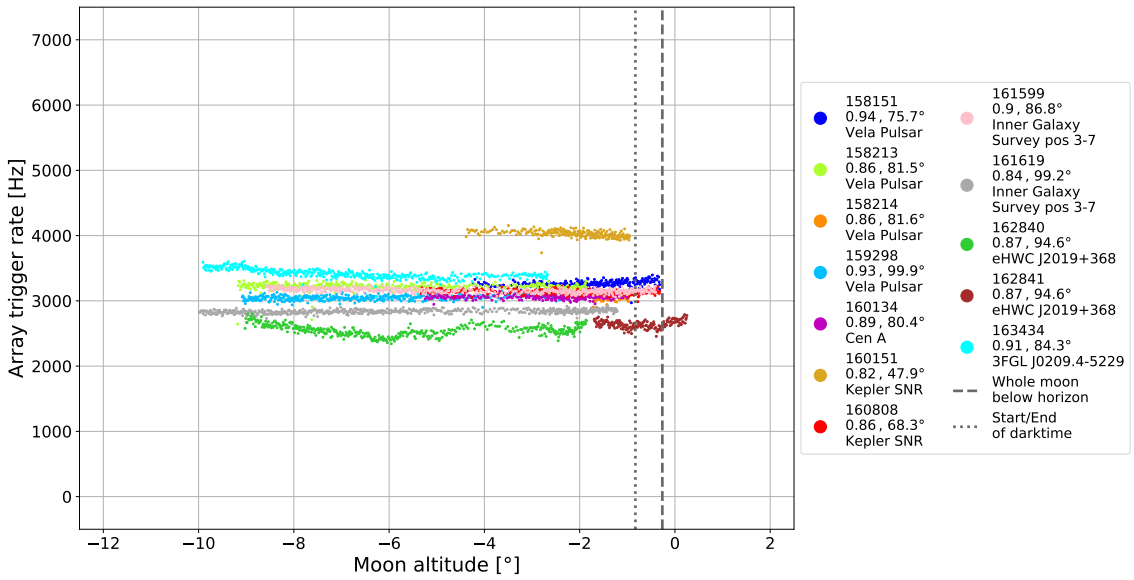

Figure 13: Array trigger rates for runs with a rising moon and a mean moon fraction between 80 % and 100 %

After looking at the runs that have a rising moon one should look at the ones with a setting moon. The array rates of these runs can be found in figure 14 and some of these rates show quite a different behavior than before. In comparison to the rates for a rising moon some rates here have a positive gradient and slowly get bigger. Run 157703 is another run in which a high part of the moon is above horizon and also the moon fraction is 93 %.

Though the angle of separation being almost 90° could be the reason that there is no visible increase in the array rates. The rates of run 160049 show an exponential decrease around horizon. More than half of the moon is above the horizon at the start of this run and the rates go down from almost 7000 Hz until they reach stable rates of about 3800 Hz below an altitude of around −1.0°. There is a visibly higher trigger rate for run 162086 when the moon is above horizon but the increase is not as sharp as for the previously discussed run. Nevertheless the changes of the trigger rates for these two runs clearly show that the moon can have a significant impact on array rates when it is around the horizon.

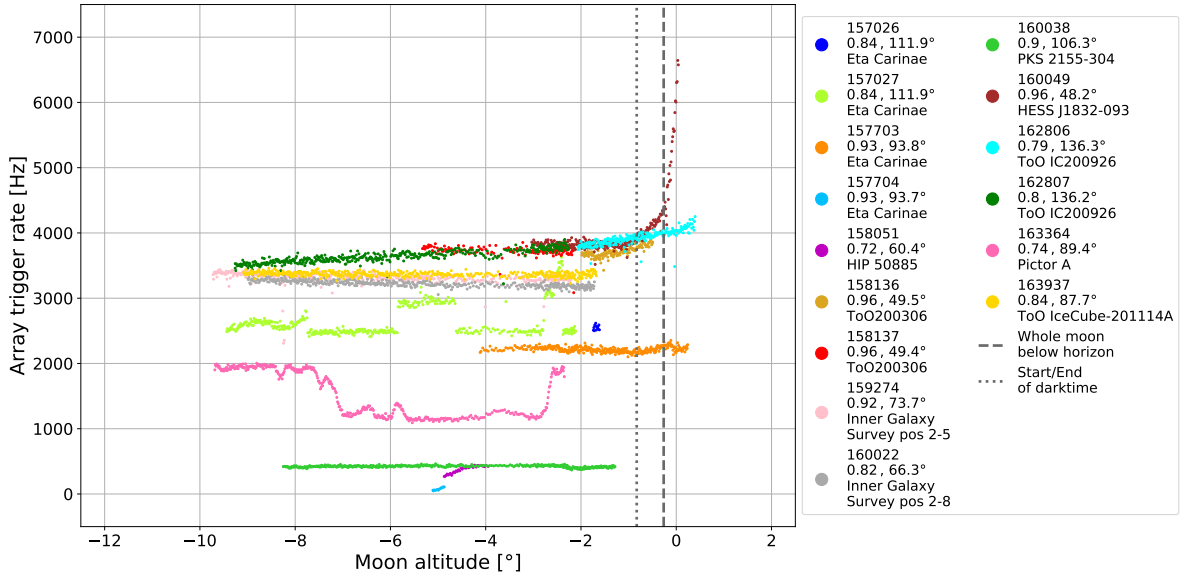

Figure 14: Array trigger rates for runs with a setting moon and a mean moon fraction between 66.66 % and 100 %

Single-telescope trigger rates

Next it is important to check the single-telescope trigger rates since during the observations high rates were reported. Also looking at the previous chapters it is clear that the single-telescope rates can go to extremely high values although it is not visible in the array rates because of the multiple telescope triggering. So one has to check if there are runs with steeply rising/decreasing rates far above ~10 kHz because this can cause problems for the individual telescopes. For the single-telescope trigger rates it is only looked at CT1 and CT5 since the rates of all small telescopes show the same behavior with only minor differences. Besides that only the trigger rates of specific runs that show an increasing/decreasing behavior are investigated because this is the main focus of this analysis. Also the moon in these runs has a mean fraction of 79 % and higher. The remaining runs can be found Appendix. It is also important to mention that for low mean moon fractions only the rates of CT1 and CT5 are displayed there. In these runs the single-telescope trigger rates are fairly constant and thus there is no interesting difference present between the rates of the four small telescopes. For high mean moon fractions the trigger rates of all five telescopes are shown there. Furthermore it should be mentioned that some runs with Eta Carinae as target show high trigger rates above the limit of the H.E.S.S. telescope which mostly likely

comes from the brightness of the source itself. Also since these increases do not appear near the horizon the runs with this target are not discussed.

The first rising trigger rate from CT1 that is looked at belongs to run 162901 can be seen in figure 15. It shows a slow increase within a range of about 2° and the exponential course is already present but in the end this rate is still below ~3000 Hz, even when the upper edge of the moon starts to move above horizon. The angle of separation is 80.9° which is optimal for moon observations. Nevertheless a moon fraction of 79 % is very high and therefore the moon near the horizon already has an impact on the trigger rates and causes them them to increase. There is not any other rising rate visible for that range of mean moon fraction.

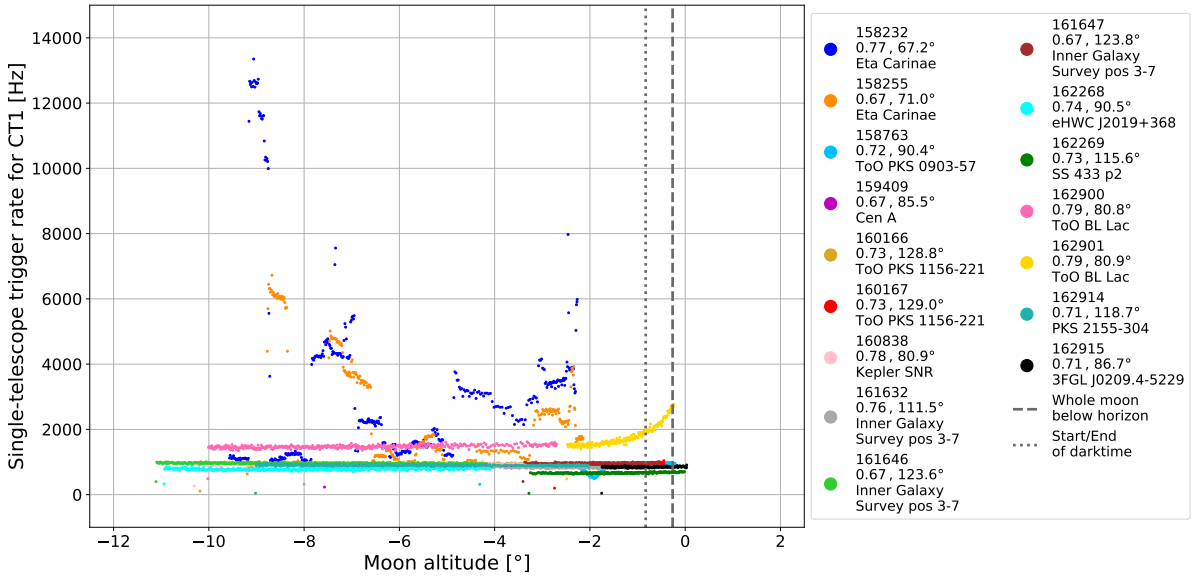

Figure 15: Single-telescope trigger rates (CT1) for runs with a rising moon and a mean moon fraction between 65 % and 80 %

Going to higher mean moon fractions gives even higher trigger rates near horizon which can be seen for run 162841 in figure 16 having a moon fraction of 87 %. For this the rate rises from less than 2 kHz to almost 8 kHz after which the moon is almost completely above horizon. It is shown that the requested start/stop altitude of −0.83° is safe for dark observations since this trigger rate is only ~2 kHz at this elevation. For some other runs there are also visible increases in the trigger rate but these are small and only go up to about 1500 Hz which is no problem for the cameras. Nevertheless this is an important information because there is also the possibility that these rates would have gone to very high values quickly if the run would have ended later.

Most importantly it should be looked at the single-telescope trigger rates that can be found in figure 17. For run 160049 rates go down from more than 50 kHz which is far above the usual range of trigger rates. Even when the upper edge of the moon is below horizon the rate is around 15 kHz. Though looking at the requested start/stop altitude it is shown that rate is not higher than about 5000 Hz which does not cause problems for the cameras. The moon does have a huge impact on this trigger rate since it has a very high

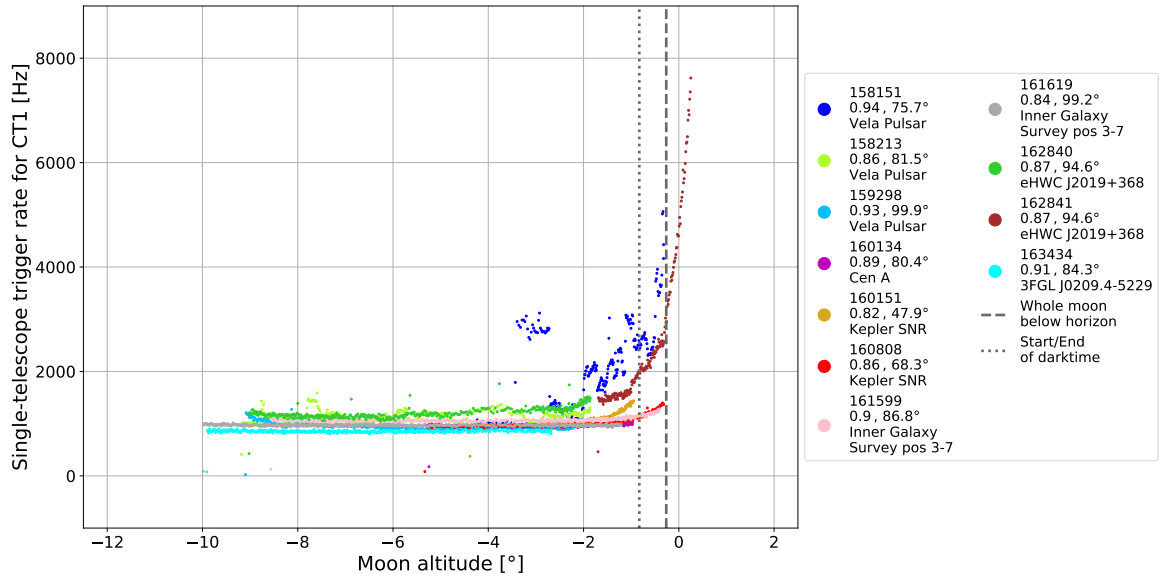

Figure 16: Single-telescope trigger rates (CT1) for runs with a rising moon and a mean moon fraction between 80 % and 100 %

moon fraction of 96 % and the angle of separation is less than 50° which is non optimal. Also for this run the rates of the other small telescopes vary between about 40 kHz and 65 kHz at the start of the run.

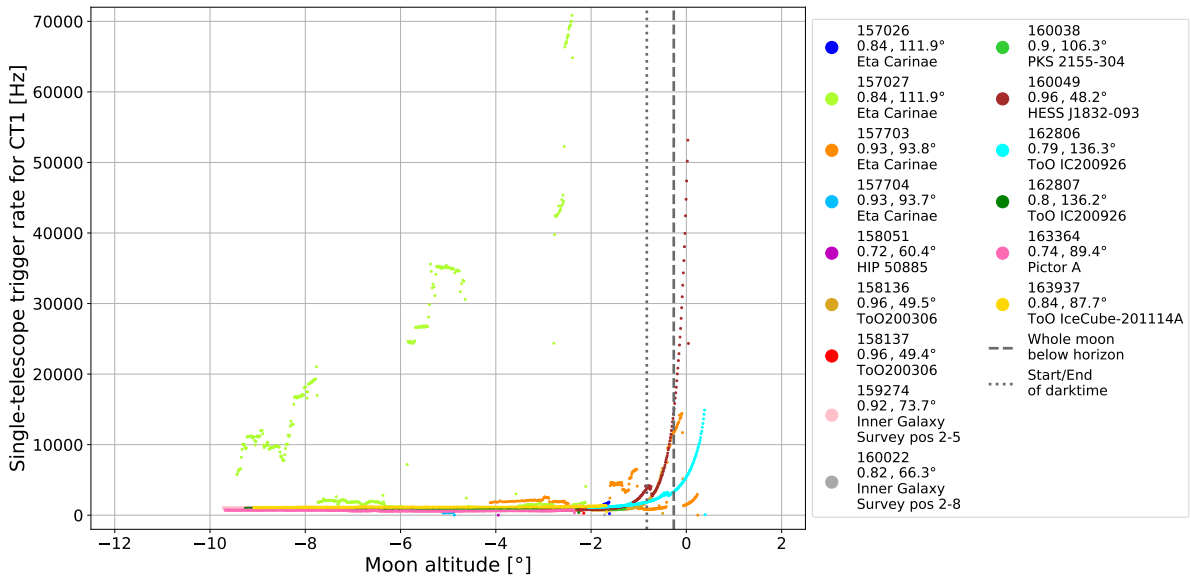

Figure 17: Single-telescope trigger rates (CT1) for runs with a setting moon and a mean moon fraction between 66.66 % and 100 %

For run 162806 the rate starts at about 15 kHz which is still too high for normal observations. Even though the moon fraction is not as high as for the other run the angle of separation goes towards 180° which causes backscattered moonlight going onto the cameras. For this run the rate does not exceed ~5000 Hz at the requested start/stop altitude of −0.83° which

shows that this limit is safe for observations regardless of the moon parameters.

Lastly the single-telescope rates of CT5 displayed in figure 18 and figure 19 have to be checked. For this it is sufficient to only look at the runs with the highest mean moon fractions since the rates of the different runs are mostly constant with one exception.

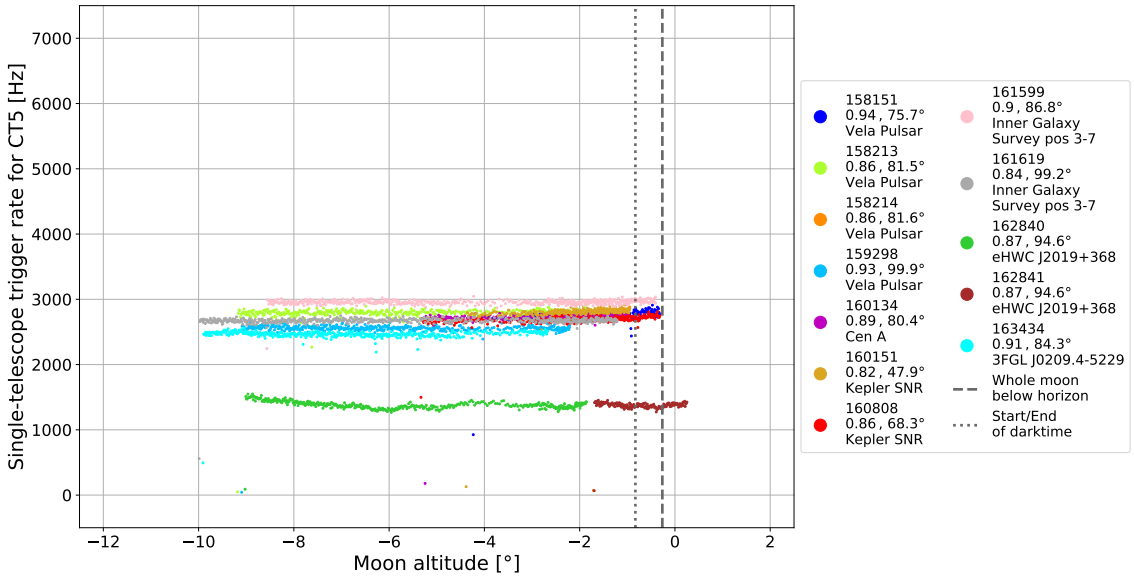

Figure 18: Single-telescope trigger rates (CT5) for runs with a rising moon and a mean moon fraction between 80 % and 100 %

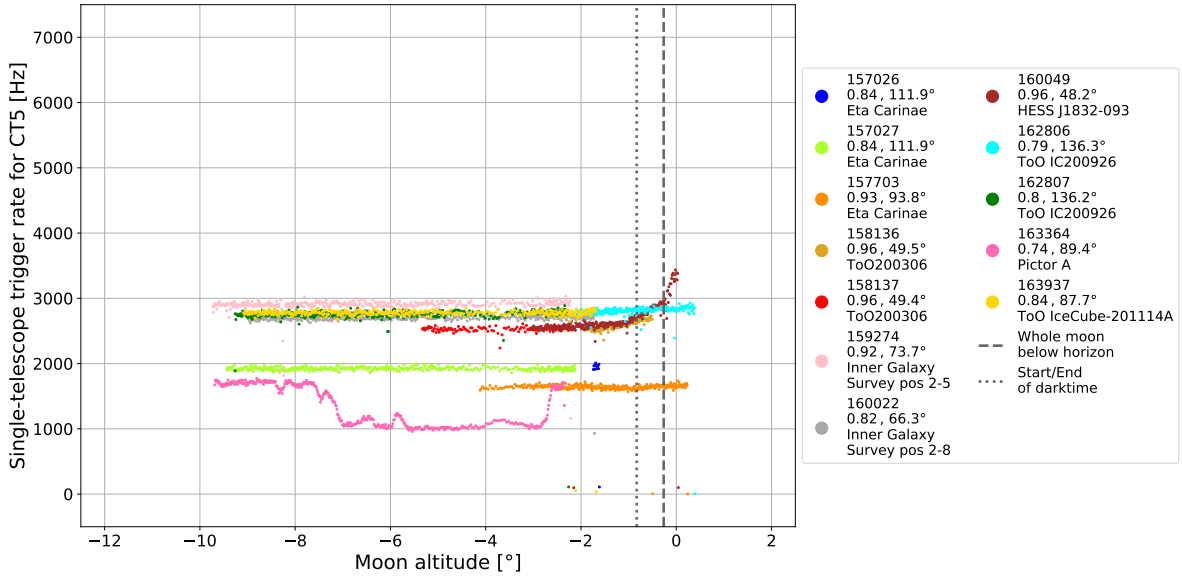

Figure 19: Single-telescope trigger rates (CT5) for runs with a setting moon and a mean moon fraction between 66.66 % and 100 %

For run 162841 there is no visibly rising trigger rate although this is the run which has exponentially rising single-telescope trigger rates up to 8 kHz for CT1-4. Even when the

moon is mostly above horizon the rate for CT5 is constant which shows that in this case the big telescope can filter NSB light coming when the moon is near the horizon. This tendency can also be seen for run 162806 which only has a rate below 3 kHz. The one rising rate occurs for run 160049 though this is a huge difference to the rates for the small telescopes because at the start of the run the CT1 rate is about 50 kHz higher. Overall for CT5 there are no rates that could cause problems to the camera even when the moon fraction is high and the moon is partly above horizon.

In summary very high single-telescope trigger rates outside the usual range occur for the small telescopes when the moon is above the requested start/stop elevation which is not the case for the big telescope. Furthermore the random coincidences are minimal because the huge increase in single-telescope trigger rates cannot be seen in the array trigger rates or only with a small increase if one stays below $-0.83°$. This shows that this altitude is a safe point to start observations at and because all of this in February of 2021 the actual start/stop altitude of dark observations is changed back to this number.

3 Analysis of camera image parameters

After comparing the different trigger rates in the previous chapter, it is important to look at the parameters that can be extracted from the camera images, in particular the Hillas parameters and the pixel intensities. In the end the NSB rate dependency of them will be investigated.
Since CT1-4 and CT5 have to be treated differently, the data is divided regarding this condition but also regarding the different run types and settings:

- CT1-4: Dark runs (5.5 p.e.), Moon runs (5.5 p.e.), Moon runs (6.5 p.e.)
- CT5: Dark runs (69 p.e.), Moon runs (69 p.e.), Moon runs (109 p.e.)

Like explained before, all ORs without moon are dark runs and the ORs and MORs with moon are moon runs. In this section they are separated regarding their pixel/trigger threshold.

For each run setting the camera images of every run are taken. With the Hillas parameters and pixel intensities taken from all those images histograms are made. The distributions in these histograms will be compared in the following. Furthermore it is important to check if and how individual runs influence these distributions and thus the Hillas parameters and pixel intensities of every run will be compared.

For the Hillas parameters a standard quality criterion was applied. For small Hillas sizes the NSB light plays a bigger role, since the number of photoelectrons being produced by air showers and NSB light is comparable. Therefore a cut was made, which excludes all images with a Hillas size of less than 60 p.e. for CT1-4 and 80 p.e. for CT5. For the investigation of the pixel intensities all cleaned camera images are used.

3.1 Hillas parameters

First the Hillas parameters, which are obtained from the camera images, have to be looked at. Since a similar behavior can be seen for the parameters for CT1-4 and CT5 respectively, it is not looked at the distributions of all parameters specifically in this section. The distribution of the pixels per image and the time development of the all parameters besides the Hillas size can be found in the Appendix.

The Hillas size of the CT1-4 data is shown in figure 20. The corresponding distributions of the Hillas length and width can be seen in figure 21. The distribution of the runs with the same pixel threshold of 5.5 p.e. look quite similar, but they differ a bit from the moon run (6.5 p.e.) data, which has a broader distribution and this tendency can be seen for all parameters.

This behavior is also visible in the statistics in table 10. For example, for the Hillas size the mean of the moon run data (5.5p.e.) is 411.8p.e., which is 1.1 times higher than the corresponding value of the dark run data. On the other hand, for a higher pixel threshold the mean goes up to 502.8p.e., which is 1.4 times higher. The mean of the other Hillas

parameters shows qualitatively same behavior and so does the median for all parameters. Regarding the mean, the difference of the moon data to the dark data is not more than about 10 % if the pixel threshold is the same but it goes up to 40 % for the higher threshold. For the median the difference is not more than 10 % and 30 % for a threshold of 5.5 p.e. and 6.5 p.e., respectively, which also shows that the distribution for the moonlight data with the lower threshold is closer to the distribution of the dark data.

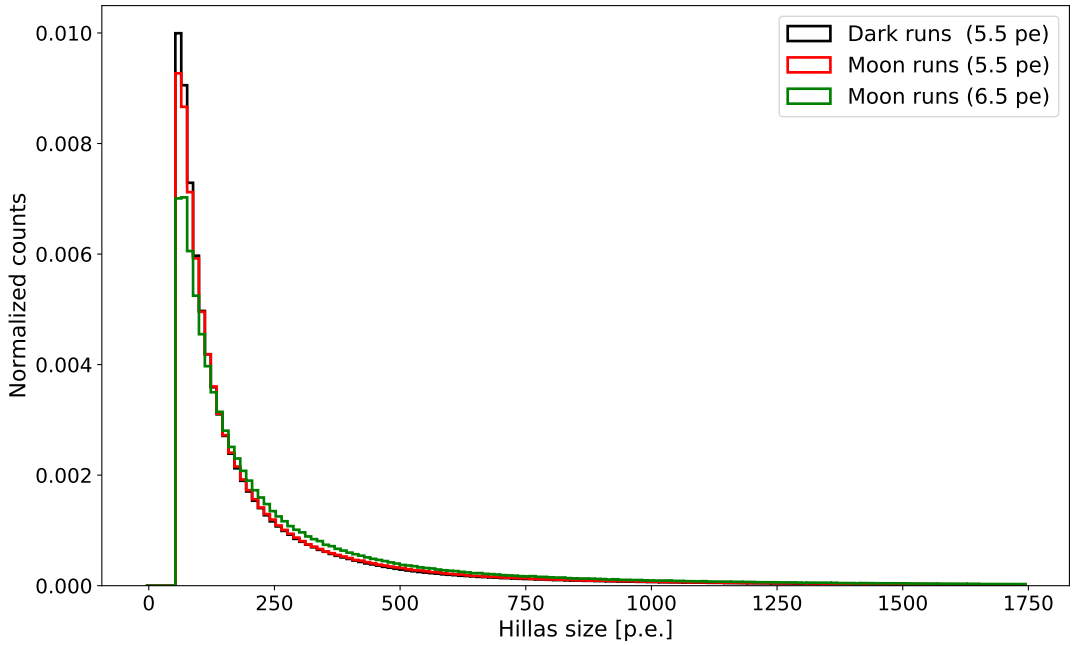

Figure 20: Distribution of the Hillas size for CT1-4

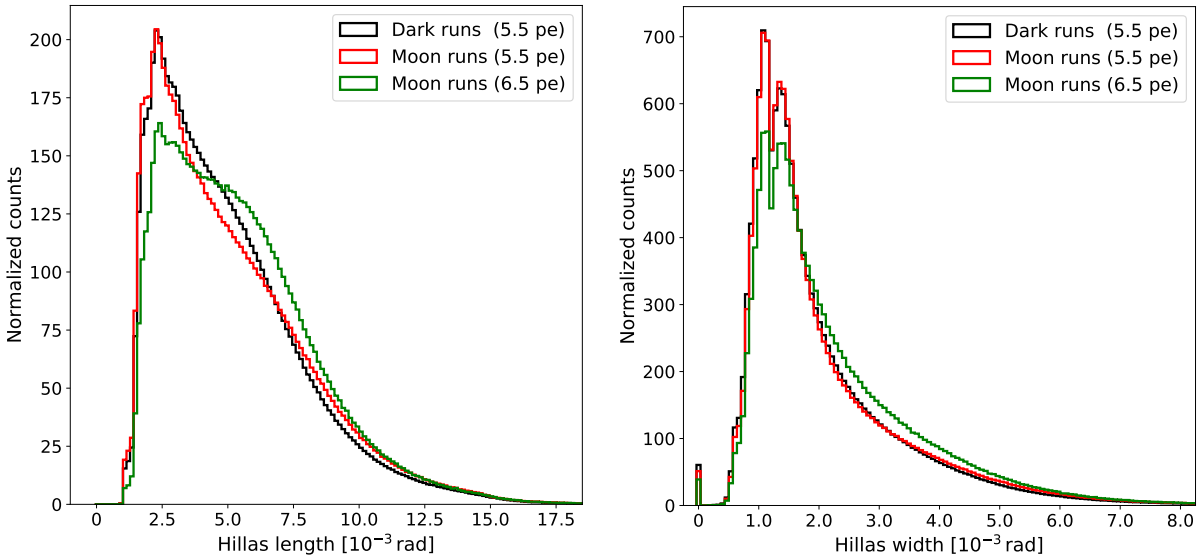

Figure 21: Distribution of the Hillas length and Hillas width for CT1-4

It is also important to look at the mode, which is the most frequently occurring value.

Here, almost no differences for both thresholds are present. This shows that all peaks are roughly at the same location, but the mean and median of the distributions are shifted to higher numbers. The similarity of the distribution for the dark runs and the moon runs with the same pixel threshold and the visible difference of the distribution for a higher threshold would imply that the NSB light that comes from the moon does not have as much impact on the data as the threshold itself. Additional moonlight that goes into the cameras changes the distributions only by a bit. If the pixel threshold is increased the difference in the distributions gets way bigger, since the Cherenkov light of the air showers goes into the cameras for a longer time period. Therefore more photoelectrons are produced, which results in average in higher Hillas sizes, which can be seen in these distributions.

Value	Run type	Hillas size [p.e.]	Pixels per image	Hillas length [10^{-3} rad]	Hillas width [10^{-3} rad]
Mean	Dark (5.5 p.e.)	370.5	17.2	5.1	2.1
	Moon (5.5 p.e.)	411.82 (1.1)	18.6 (1.1)	5.2 (1.0)	2.2 (1.0)
	Moon (6.5 p.e.)	502.79 (1.4)	21.3 (1.2)	5.6 (1.1)	2.3 (1.1)
Median	Dark (5.5 p.e.)	136.4	11.0	4.5	1.6
	Moon (5.5 p.e.)	141.71 (1.0)	11.0 (1.0)	4.6 (1.0)	1.7 (1.0)
	Moon (6.5 p.e.)	169.38 (1.2)	13.0 (1.2)	5.1 (1.1)	1.9 (1.1)
Mode	Dark (5.5 p.e.)	100.5	7.0	10.1	1.2
	Moon (5.5 p.e.)	100.13 (1.0)	7.0 (1.0)	10.4 (1.0)	1.1 (1.0)
	Moon (6.5 p.e.)	102.34 (1.0)	7.0 (1.0)	10.0 (1.0)	1.2 (1.0)

Table 10: Mean, median and mode of the Hillas parameters for different run settings (CT1-4)

It has to be looked at every Hillas parameter per individual run to see if the same tendency is present there or if specific runs distort the distributions. The development of the Hillas size over time is shown in figure 22. The other Hillas parameters show similar behavior. One can see that large fluctuations are present for the different parameters and they change significantly over time. Looking only at the runs of 2019 it is clearly visible that the Hillas size of the moon run with a pixel threshold of 6.5 p.e. is way higher than the other moon runs with a lower threshold, which is also the case for the moon runs that were taken in September of 2020. The Hillas size is significantly higher, although all observations were made in about one week. This comes mostly from the higher threshold, since more photoelectrons are needed to trigger the telescope, which causes an increase of the Hillas size. Looking at the moon runs with a threshold of 5.5 p.e. and all dark runs one can see that the average Hillas size decreases from about 160 p.e. to about 135 p.e. around the beginning of September in 2020, which could come from a change of PKS 2155-304.

Overall for CT1-4 dark and moon runs with the same threshold show relatively equal values for the Hillas parameters, although some differences are present. Because of these minor fluctuations more observations have to be made to further investigate the differences. On the other hand moon runs with a higher pixel threshold result in higher values of all

studied Hillas parameters. Therefore it is difficult to directly compare these runs to dark runs. For the moon characteristics that were present during all those runs one can say that data can be gathered that is similar to data taken during dark nights.

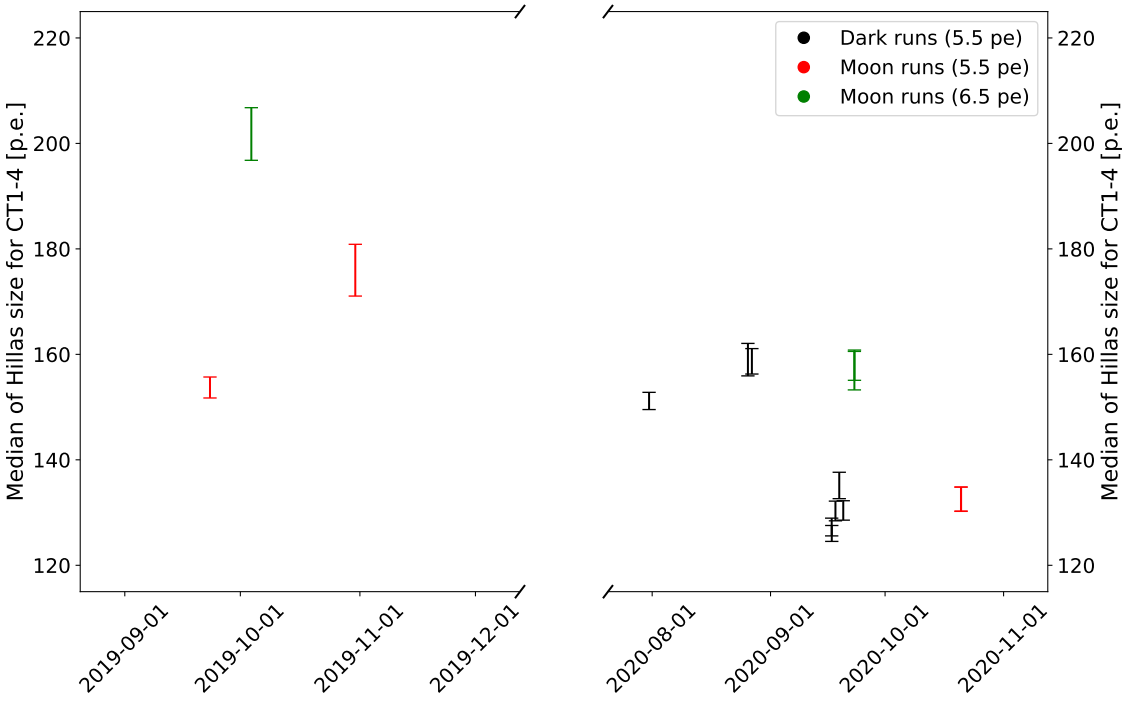

Figure 22: Hillas size per run over time for CT1-4

After looking at the distributions for CT1-4, the ones for CT5 have to be discussed as well. Figure 23 and figure 24 show the distributions of the Hillas size, length and width for CT5. It can be seen that the data of the dark and moon runs with a threshold of 69 photoelectrons is distributed similarly and there is only a slight visible difference. On the other hand the data of the moon runs (104 p.e.) shows a much broader distribution that significantly differs from the other ones. As previously mentioned the pixel threshold of these runs is about 50 % higher than the threshold of the other runs. This specific behavior that is similar for all Hillas parameters can also be seen for the pixels per image.

In table 11 the data for the different run types are compared. For the mean and the median the highest change for moon runs (69 p.e.) and moon runs (104 p.e.) in comparison to dark runs is about 10 % and 50 % respectively. The mode for moon runs with the lower threshold is not more than 10 % off but for the runs with a higher threshold it goes up to 50 %, which results in a very different peak location. This shows that the moon runs (104 p.e.) are significantly different to the data from dark runs and like for CT1-4 this implies that the chosen threshold has more impact on the data than the moonlight itself. Next it has to be looked at the Hillas parameters for every individual run to see again if a specific run deviates from the other runs.

The Hillas size of every CT5 run can be seen in figure 25 and it shows the time development of that parameter.

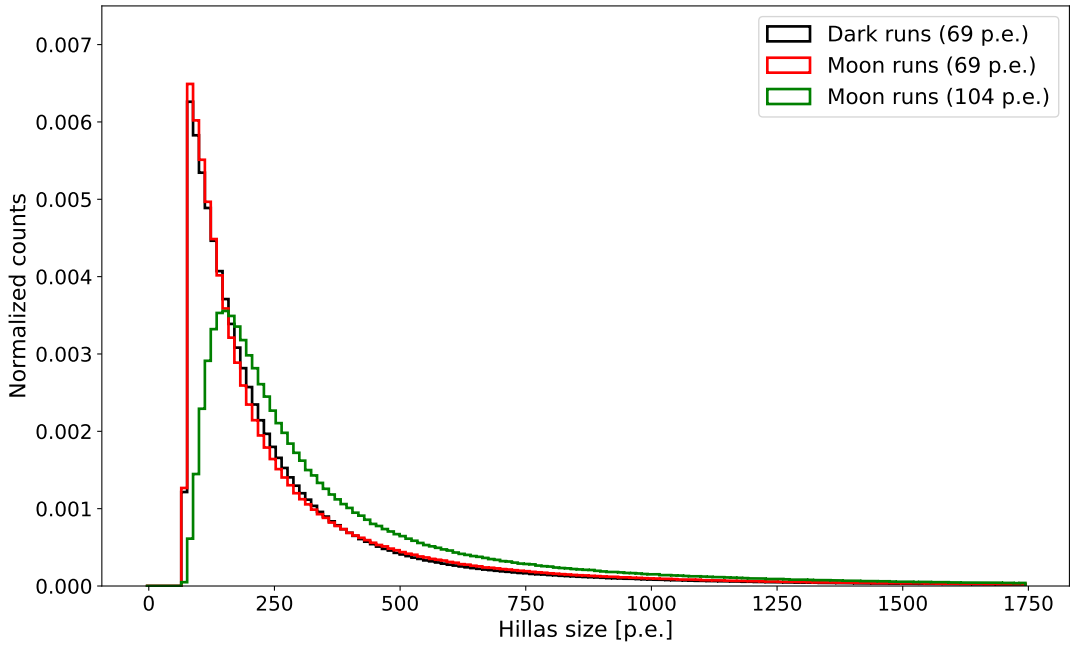

Figure 23: Distribution of the Hillas size for CT5

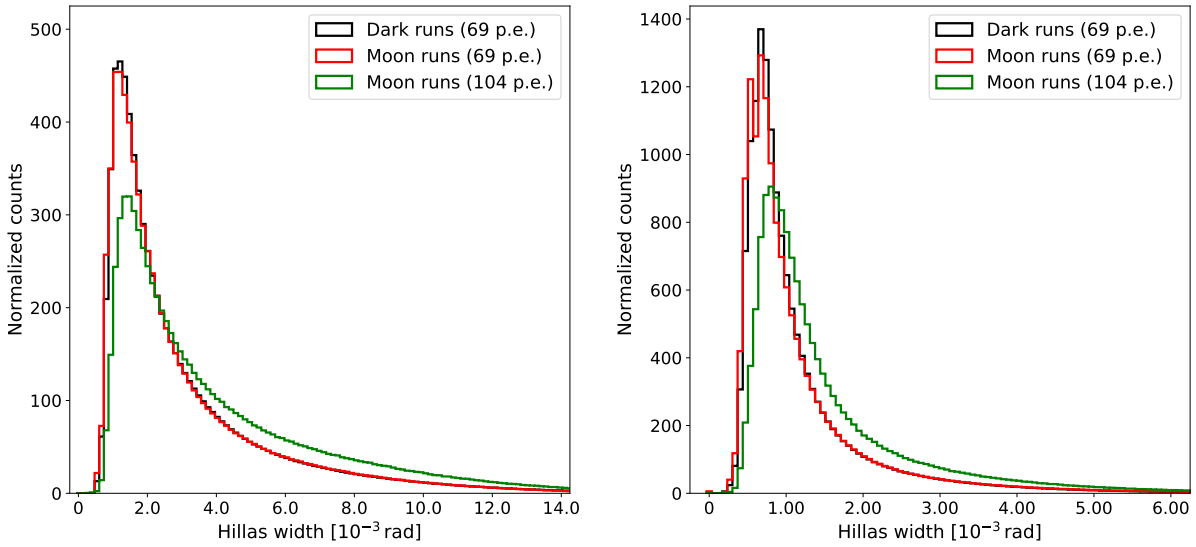

Figure 24: Distribution of the Hillas length and Hillas width for CT5

Since the runs of each run setting happened within a short time period, it is difficult to investigate the overall time development of the Hillas parameters. Nevertheless one can see that the Hillas sizes of the runs with the lower threshold are around the same value of about 190 p.e., which implies that the moon does not have a significant impact on the data, since the pixel threshold is the same for both run types. For the moon runs (104 p.e.) the Hillas size is about 50 % higher, which comes from the higher threshold that is present for these runs. The last interesting thing which can be seen is the decreasing course of the Hillas size of the dark runs within a few days.

Based on the analyzed runs, it looks like using CT5 during nights with moon results in

Value	Run type	Hillas size [p.e.]	Pixels per image	Hillas length [10^{-3} rad]	Hillas width [10^{-3} rad]
Mean	Dark (69 p.e.)	470.9	25.7	3.2	1.2
	Moon (69 p.e.)	537.0 (1.1)	24.3 (0.9)	3.1 (1.0)	1.2 (1.0)
	Moon (104 p.e.)	711.2 (1.5)	38.2 (1.5)	4.1 (1.3)	1.6 (1.3)
Median	Dark (69 p.e.)	194.1	14.0	2.2	0.9
	Moon (69 p.e.)	194.6 (1.0)	13.0 (0.9)	2.2 (1.0)	0.9 (1.0)
	Moon (104 p.e.)	280.2 (1.4)	21.0 (1.5)	3.0 (1.4)	1.2 (1.3)
Mode	Dark (69 p.e.)	102.7	8.0	1.3	1.0
	Moon (69 p.e.)	109.6 (1.1)	7.0 (0.9)	1.2 (0.9)	1.1 (1.0)
	Moon (104 p.e.)	146.9 (1.4)	12.0 (1.5)	1.7 (1.3)	1.1 (1.1)

Table 11: Mean, median and mode of the Hillas parameters for different run settings (CT5)

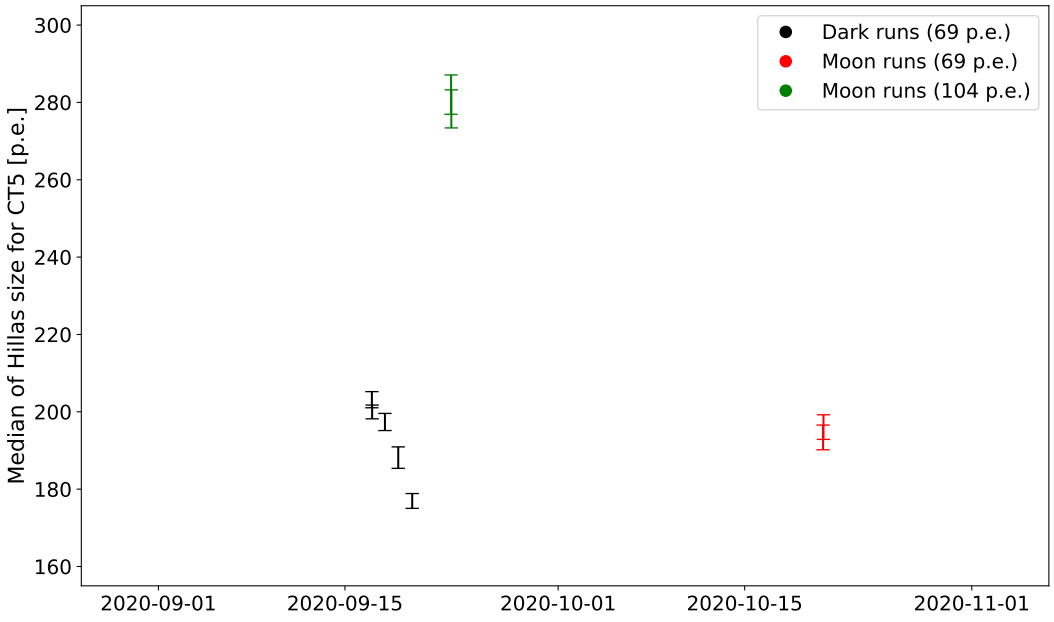

Figure 25: Hillas size per run over time for CT5

Hillas parameters that are fairly comparable to the parameters taken during dark moonless nights. The different characteristics of the images must be account for in the subsequent analysis. Also since only a few observations with moon happened, more moon runs that include CT5 have to made to better compare the different data.

3.2 Pixel intensities

Next the signal intensities in individual pixels were investigated. For this it is looked at the summed signal in three pixels with the highest intensity that are present after the images are cleaned. In the following this value is referred to as "three hottest pixels".

Figure 26 shows the distribution of the three hottest pixels for CT1-4. The data of dark runs and moon runs with a pixel threshold of 5.5 p.e. show a similar course. On the other hand the distribution of the moon runs with a higher threshold of 6.5 p.e. is a bit broader in comparison.

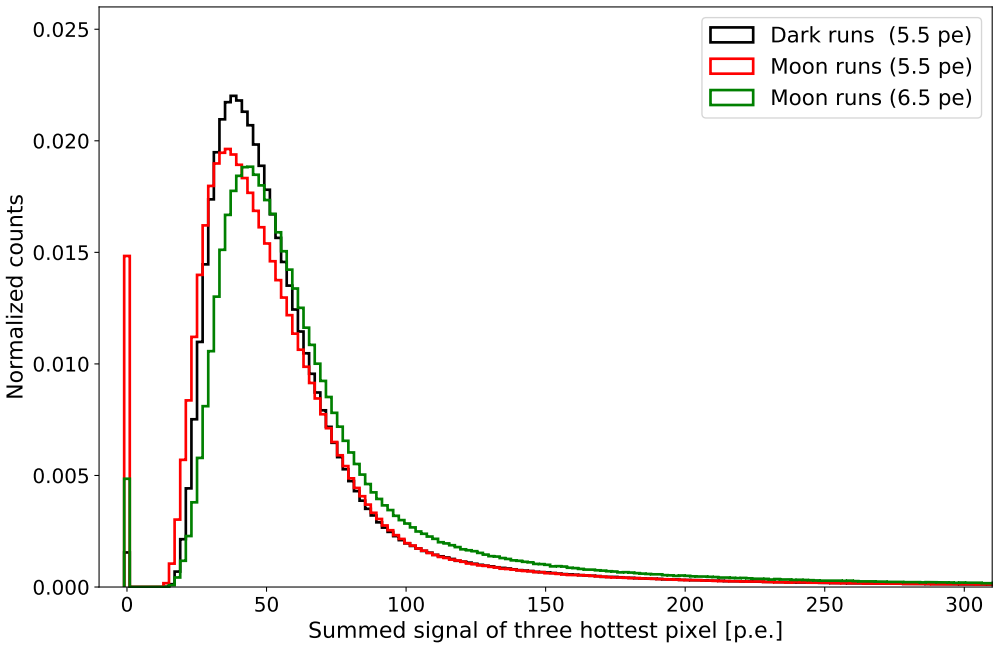

Figure 26: Distribution of the three hottest pixels for CT1-4

In table 12 one can see that the mean and the median of the three hottest pixels for moon runs (5.5 p.e.) differ by less than 10 % in comparison to the dark run data. For moon runs with a higher threshold that difference is significantly bigger, since the mean and the median for this run data is 10 % – 30 % higher. This tendency changes a bit for the mode, which represents the peak of the distribution. For moon runs with a threshold of 6.5 p.e. the value gets smaller in comparison to the dark runs. Though overall the pixel intensities are more similar if the pixel threshold is the same for dark and moon runs for CT1-4 and if the threshold is higher the distribution is broader.

This behavior is similar to that of the Hillas parameters. Likewise it is important to look at the pixel intensities of the individual runs. The change of the three hottest pixels over time can be seen in figure 27. It is clearly visible that with one exception all runs that have a pixel threshold of 5.5 p.e. fluctuate around 52 p.e. and the runs with a higher threshold in average result in higher values. It is also important to remember that for the pixel intensities no cut was made and thus all images are included. One can see that at the beginning of September in 2020 the average value for the three hottest pixels goes down by a bit and stays there with the exception of the moon runs with the higher pixel threshold. Because of the higher threshold more photoelectrons are needed to fulfill the trigger conditions and this results in a higher value.

The course of the different runs in 2020 shows that the pixel intensities between dark and moon runs with a threshold of 5.5 p.e. are comparable. Also like for the Hillas parameters

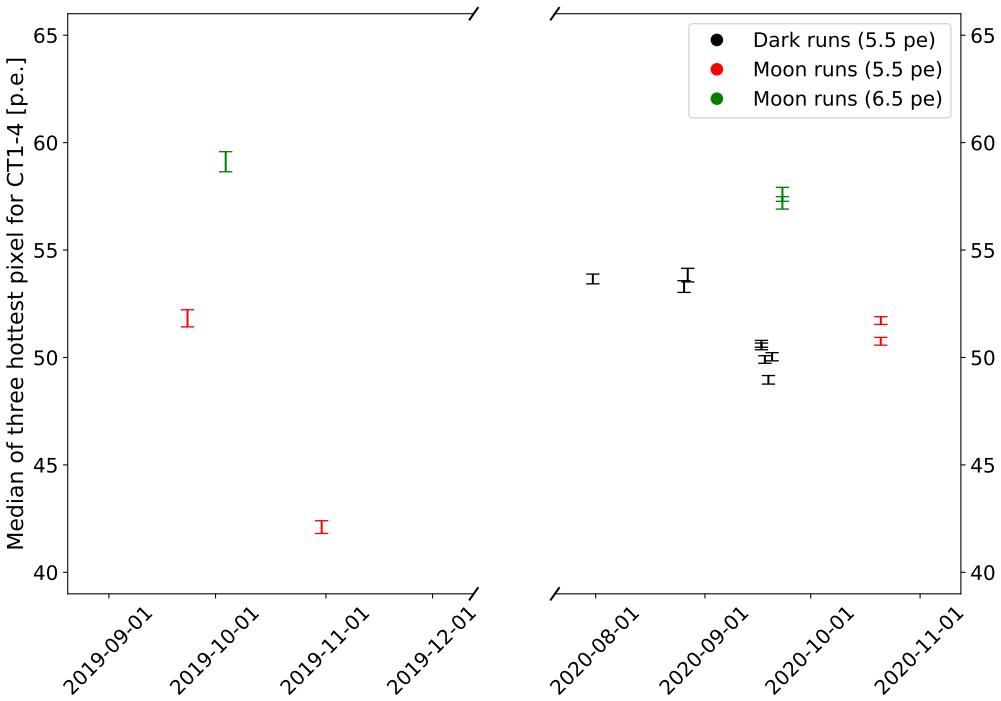

Figure 27: Summed signal of three hottest pixels per run over time for CT1-4

it is clear that a higher threshold results in higher values in average.

Looking at the pixel intensities in figure 28 all three run types show a different course and none of them is very similar. The dark runs show the broadest distribution and that data lies between the data of the other two run types. For moon runs (69 p.e.) the data is similar for small intensities, but the distribution is not as broad. On the other hand the data of the moon runs (104 p.e.) is shifted to higher numbers in total.

This behavior is also represented in table 12. The mean, median and mode of the moon runs (69 p.e.) is about 10 % smaller than for dark runs and for the data of the moon runs (104 p.e.) these values are up to 20 % higher. This shows that overall the dark and moon runs with the same threshold have less differences and that the moonlight does not have a significant impact on the values. Going to higher thresholds results in higher differences between the pixel intensities of the different run types.

To see where this tendency of the various run types comes from it has to be looked at the individual runs. This can be seen in figure 29. The course of the pixel intensities over time looks similar to the course of the Hillas parameters with one visible difference. The pixel intensities of the dark runs start very high and steeply decrease within a time period of a few days, which was also happened for the Hillas parameters but not that drastically. The reason for this cannot be the moonlight, since no moon was present during the observations. Therefore something else has to be responsible for these rapid changes. All these runs happened within a time period of around three days. The variability of PKS 2155-304 could be a reason, since it is known that the flux of the source can change significantly within days and even hours [17]. The high pixel intensities for the moon runs (104 p.e.) come again from the higher pixel threshold that needs more photoelectrons to

trigger.

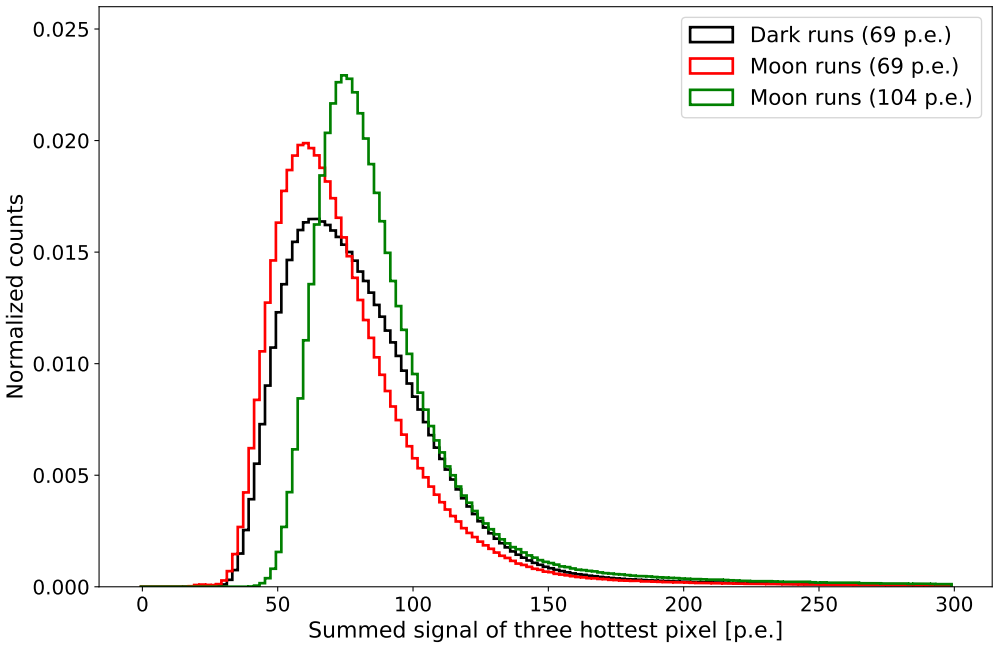

Figure 28: Distribution of the three hottest pixels for CT5

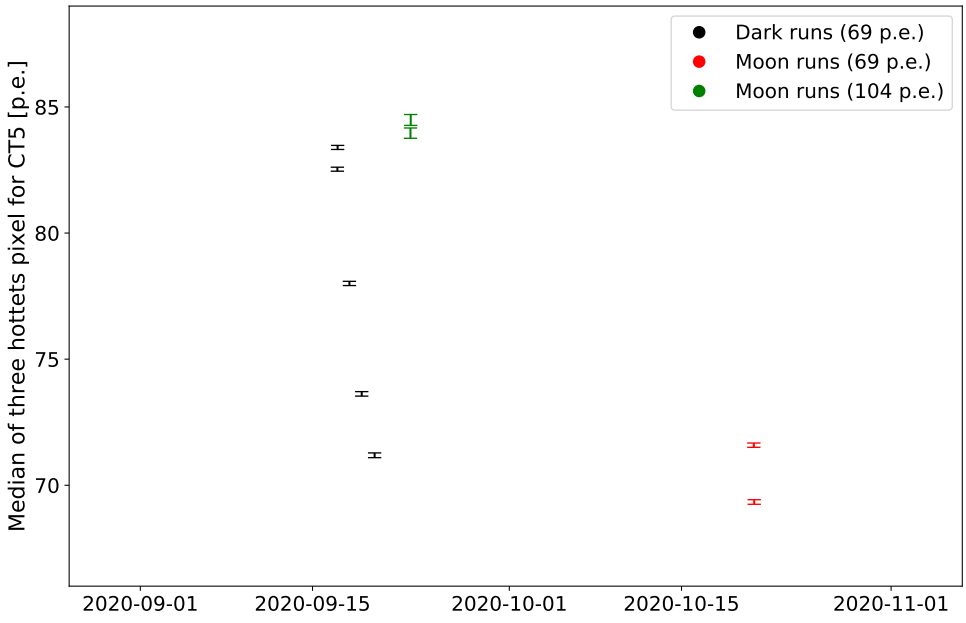

Figure 29: Summed signal of three hottest pixels per run over time for CT5

Overall it seems that the pixel intensities behave similarly to the Hillas parameters. Since these large differences for the dark runs are present, it is important to do more observations at different dates, because it is likely that some factors are the reason for the varying values during this short time period. Nevertheless it looks like regarding the pixel intensities of

CT5, data obtained during dark moonless nights is comparable to data taken while the moon is up.

Value	Run type CT1-4	Three hottest pixels [p.e.]	Run type CT5	Three hottest pixels [p.e.]
Mean	Dark (5.5 p.e.)	83.6	Dark (69 p.e.)	93.7
	Moon (5.5 p.e.)	83.7 (1.0)	Moon (69 p.e.)	86.3 (0.9)
	Moon (6.5 p.e.)	106.5 (1.3)	Moon (104 p.e.)	110.6 (1.2)
Median	Dark (5.5 p.e.)	51.0	Dark (69 p.e.)	77.7
	Moon (5.5 p.e.)	50.4 (1.0)	Moon (69 p.e.)	70.6 (0.9)
	Moon (6.5 p.e.)	58.2 (1.1)	Moon (104 p.e.)	84.2 (1.1)
Mode	Dark (5.5 p.e.)	45.5	Dark (69 p.e.)	69.0
	Moon (5.5 p.e.)	45.7 (1.0)	Moon (69 p.e.)	66.1 (1.0)
	Moon (6.5 p.e.)	42.5 (0.9)	Moon (104 p.e.)	71.8 (1.0)

Table 12: Mean, median and mode for the pixel intensity for different run settings (CT1-4)

Lastly the ratio of images in which all pixels are set to zero caused by the cleaning process are investigated for the different run types. In the following these images are referred to as “null images”. This kind of images occur, because of random coincidences from NSB light passing the trigger criterion, but not surviving the cleaning, thus being set to zero by the algorithm. The ratio of null images for both CT1-4 and CT5 can be found in table 13.

One can say that the ratio of null images is an approximation of how much observation time and information is lost. Whenever the the moonlight light fulfills the trigger criteria, the images are read out and this during this time no photon coming from the air shower can be detected. Overall this results in less detection time. Looking at CT1-4, for less than 3 % of all images the pixels are set to zero and for CT5 less than 0.2 %. This shows that only a relatively small part of the taken images is read out because of moonlight.

For CT1-4 the ratio of null images for moon runs is almost 10 times higher than for dark runs if the pixel threshold is the same. This shows that a lot of time that would be used for detection of Cherenkov radiation is lost due to the moonlight causing the read-out of images. For a threshold of 6.5 p.e. for moon runs the ratio of null images is only 3 times higher. This comes from the fact for a higher threshold it is not as easy to fulfill the trigger requirements by random coincidences from moonlight going into the camera. Thus increasing the pixel threshold would mostly likely result in an even smaller ratio.

For CT5 there is a significant difference for the ratio of null images for the dark and moon runs with the same threshold. Like for CT1-4 this likely comes from the additional light from the moon. On the other hand the ratio for moon runs (104 p.e.) is even less than for dark runs, which comes from the threshold that is about 50 % higher than the threshold for the other run types and thus for this run setting the moonlight does have the least impact.

Overall moonlight increases the ratio of images in which no pixels survive the cleaning

and an increase of the threshold lowers that ratio.

Run type CT1-4	Ratio of null images CT1-4 [%]	Run type CT5	Ratio of null images CT5 [%]
Dark (5.5 p.e.)	0.31	Dark runs (69 p.e.)	0.026
Moon (5.5 p.e.)	2.94 (9.58)	Moon runs (69 p.e.)	0.193 (7.304)
Moon (6.5 p.e.)	0.95 (3.11)	Moon runs (104 p.e.)	0.001 (0.039)

Table 13: Ratio of the null images for all run settings for CT1-4 and CT5

3.3 NSB rate dependency

After looking at the different camera image parameters, it is important to check the NSB rate dependency of all parameters to see how the moon affects the data of every individual run. For CT1-4 the mean NSB rate of all four telescopes is used. The systematic uncertainty[3] of the NSB rate is estimated to be between 10 % and 20 % of the value itself. In the following a mean systematic uncertainty of 15 % of the NSB rate is used. Since all parameters show quite similar behavior like in the previous section, it will only looked at the Hillas size for CT1-4 and CT5 respectively, but visible differences between the parameters will be mentioned. The plots that show the NSB dependency of the other parameters can be found in the Appendix.

In figure 30 the NSB dependency of the Hillas size for CT1-4 is shown. All moon runs except for one have a significantly higher NSB rate than the dark runs, which is caused by the moonlight. The moon run (5.5 p.e.) that has a relatively low NSB rate of about 60 MHz is MOR 155278. This is the run that has heavily fluctuating trigger rates caused by scattering of Cherenkov light off clouds. This run is an outlier and this can also be seen for the pixels per image, the Hillas length and width. Looking at the pixel intensities the median of this outlier run is way lower than for any other run. Though both cases cannot directly be compared, since for the Hillas parameters a cut was made regarding the Hillas size, but not for the pixel intensities. With the exception of the previously discussed run the Hillas size of all dark runs and moon runs with the same pixel threshold are around the same range of about 140 p.e. to 160 p.e., which is not the case for the runs with the higher threshold. Although the NSB rate of these runs is comparable, the Hillas size of these varies between about 160 p.e. to 200 p.e., which is in average higher range than for the other runs. This tendency is also present for the other parameters and the pixel intensities. With the exception of the two runs with the highest Hillas size the runs are visibly divided into two groups. The one is around 155 p.e. and the other one is around 130 p.e., but this separation rather comes from the variability of PKS 2155-304 than from the moon. These groups are also present for the Hillas width and the pixel intensities.

Overall for CT1-4 for these viewed runs the data of the dark and moon runs (5.5 p.e.) is not heavily affected by a way higher NSB rate caused by the moonlight. Nevertheless special

[3]Private communication V. Marandon

conditions like clouds can change that and thus one has to pay attention to this factor. Also increasing the pixel threshold results in higher values for the different parameters.

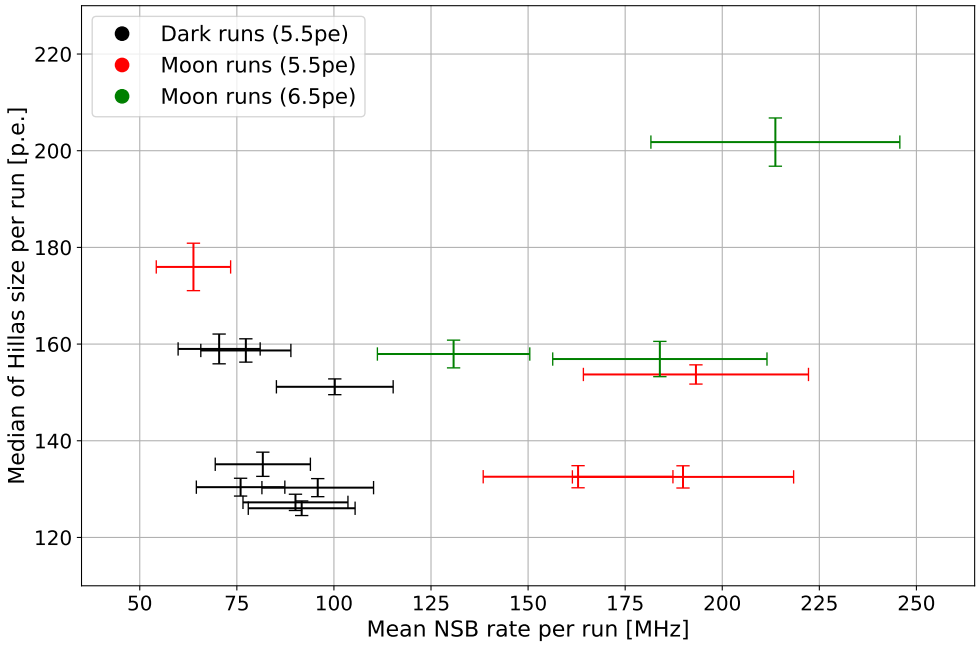

Figure 30: NSB dependency of the Hillas size for CT1-4

The NSB dependency of the Hillas size for CT5 is shown in figure 31.

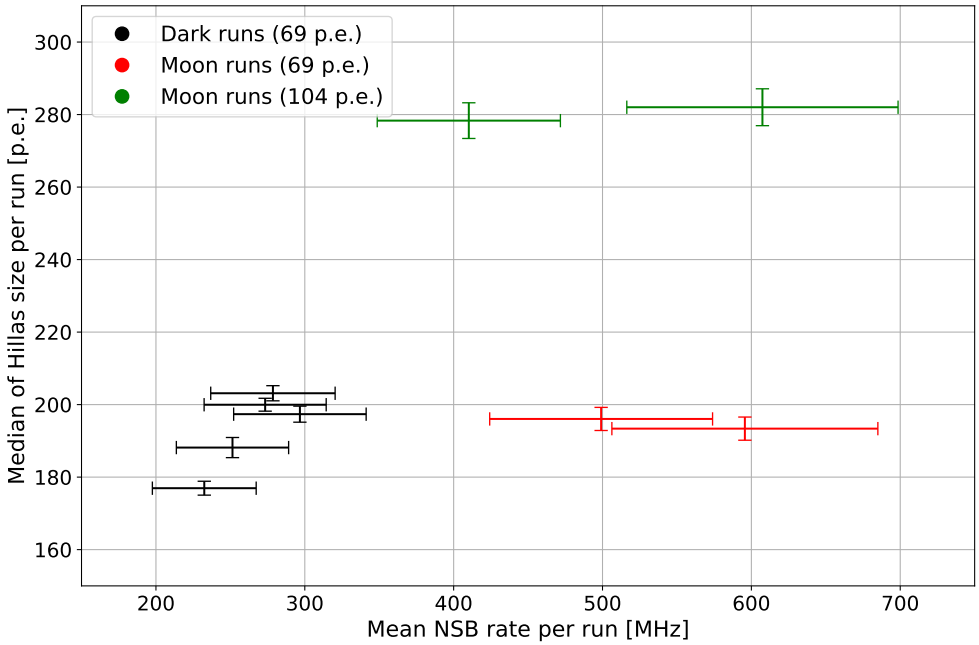

Figure 31: NSB dependency of the Hillas amplitude for CT5

It is clearly visible that the median of the Hillas size for runs with a threshold of 69 p.e. are within the same range of about 180 p.e. to 200 p.e which is not the case for the runs with

a higher threshold. The values of these runs are way higher at around 280 p.e. which is a big difference caused by the higher pixel threshold of CT5. Like seen for CT1-4, for moon runs a higher NSB rate was present than for dark runs, which comes from the additional light from the moon that goes into the cameras. This behavior can also be seen for the pixels per image, the Hillas length and width. Not all intensities of the dark run data are around the same value and it is shown that these heavily vary. Some dark runs have intensities around the level of the moon runs (69 p.e.), but others go up to the values of the moon runs (104 p.e.). It is important to remember that also for CT5 a cut for the Hillas parameters was made but not for the pixel intensities and therefore they are not directly comparable.

All in all for CT5 for the viewed runs the different parameters do not change significantly if the same run setting is used. Although the NSB rate is higher for the moon runs (69 p.e.) the impact of the moonlight itself on the different parameters is minimal. Also the increase of the values for moon runs (104 p.e.) comes from the higher pixel threshold itself rather than the moonlight.

4 Summary and outlook

In this thesis data taken from observations with relatively weak moonlight were analyzed and compared to data obtained during dark moonless nights. The blazar PKS 2155-304 was the gamma-ray source for all of these observations. In summary a lot of conclusions can be drawn after comparing the different data.

In this study it was looked at the data from 16 different runs (stereo, hybrid and mono configuration), which all happened between September 2019 and November 2020. All runs that included CT5 happened after the telescope had received its "FlashCam" upgrade. In all moonlight runs the moon had a fraction of less than 40 % and the angle of separation between moon and target was between 45° and 135°. The trigger rates and camera image parameters of all runs were investigated.

For the array trigger rate there was no visible change that could come from moonlight. The only varying trigger rates that appeared were caused by clouds that scattered the NSB light. This shows that the accidental coincidences are low due to the multiple telescope triggering. For the single-telescope rates the impact of the moon could be seen for CT1-4. The two "ObservationRun (OR)" with moon showed a slowly changing rate with the decreasing moon. The single-telescope rate of the one "MoonlightObservationRun (MOR)" went up to more than 25 kHz, which is far above the usual measured trigger rates and could damage the PMTs of the telescopes. On the other hand for CT5 there were no changes in the trigger rates that could have been caused by moonlight. Also for some runs the mean value of the array and single-telescope trigger rate is significantly lower than for others, but this comes from the trigger threshold that is 50 % and not from the light of the moon. For CT1-4 pixel thresholds of 5.5 p.e. were used for ORs and 5.5 p.e./6.5 p.e. for MORs. For CT5 the trigger thresholds were 69 p.e. for ORs and 104 p.e. for MORs.

The different camera image parameters showed a behavior that is mostly independent from the moon. It was looked at the Hillas size, the Hillas length, the Hillas width and the number of pixels per taken image. For both CT1-4 and CT5 no significant changes appeared and only minor fluctuations were present for runs that have the same threshold. Overall going to a higher trigger threshold increases the mean value of all the parameters. Looking at the time development of the parameters of CT1-4 the mean value of the parameters decreased at some point in time, which most likely comes from a factor that is not the moon. This effect was not seen for CT5, but that most likely comes from the fact that all runs that include CT5 were taken within about a month. The first and last CT1-4 run was taken a bit more than a year apart.

Looking into the future with H.E.S.S., it is clear that observations during nights with moon can and should be made. If the night sky background rate is acceptable, such observations can result in data comparable to data taken during dark moonless nights. Additional observation time can be gained and transient events can be targeted, even while the moon is up.

Nevertheless there are things have to be done to properly do measurements during nights with moon. Although the dark and moonlight data looked at in this study are qualitatively similar, it should be thought about possibly adjusting the pixel threshold of CT1-4 because

of the high single-telescope trigger rates that occurred. For CT5 it does look like that for the current moonlight settings no changes have to be made. No changes of trigger rates caused by the moon appeared and thus the settings should be used for further observations. Looking at the camera image parameters, it can be seen that more observations in total have to be made to investigate the time development of the different parameters better. This especially applies to CT5 because there were only three short time periods in which all runs happened. Lastly it is important to think about making adjustments for the analysis of the moonlight data coming from runs with a higher trigger threshold, since this data is qualitatively different to the dark and moonlight data coming from runs with a lower trigger threshold.

Appendix

Single-telescope trigger rates for PKS 2155-304

The legend contains the run type and the run number. It also includes the mean moon fraction, mean angle of separation but also the mean moon altitude with its movement direction.

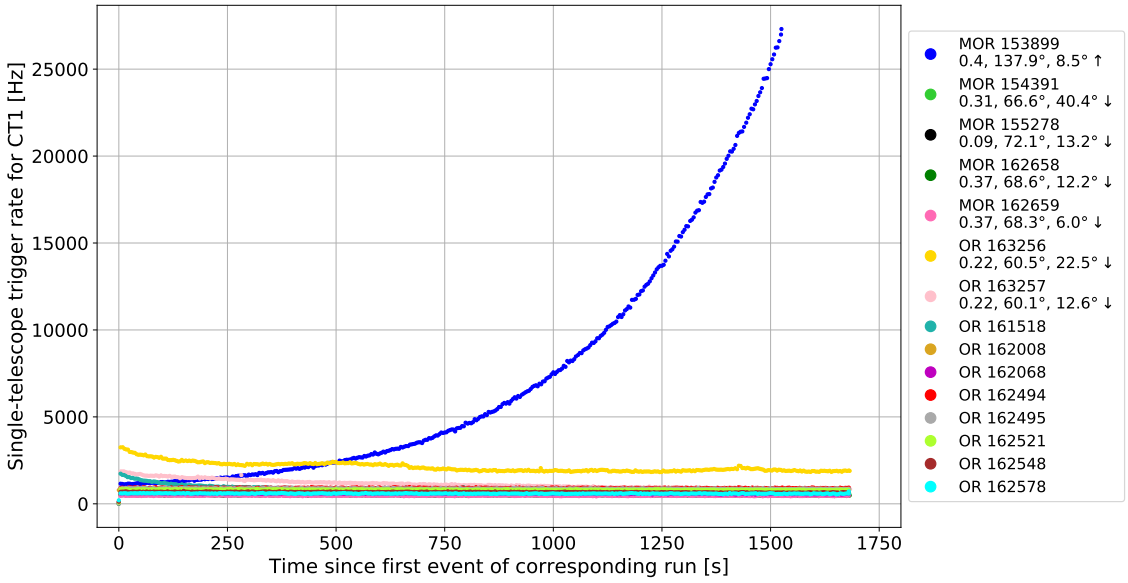

Figure 32: Single-telescope trigger rates for CT1

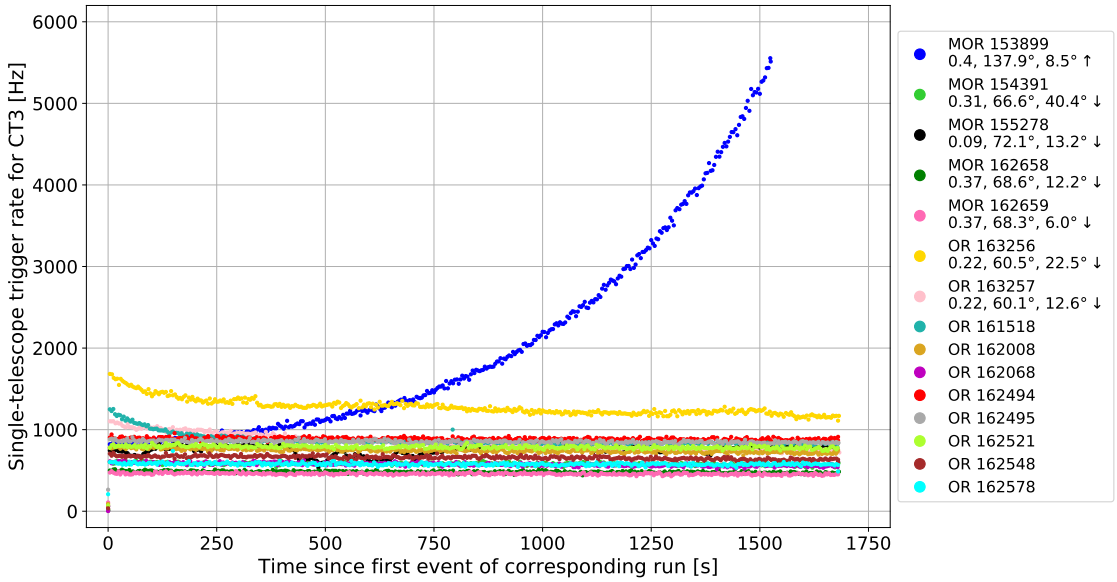

Figure 33: Single-telescope trigger rates for CT3

Run number	Mean μ [Hz]	Standard deviation σ [Hz]	Coefficient of variation σ/μ [%]	Moon fraction	NSB rate [MHz]
153899	7232.5	6868.8	95.0	0.40	192.73
154391	589.5	32.3	5.5	0.31	213.99
155278	763.1	68.5	9.0	0.09	63.11
162658	484.7	26.0	5.4	0.37	181.35
162659	462.6	21.0	4.5	0.37	128.53
163256	2110.7	294.7	14.0	0.22	188.45
163257	1119.6	251.7	22.5	0.22	161.25
161518	914.2	149.1	16.3	-	98.23
162008	752.2	19.4	2.6	-	68.94
162068	579.0	29.8	5.1	-	75.33
162494	913.8	42.6	4.7	-	88.68
162495	877.4	45.3	5.2	-	90.35
162521	808.6	39.7	4.9	-	94.03
162548	673.9	33.7	5.0	-	80.2
162578	589.6	24.3	4.1	-	74.21

Table 14: Statistical parameters for the single-telescope trigger rates of CT1

Run number	Mean μ [Hz]	Standard deviation σ [Hz]	Coefficient of variation σ/μ [%]	Moon fraction	NSB rate [MHz]
153899	2026.8	1268.0	62.6	0.40	193.19
154391	579.7	31.4	5.4	0.31	214.44
155278	752.9	67.6	9.0	0.09	65.03
162658	479.1	25.6	5.3	0.37	183.97
162659	457.8	20.4	4.5	0.37	130.98
163256	1274.8	114.9	9.0	0.22	190.63
163257	840.2	103.4	12.3	0.22	164.01
161518	869.3	85.4	9.8	-	100.25
162008	741.1	38.7	5.2	-	70.9
162068	573.3	33.9	5.9	-	77.8
162494	885.7	43.4	4.9	-	89.87
162495	850.4	33.5	3.9	-	91.41
162521	784.9	38.8	4.9	-	95.89
162548	656.5	36.5	5.6	-	81.71
162578	577.0	24.2	4.2	-	76.09

Table 15: Statistical parameters for the single-telescope trigger rates of CT3

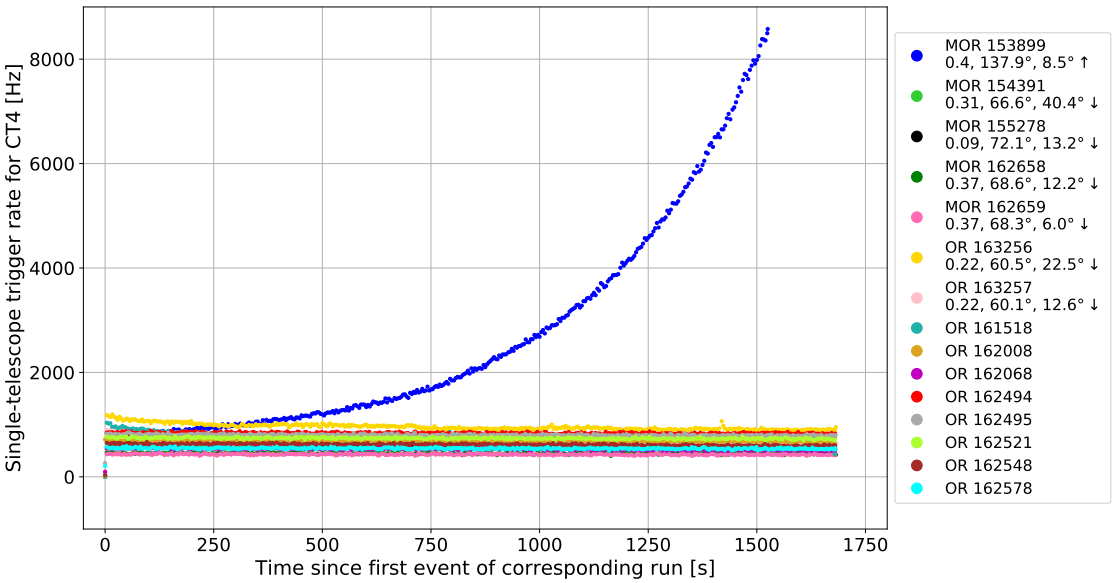

Figure 34: Single-telescope trigger rates for CT4

Run number	Mean μ [Hz]	Standard deviation σ [Hz]	Coefficient of variation σ/μ [%]	Moon fraction	NSB rate [MHz]
153899	2648.1	2050.3	77.4	0.40	198.29
154391	546.2	31.5	5.8	0.31	214.95
155278	702.7	61.4	8.7	0.09	63.71
162658	445.1	24.5	5.5	0.37	175.61
162659	429.5	19.8	4.6	0.37	125.08
163256	955.1	75.0	7.9	0.22	179.86
163257	711.5	62.4	8.8	0.22	154.45
161518	799.5	61.3	7.7	-	96.33
162008	688.4	18.0	2.6	-	67.57
162068	530.9	27.3	5.1	-	74.40
162494	833.9	43.0	5.2	-	86.73
162495	799.3	30.7	3.8	-	88.38
162521	736.9	37.9	5.1	-	91.97
162548	615.2	33.5	5.5	-	78.51
162578	543.2	21.3	3.9	-	73.21

Table 16: Statistical parameters for the single-telescope trigger rates of CT4

Array trigger rates for the moon being around horizon

The legend contains the run number, the mean moon fraction, the mean angle of separation and the target name.

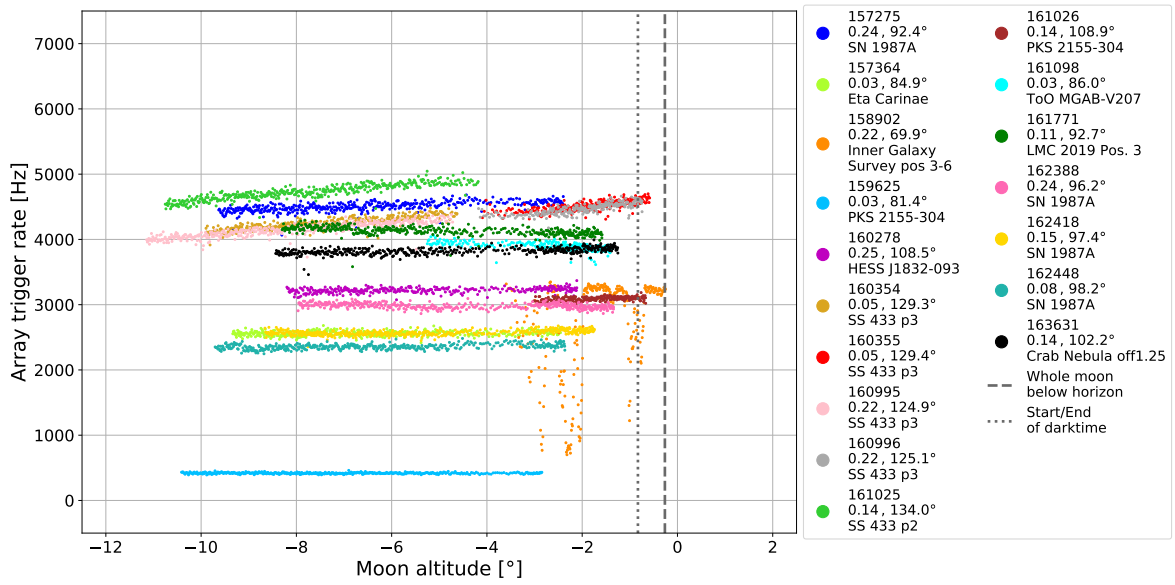

Figure 35: Array trigger rates for runs with a rising moon and a mean moon fraction between 0 % and 25 %

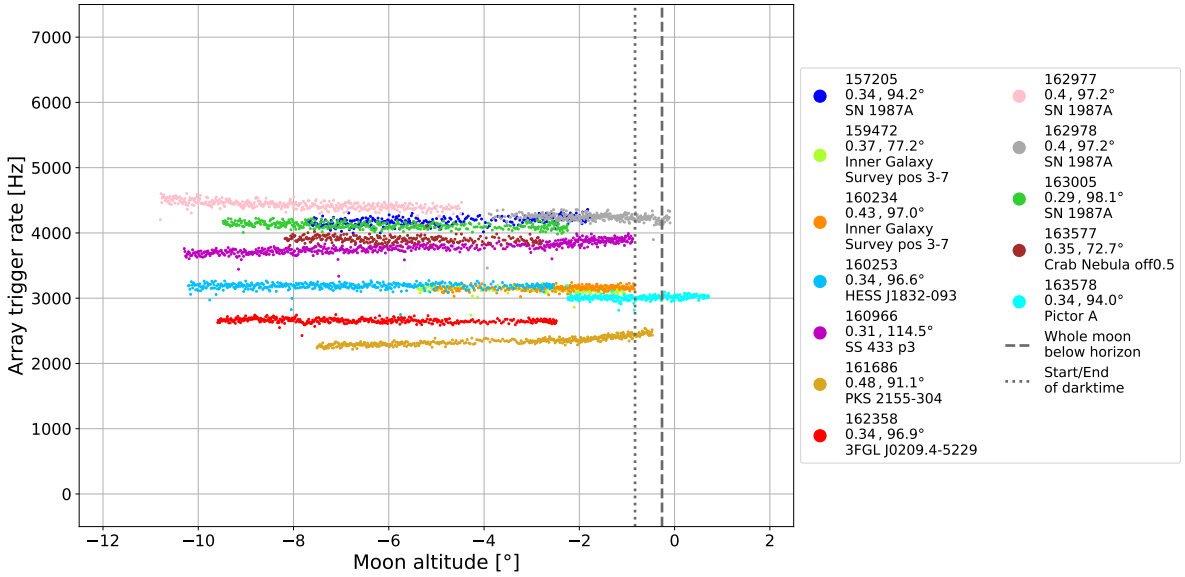

Figure 36: Array trigger rates for runs with a rising moon and a mean moon fraction between 25 % and 50 %

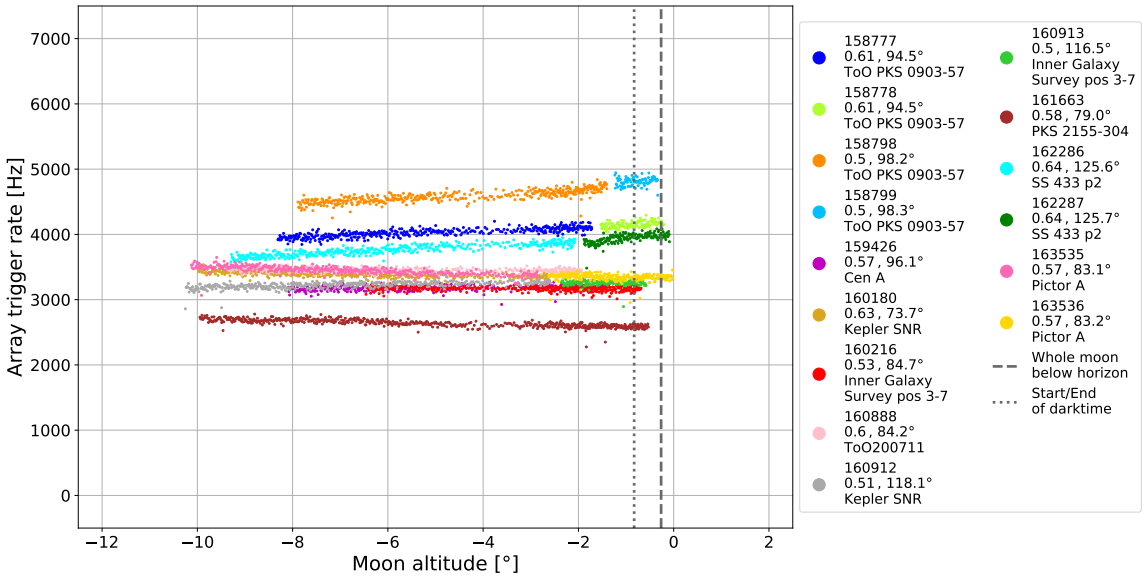

Figure 37: Array trigger rates for runs with a rising moon and a mean moon fraction between 50 % and 65 %

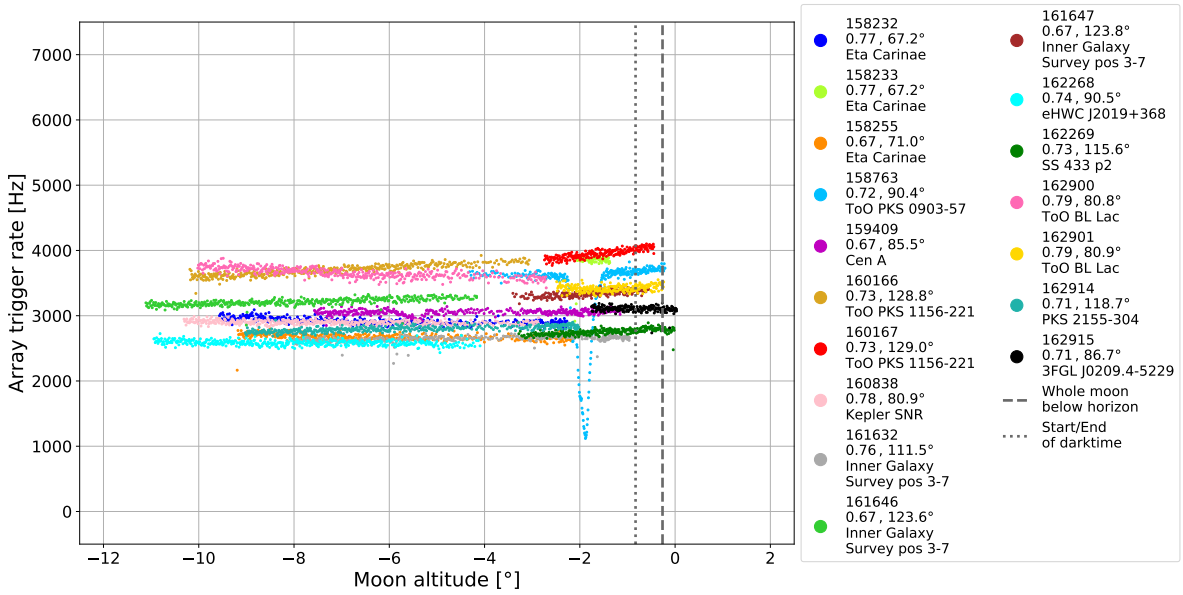

Figure 38: Array trigger rates for runs with a rising moon and a mean moon fraction between 65 % and 80 %

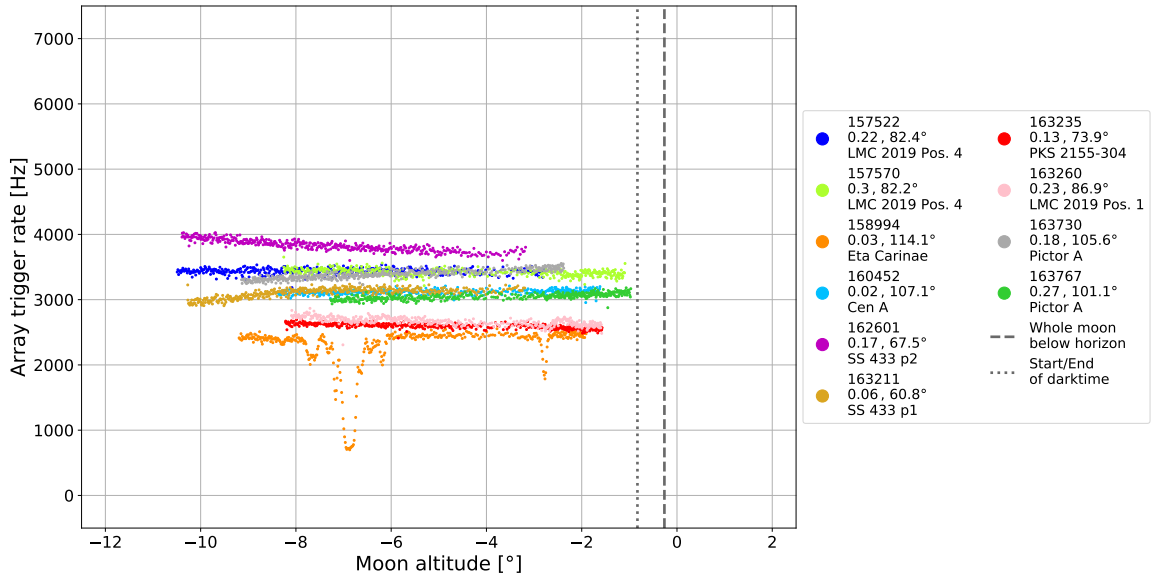

Figure 39: Array trigger rates for runs with a setting moon and a mean moon fraction between 0 % and 33.33 %

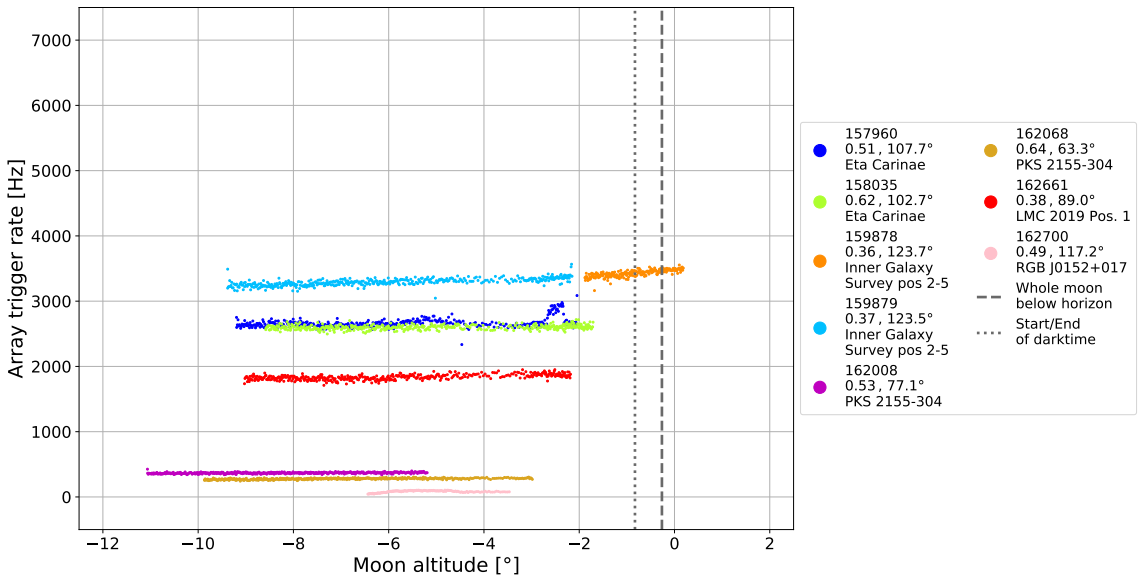

Figure 40: Array trigger rates for runs with a setting moon and a mean moon fraction between 33.33 % and 66.66 %

Single-telescope trigger rates for the moon being around horizon

The legend contains the run number, the mean moon fraction, the mean angle of separation and the target name.

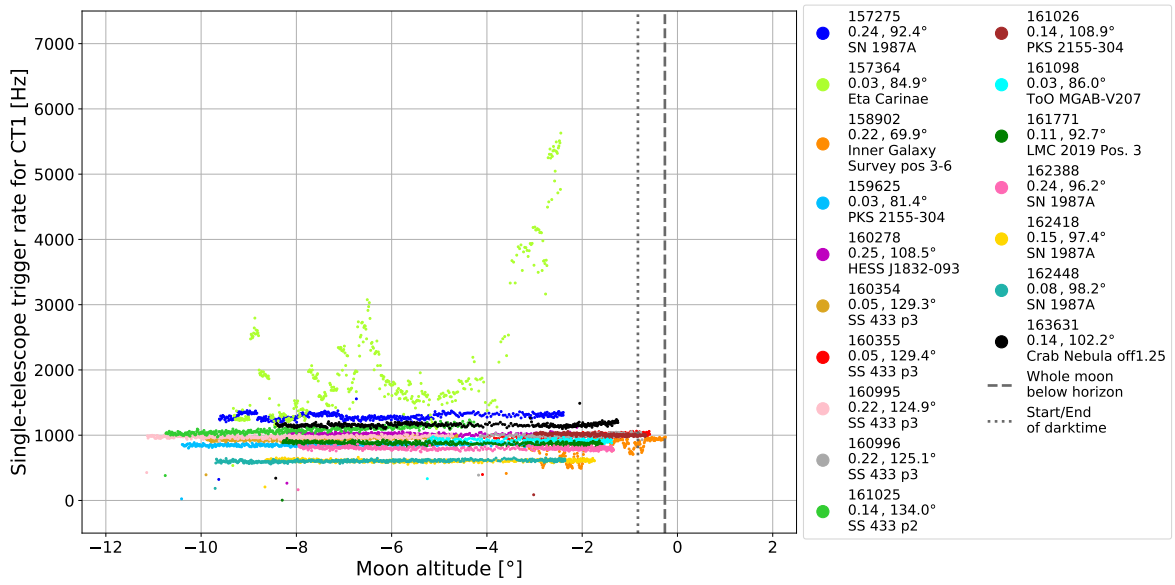

Figure 41: Single-telescope trigger rates (CT1) for runs with a rising moon and a mean moon fraction between 0 % and 25 %

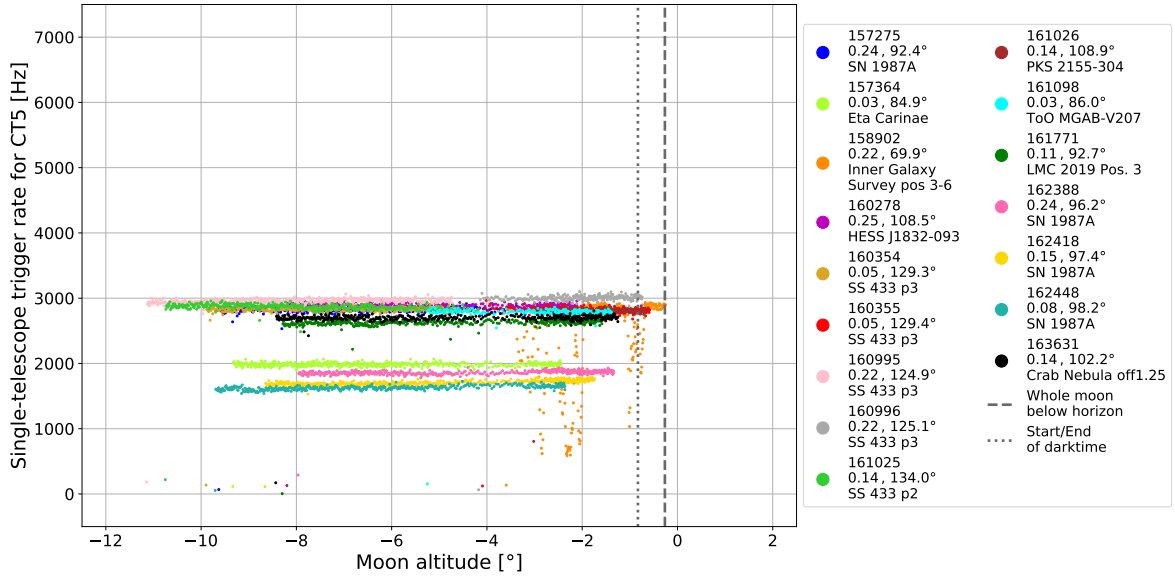

Figure 42: Single-telescope trigger rates (CT5) for runs with a rising moon and a mean moon fraction between 0 % and 25 %

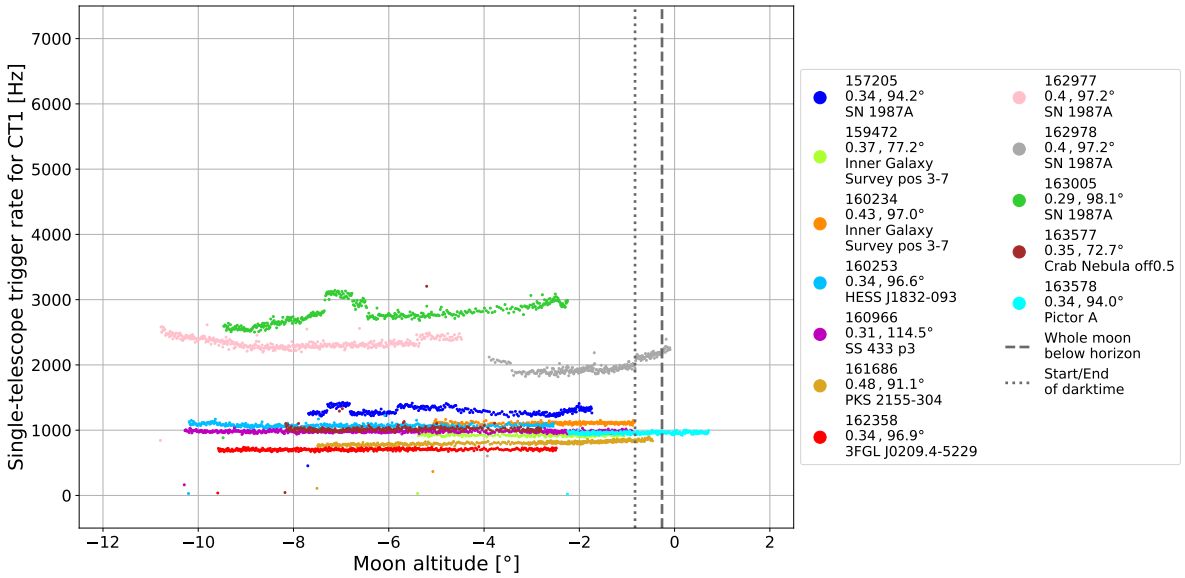

Figure 43: Single-telescope trigger rates (CT1) for runs with a rising moon and a mean moon fraction between 25 % and 50 %

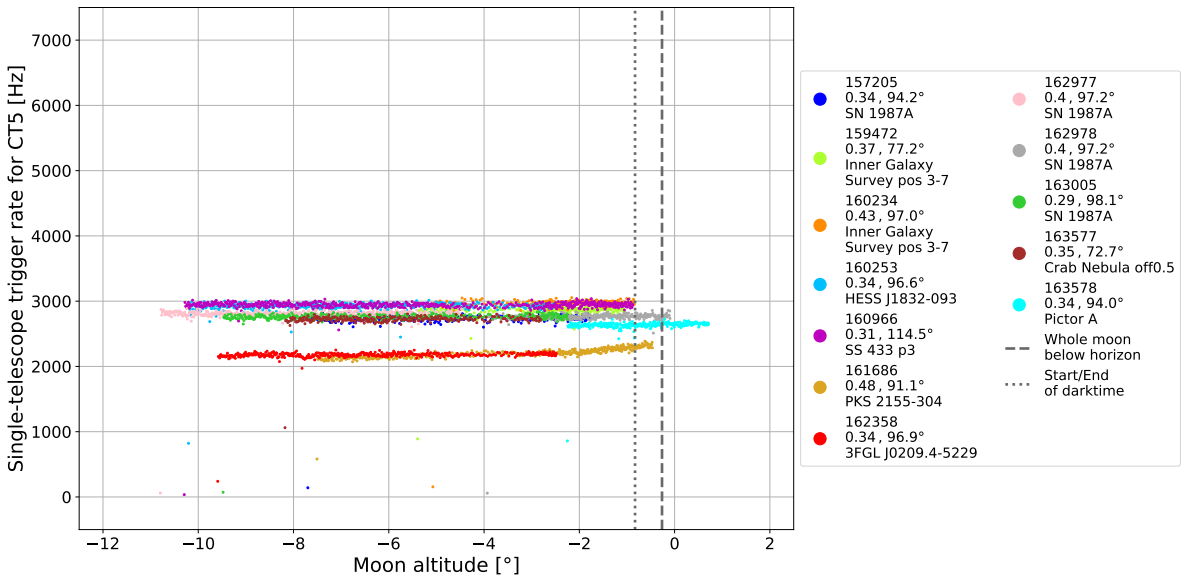

Figure 44: Single-telescope trigger rates (CT5) for runs with a rising moon and a mean moon fraction between 25 % and 50 %

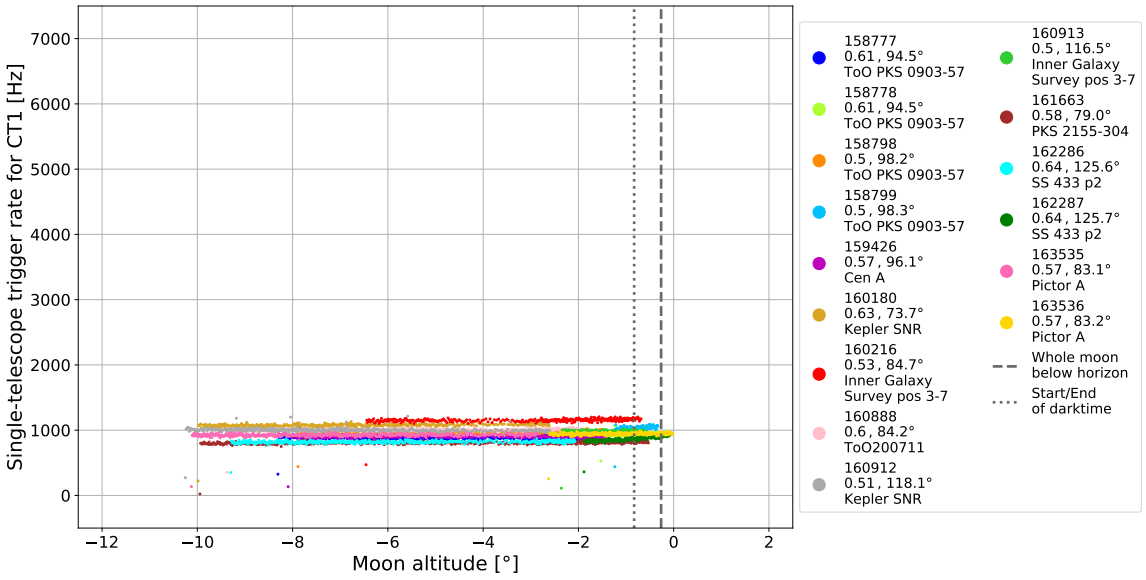

Figure 45: Single-telescope trigger rates (CT1) for runs with a rising moon and a mean moon fraction between 50 % and 65 %

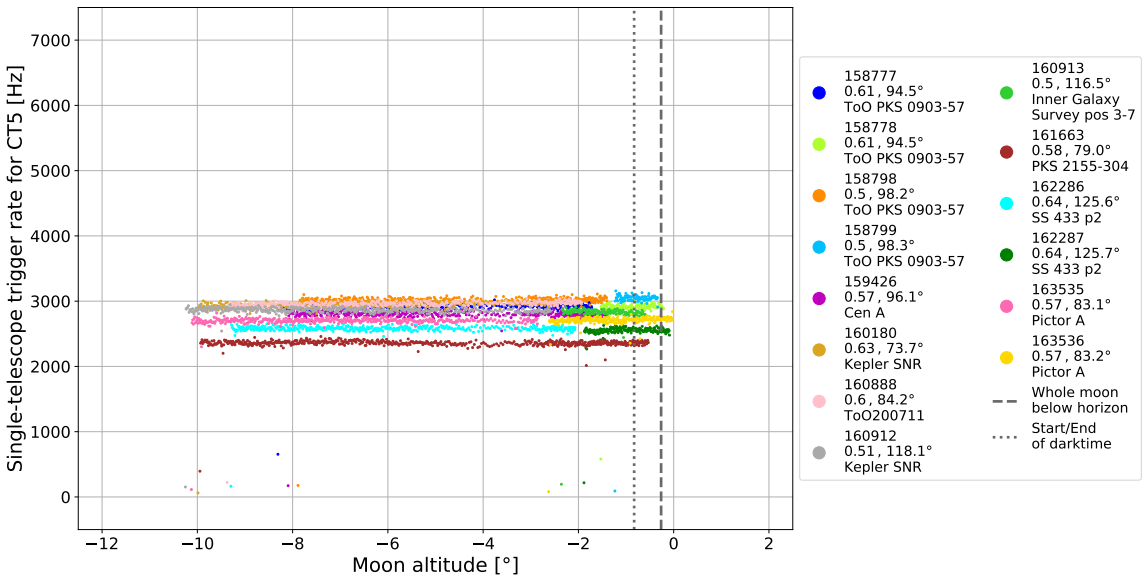

Figure 46: Single-telescope trigger rates (CT5) for runs with a rising moon and a mean moon fraction between 50 % and 65 %

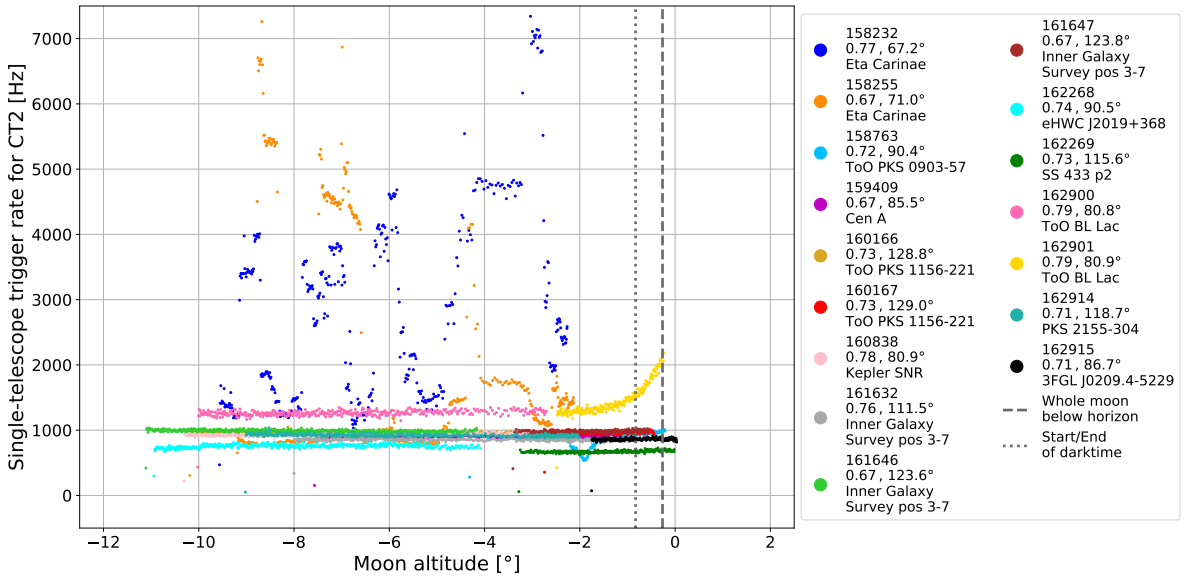

Figure 47: Single-telescope trigger rates (CT2) for runs with a rising moon and a mean moon fraction between 65 % and 80 %

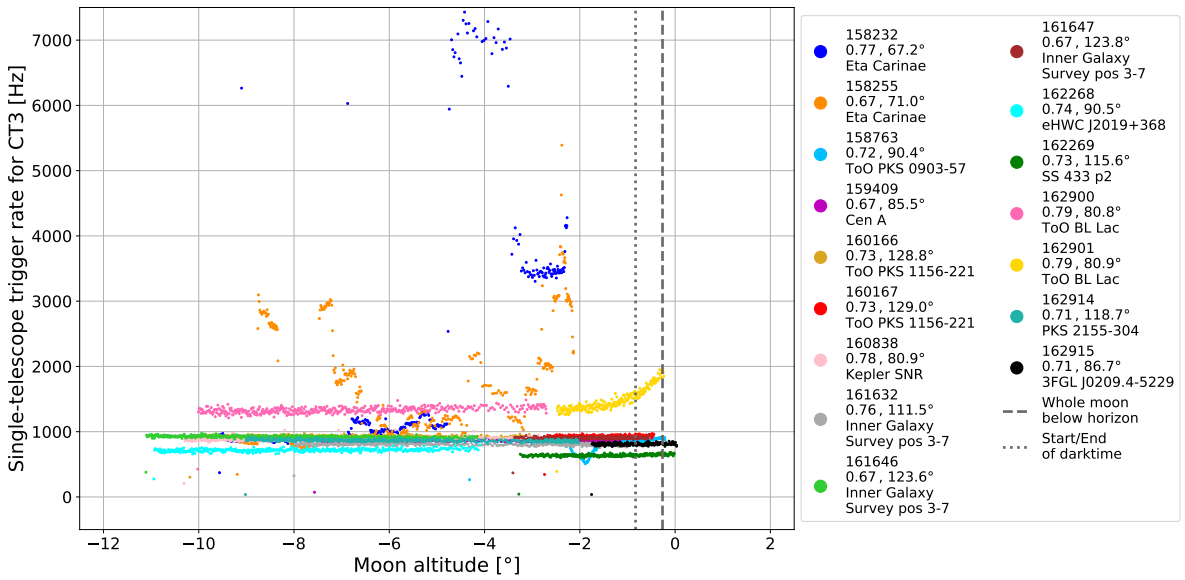

Figure 48: Single-telescope trigger rates (CT3) for runs with a rising moon and a mean moon fraction between 65 % and 80 %

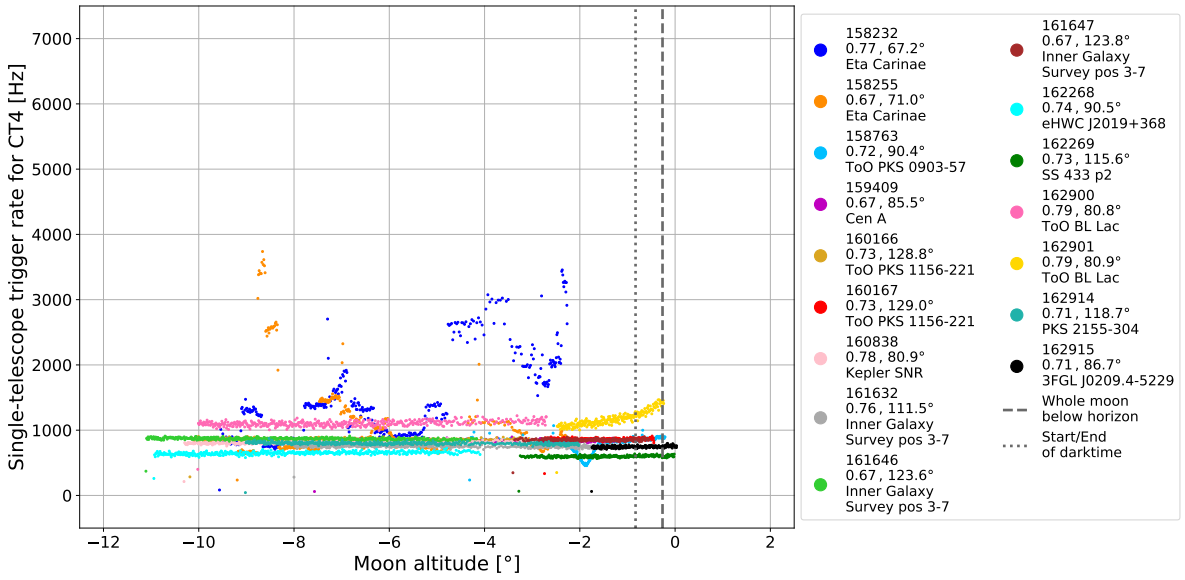

Figure 49: Single-telescope trigger rates (CT4) for runs with a rising moon and a mean moon fraction between 65 % and 80 %

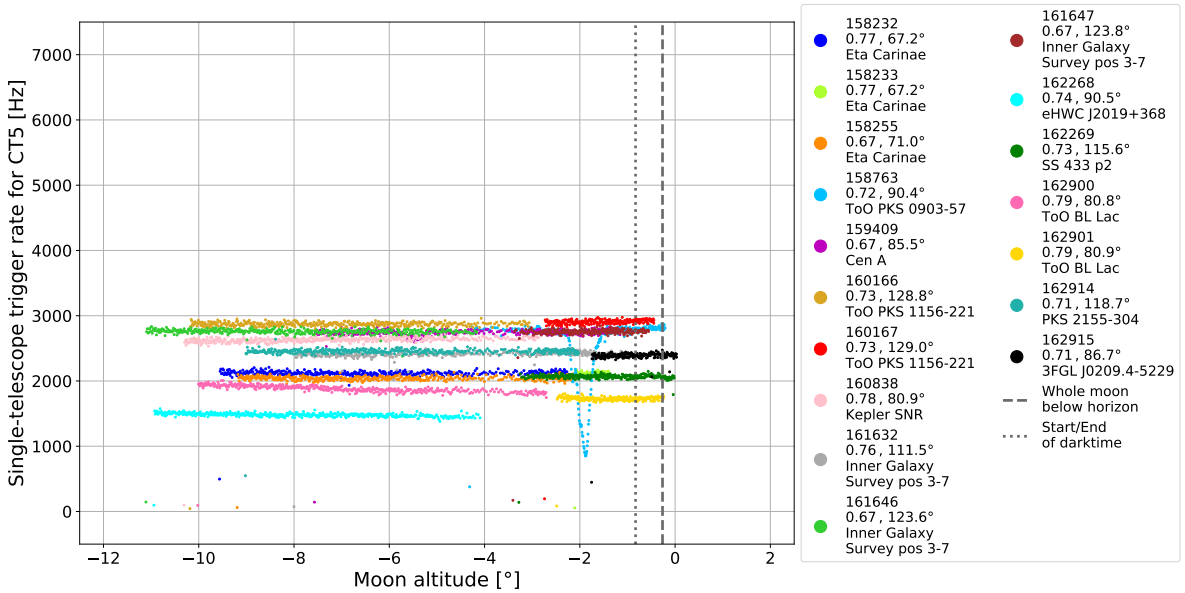

Figure 50: Single-telescope trigger rates (CT5) for runs with a rising moon and a mean moon fraction between 65 % and 80 %

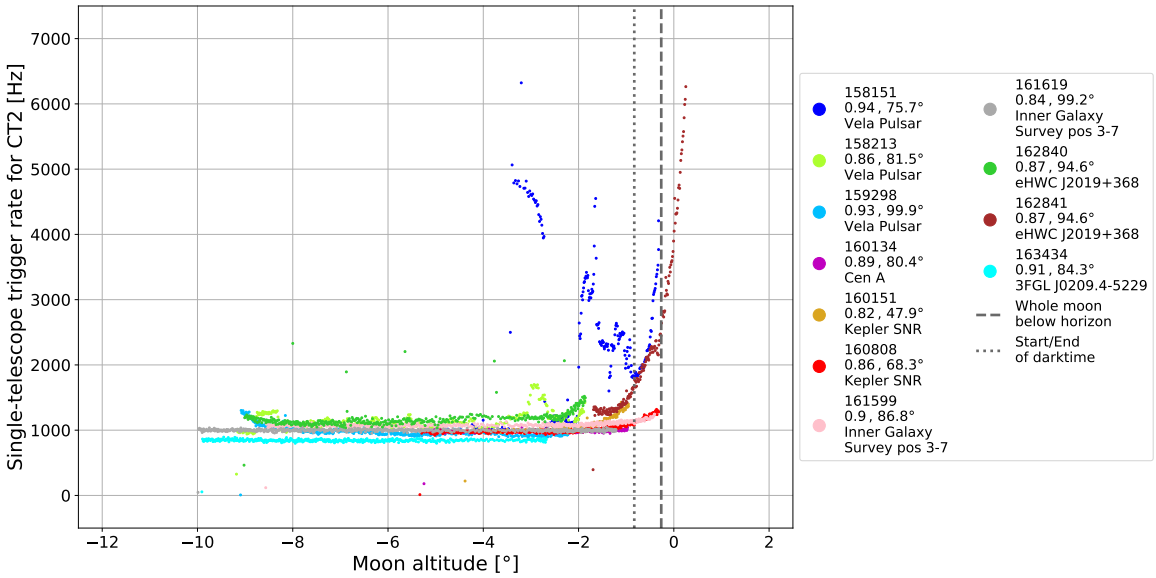

Figure 51: Single-telescope trigger rates (CT2) for runs with a rising moon and a mean moon fraction between 80 % and 100 %

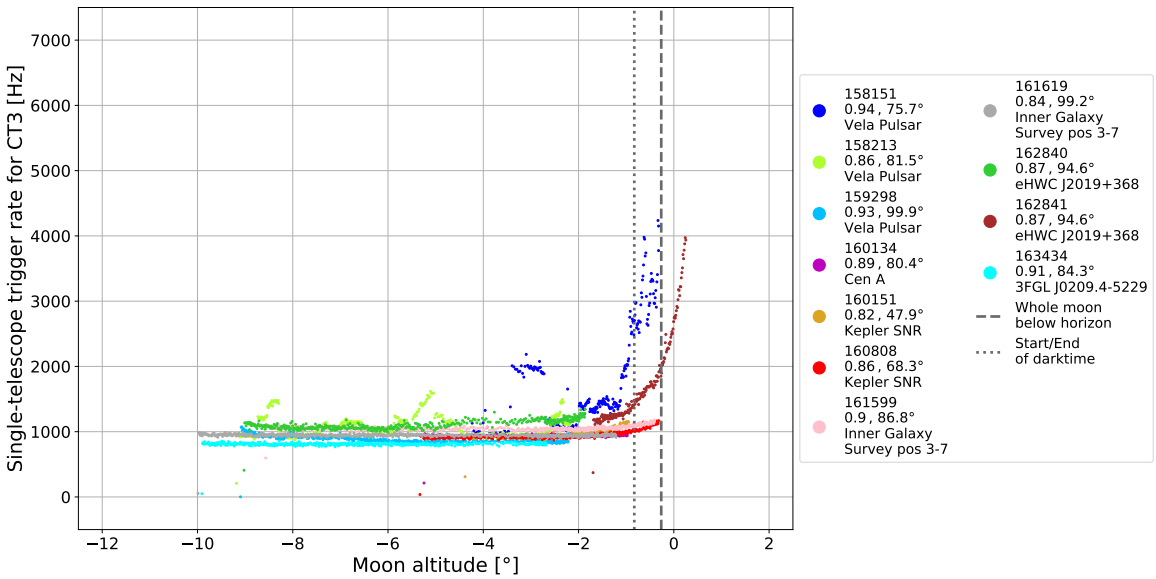

Figure 52: Single-telescope trigger rates (CT3) for runs with a rising moon and a mean moon fraction between 80 % and 100 %

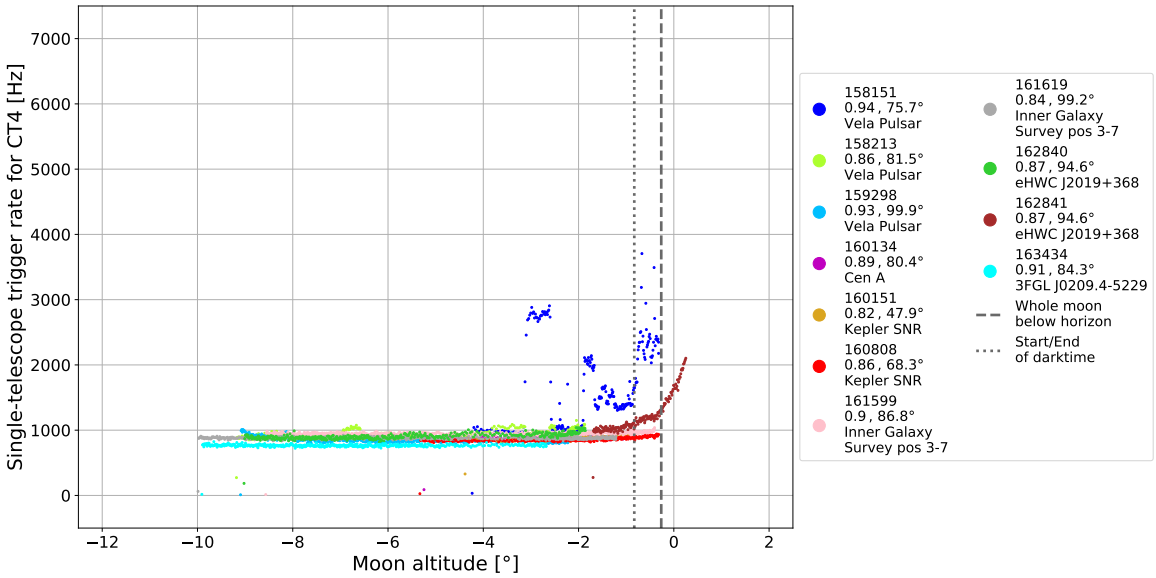

Figure 53: Single-telescope trigger rates (CT4) for runs with a rising moon and a mean moon fraction between 80 % and 100 %

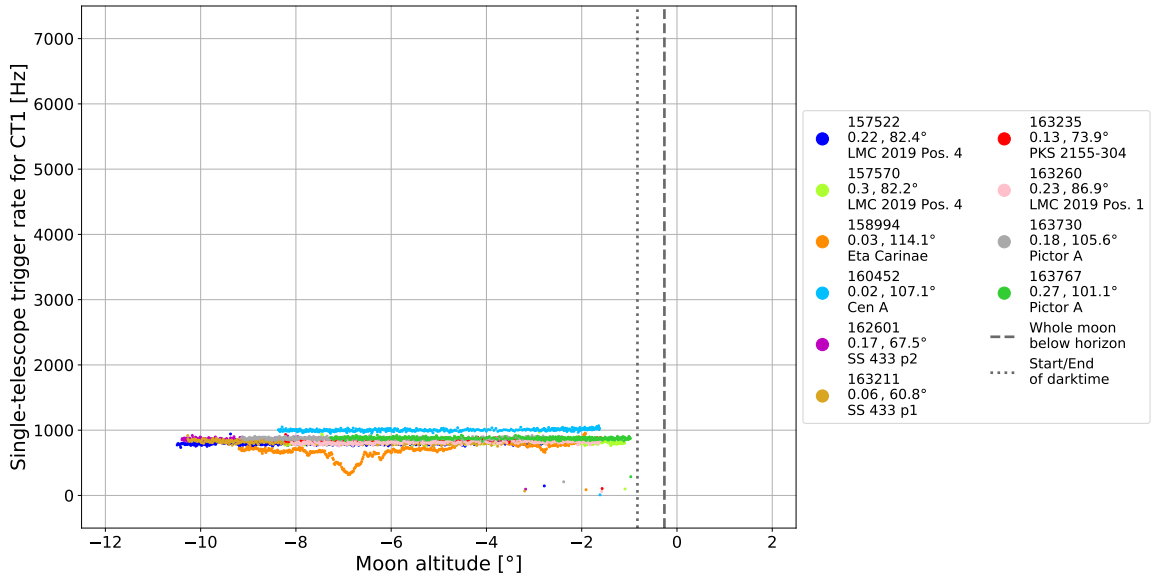

Figure 54: Single-telescope trigger rates (CT1) for runs with a setting moon and a mean moon fraction between 0 % and 33.33 %

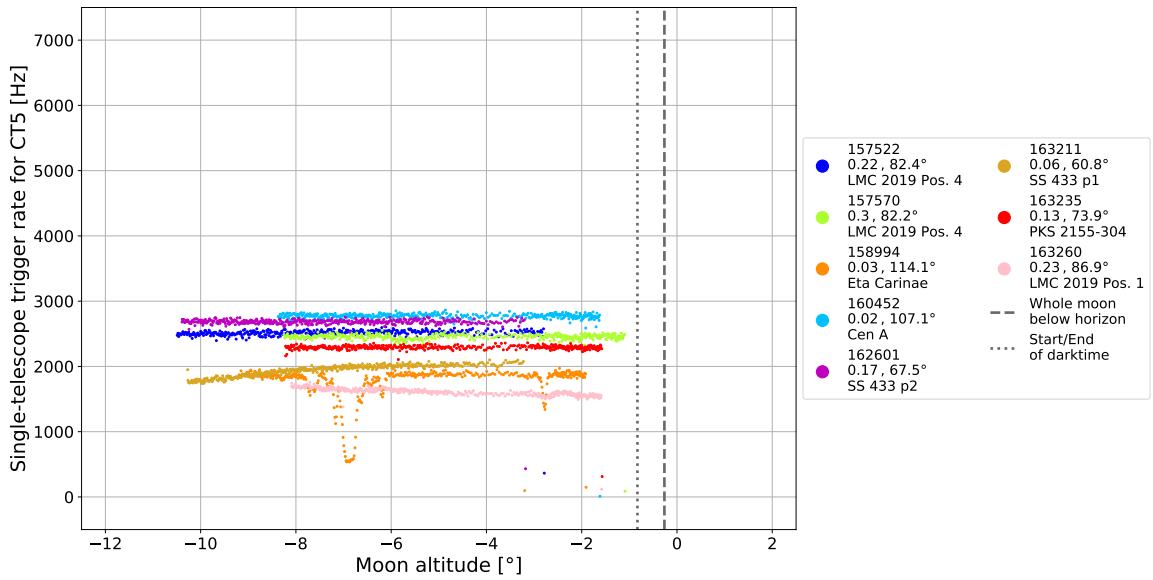

Figure 55: Single-telescope trigger rates (CT5) for runs with a setting moon and a mean moon fraction between 0 % and 33.33 %

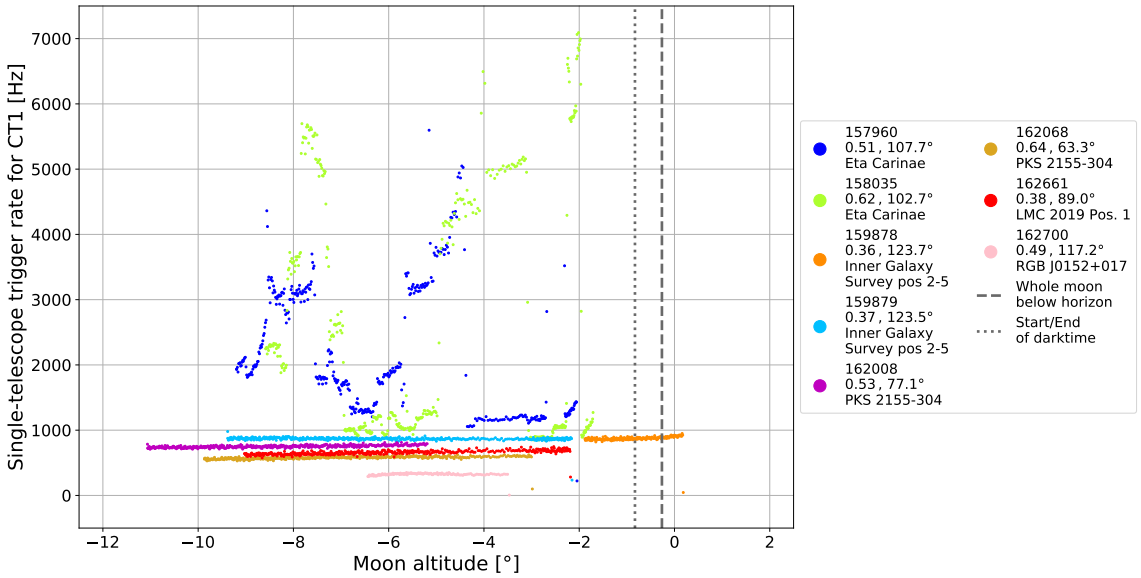

Figure 56: Single-telescope trigger rates (CT1) for runs with a setting moon and a mean moon fraction between 33.33 % and 66.66 %

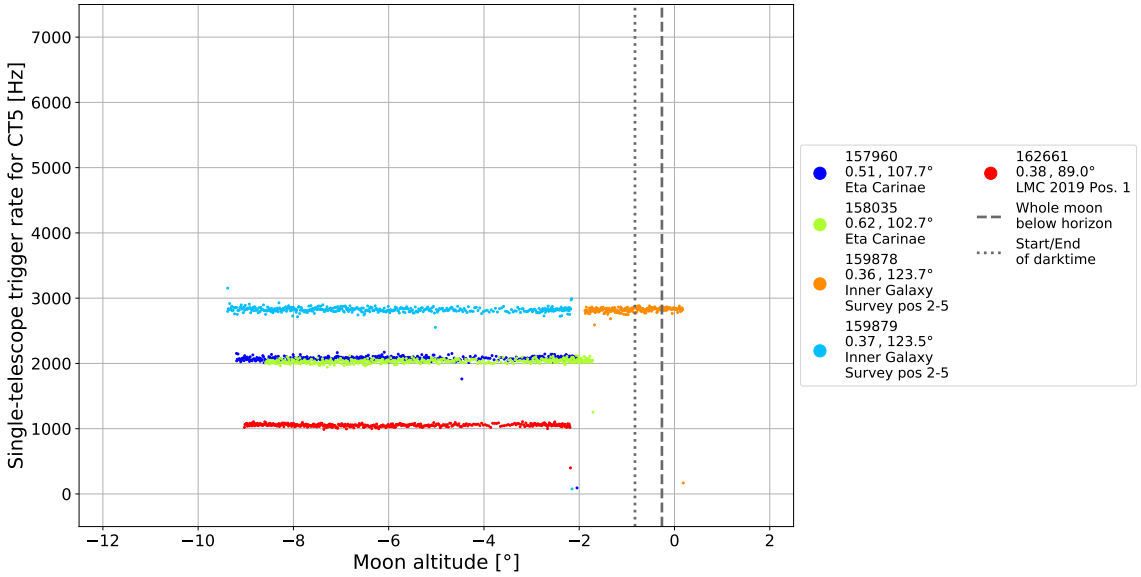

Figure 57: Single-telescope trigger rates (CT5) for runs with a setting moon and a mean moon fraction between 33.33 % and 66.66 %

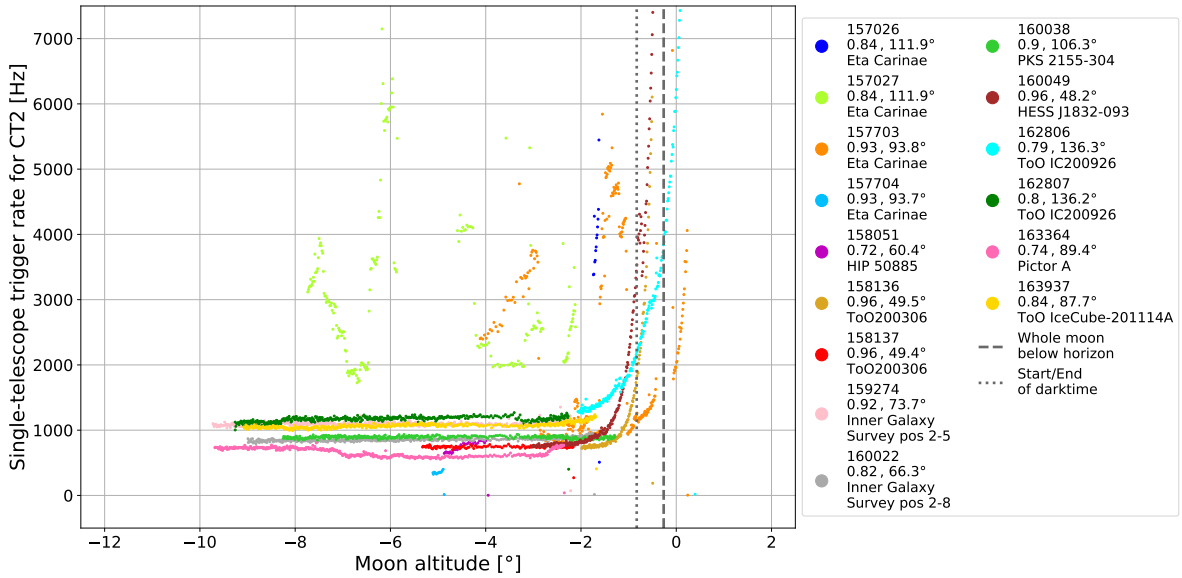

Figure 58: Single-telescope trigger rates (CT2) for runs with a setting moon and a mean moon fraction between 66.66 % and 100 %

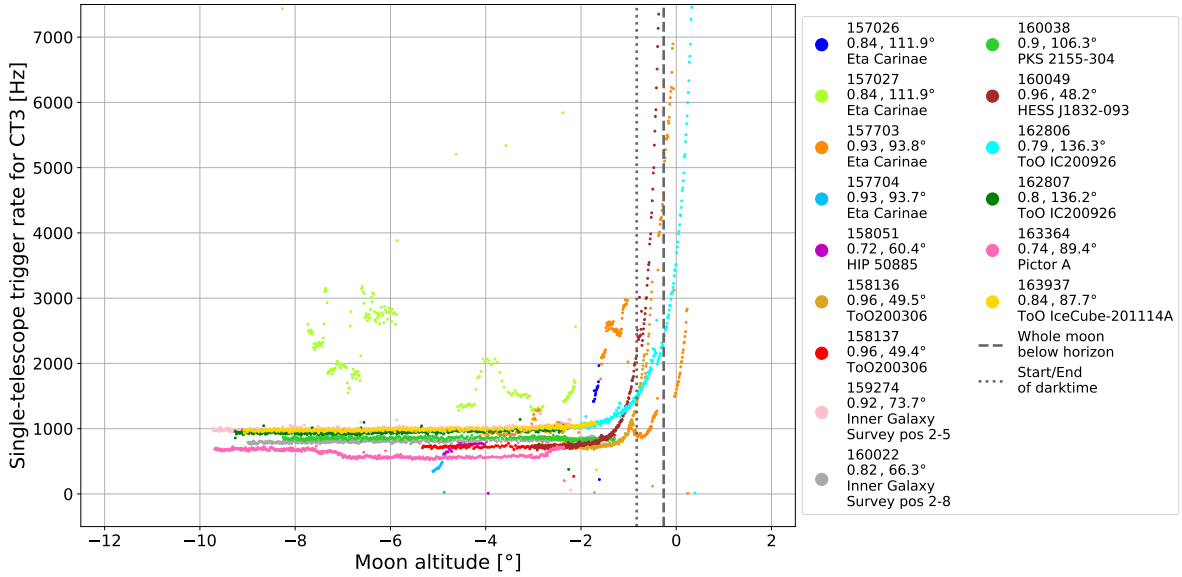

Figure 59: Single-telescope trigger rates (CT3) for runs with a setting moon and a mean moon fraction between 66.66 % and 100 %

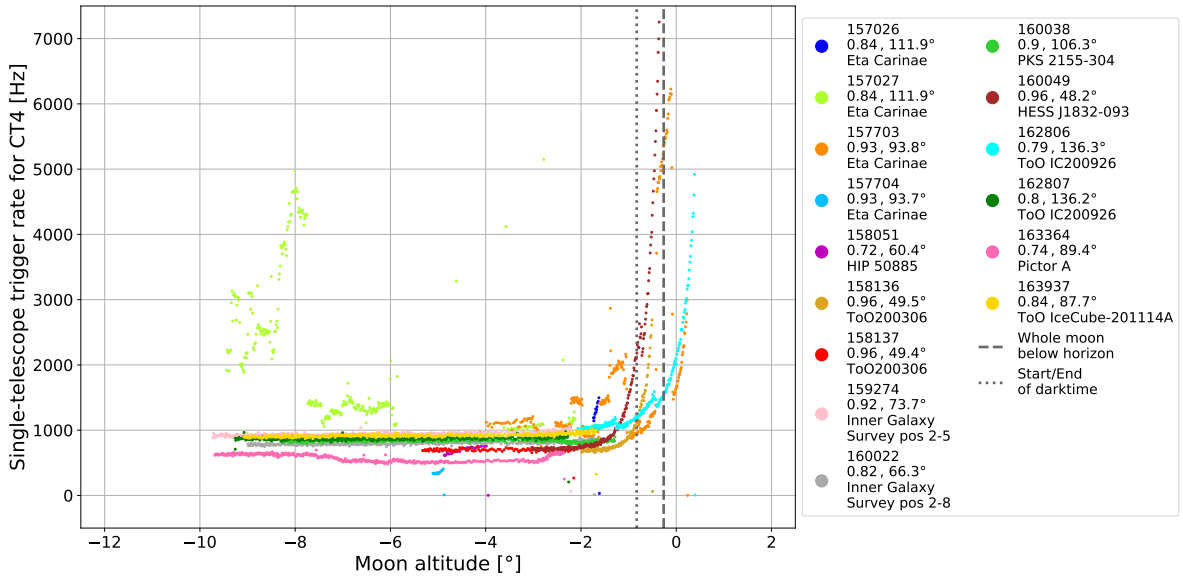

Figure 60: Single-telescope trigger rates (CT4) for runs with a setting moon and a mean moon fraction between 66.66 % and 100 %

Hillas parameters

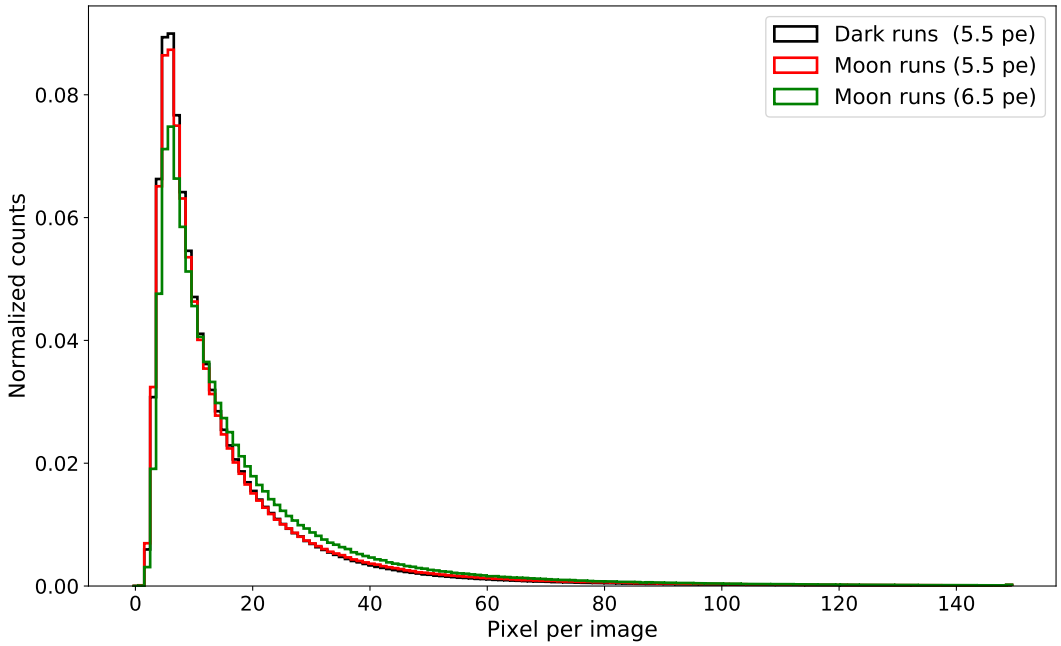

Figure 61: Distribution of the pixels per image for CT1-4

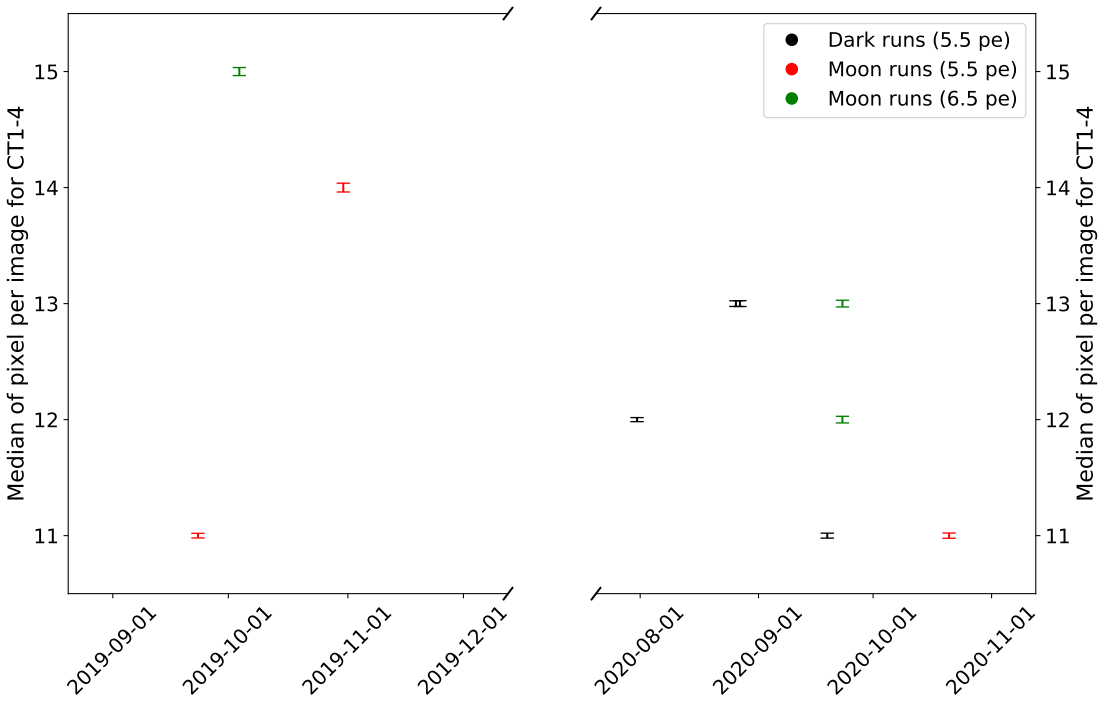

Figure 62: Pixels per image per run over time for CT1-4

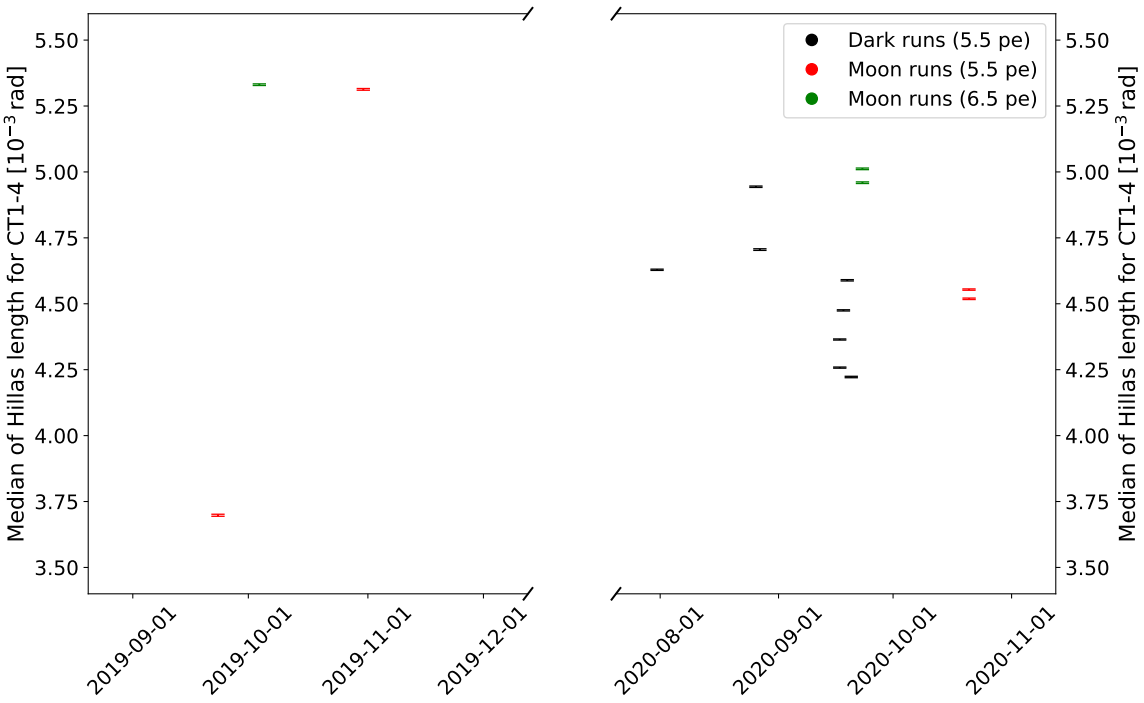

Figure 63: Hillas length per run over time for CT1-4

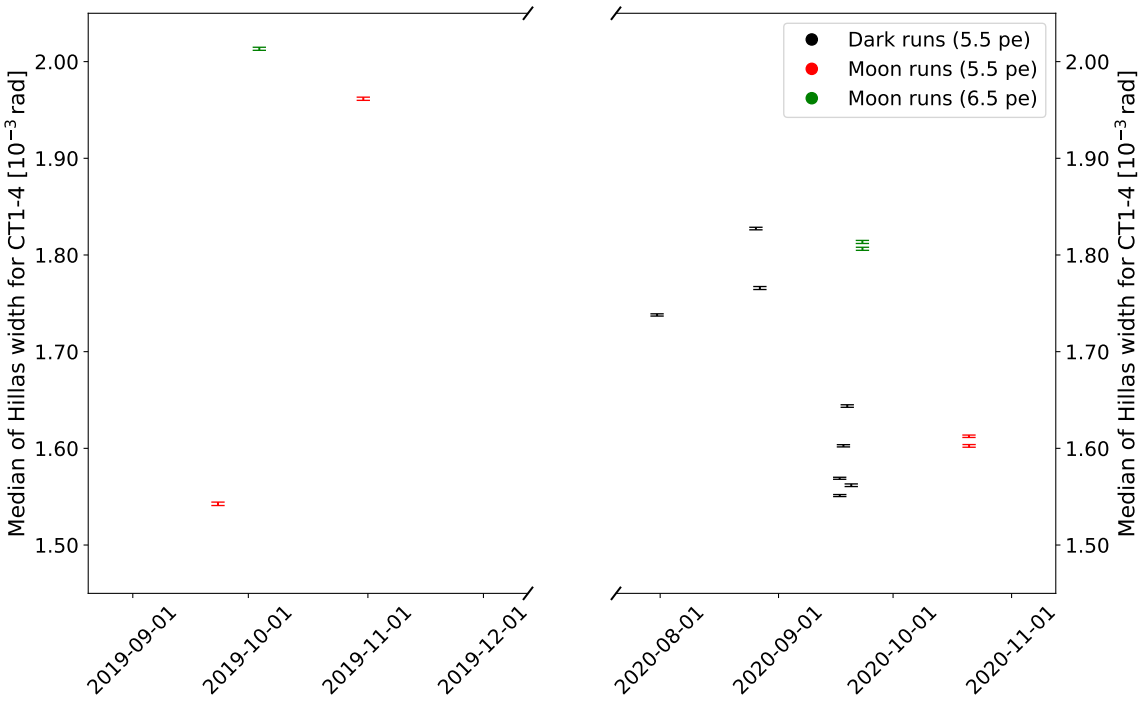

Figure 64: Hillas width per run over time for CT1-4

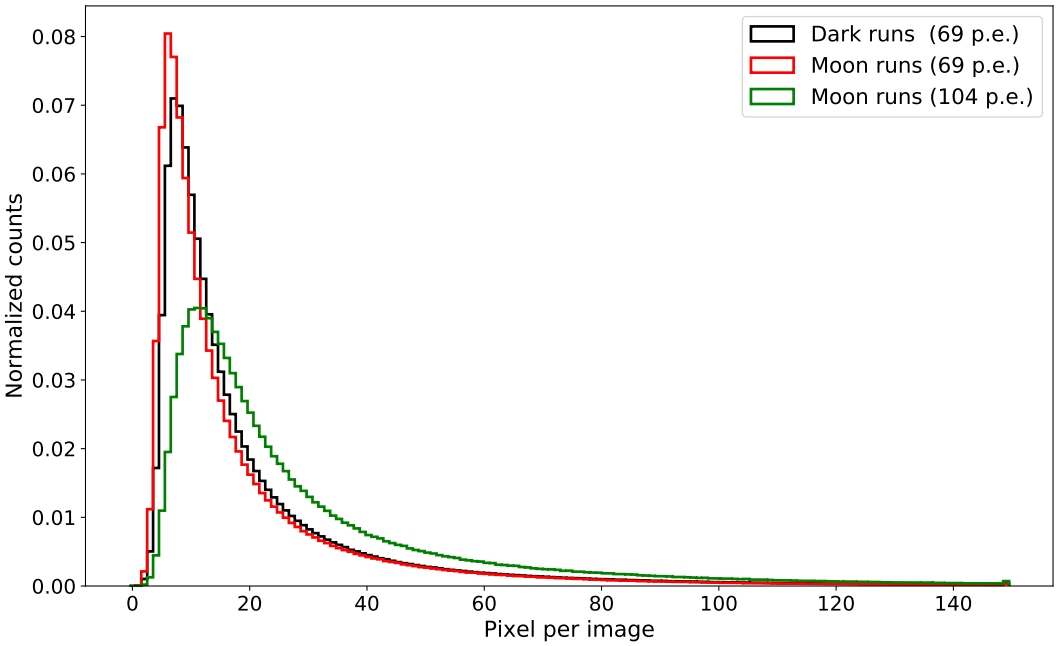

Figure 65: Distribution of the pixels per image for CT5

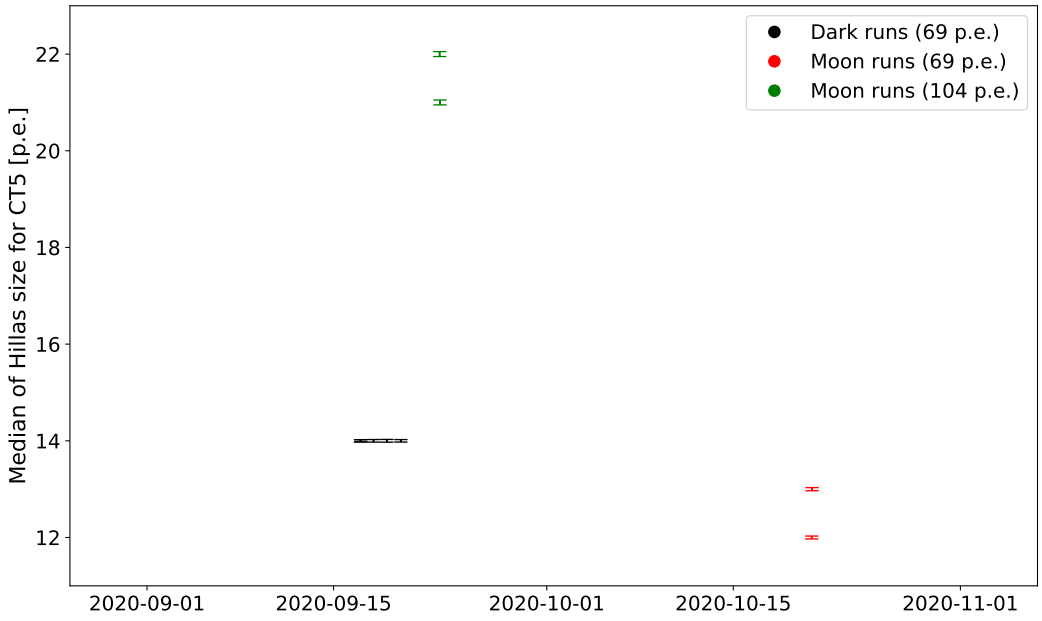

Figure 66: Pixels per image per run over time for CT5

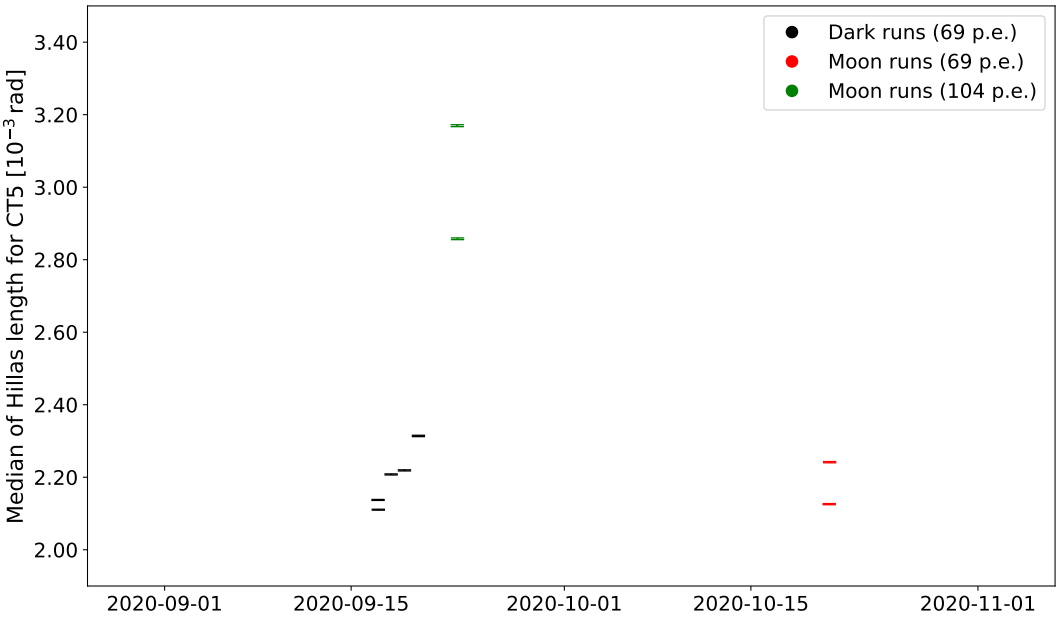

Figure 67: Hillas length per run over time for CT5

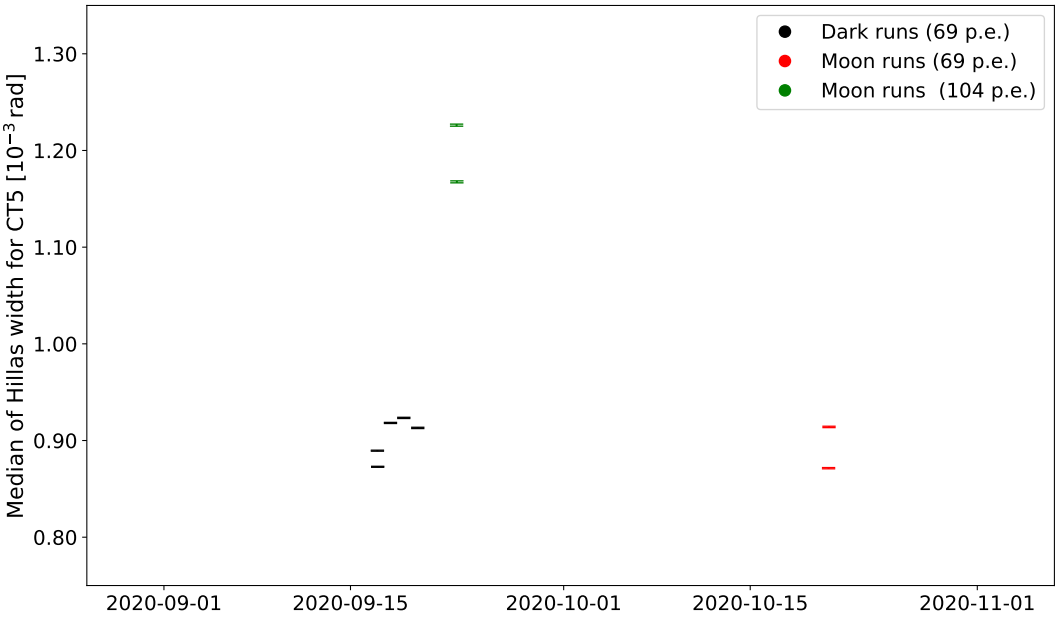

Figure 68: Hillas width per run over time for CT5

NSB dependency

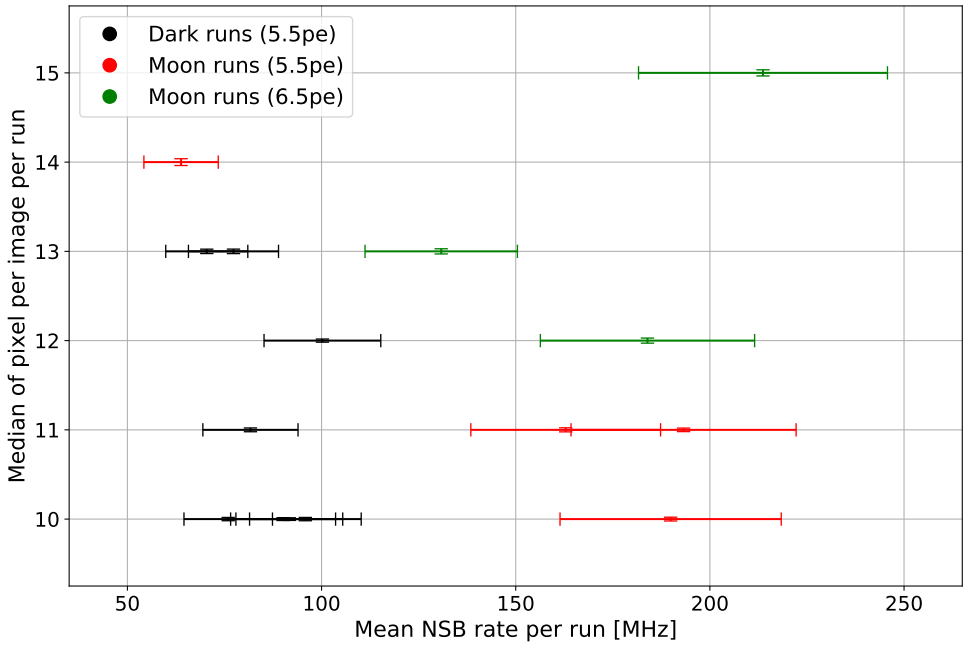

Figure 69: NSB dependency of the pixels per image per run for CT5

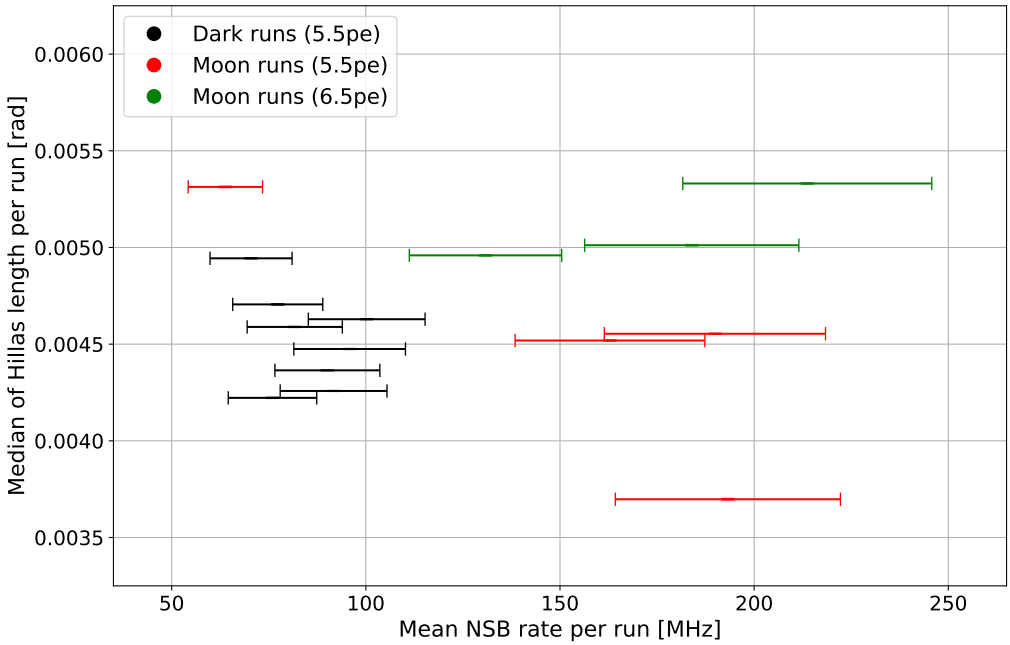

Figure 70: NSB dependency of the Hillas length per run for CT1-4

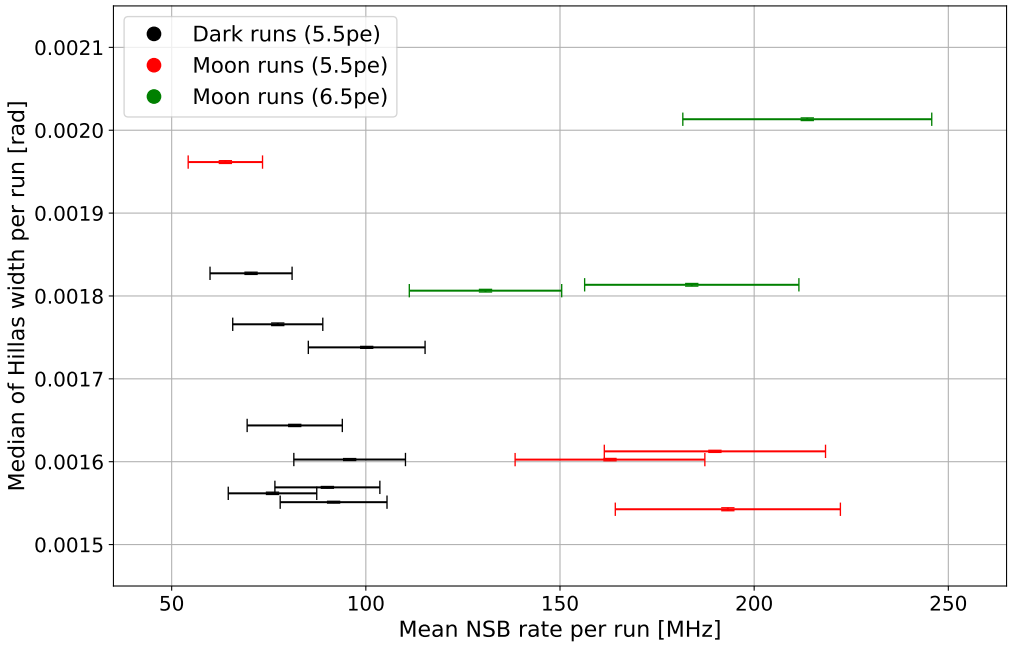

Figure 71: NSB dependency of the Hillas width per run for CT1-4

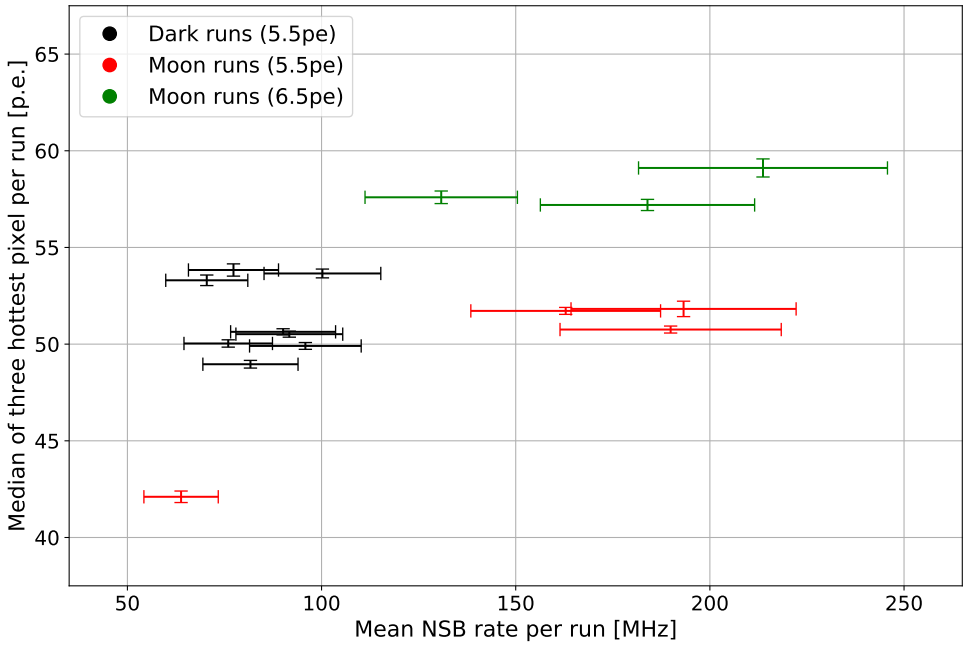

Figure 72: NSB dependency of the three hottest pixels per image per run for CT1-4

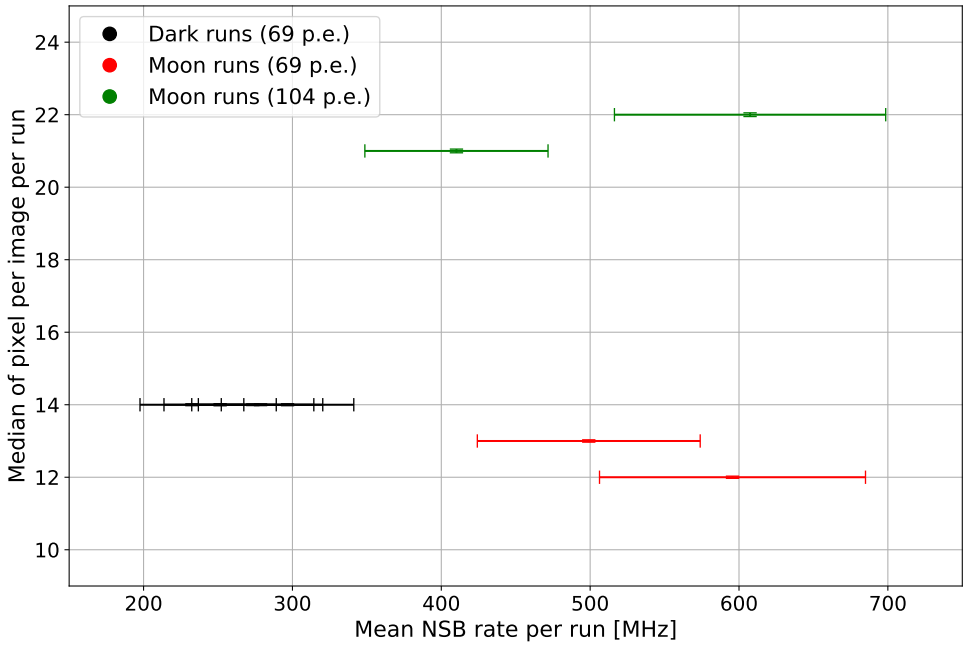

Figure 73: NSB dependency of the pixels per image per run for CT5

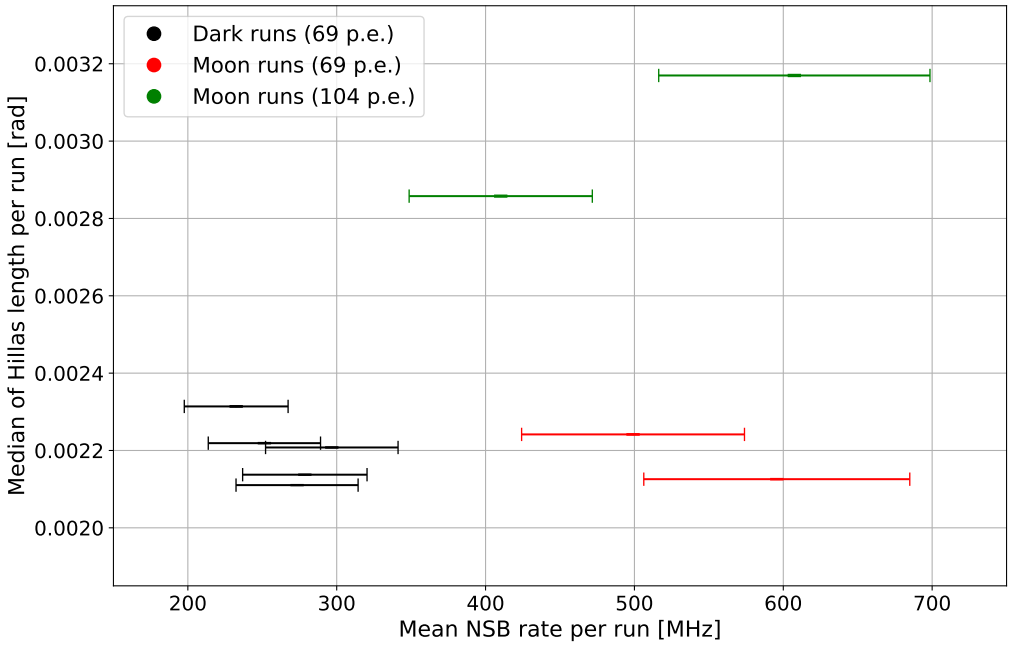

Figure 74: NSB dependency of the Hillas length per run for CT5

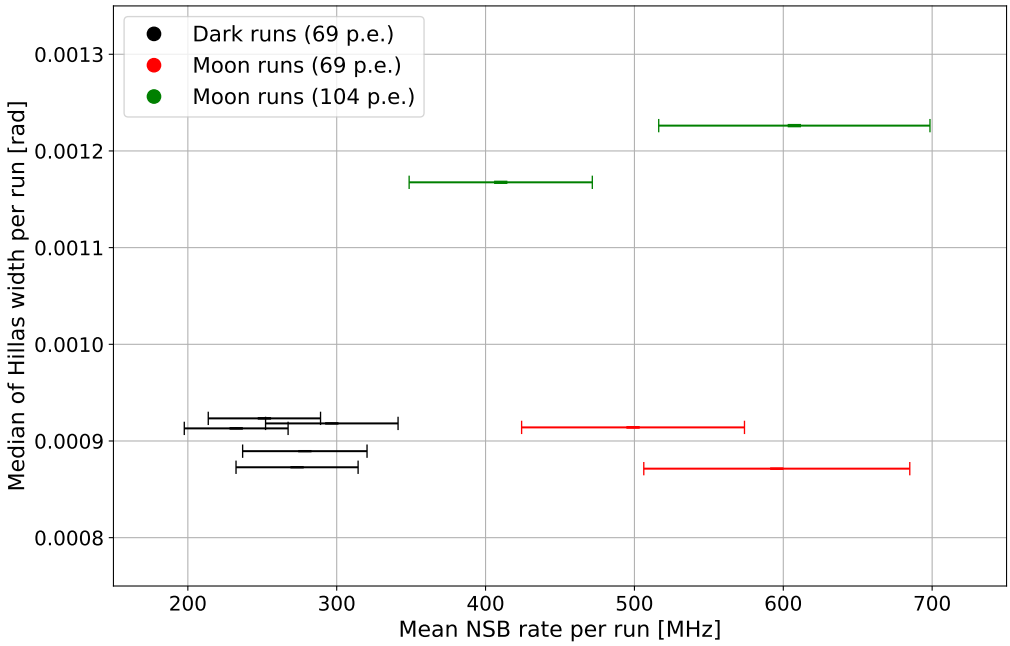

Figure 75: NSB dependency of the Hillas width per run for CT5

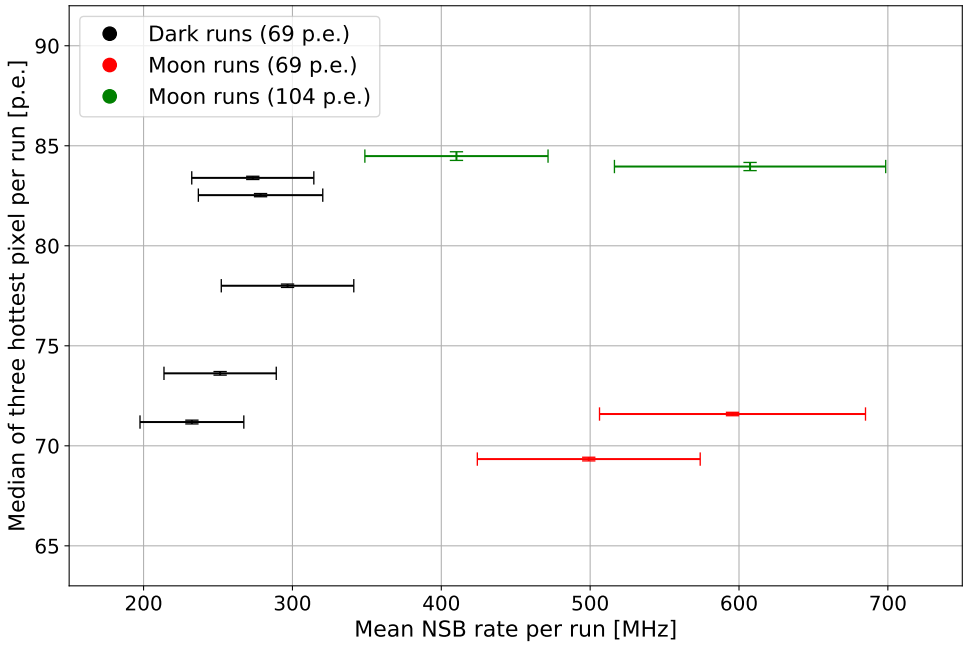

Figure 76: NSB dependency of the three hottest pixels per image per run for CT5

References

[1] T. Ashton et al. "A NECTAr-based upgrade for the Cherenkov cameras of the H.E.S.S. 12-meter telescopes". In: *Astroparticle Physics* 118 (2020), p. 102425. ISSN: 0927-6505. DOI: 10.1016/j.astropartphys.2019.102425. URL: http://dx.doi.org/10.1016/j.astropartphys.2019.102425.

[2] Bernard Degrange and Gérard Fontaine. "Introduction to high-energy gamma-ray astronomy". In: *Comptes Rendus Physique* 16.6-7 (2015), 587–599. ISSN: 1631-0705. DOI: 10.1016/j.crhy.2015.07.003. URL: http://dx.doi.org/10.1016/j.crhy.2015.07.003.

[3] E. Lorenz and R. Wagner. "Very-high energy gamma-ray astronomy". In: *The European Physical Journal H* 37.3 (2012), 459–513. ISSN: 2102-6467. DOI: 10.1140/epjh/e2012-30016-x. URL: http://dx.doi.org/10.1140/epjh/e2012-30016-x.

[4] Stefan Funk. "Ground- and Space-Based Gamma-Ray Astronomy". In: *Annual Review of Nuclear and Particle Science* 65.1 (2015), 245–277. ISSN: 1545-4134. DOI: 10.1146/annurev-nucl-102014-022036. URL: http://dx.doi.org/10.1146/annurev-nucl-102014-022036.

[5] Stefan Funk. "A new population of very high-energy γ-ray sources detected with H.E.S.S. in the inner part of the Milky Way". PhD thesis. 2005.

[6] *H.E.S.S. - The High Energy Stereoscopic System.* https://www.mpi-hd.mpg.de/hfm/HESS/.

[7] Andreas Zech and H. E. S. S. Collaboration. *News from the very-high-energy sky seen with H.E.S.S.* 2019. arXiv: 1910.08959 [astro-ph.HE].

[8] S. Funk et al. "The trigger system of the H.E.S.S. telescope array". In: *Astroparticle Physics* 22.3-4 (2004), 285–296. ISSN: 0927-6505. DOI: 10.1016/j.astropartphys.2004.08.001. URL: http://dx.doi.org/10.1016/j.astropartphys.2004.08.001.

[9] Y. Moudden et al. "The topological second-level trigger of the HESS phase 2 telescope". In: *Astroparticle Physics* 34.7 (2011), 568–574. ISSN: 0927-6505. DOI: 10.1016/j.astropartphys.2010.12.003. URL: http://dx.doi.org/10.1016/j.astropartphys.2010.12.003.

[10] F. Aharonian et al. "Observations of the Crab nebula with HESS". In: *Astronomy & Astrophysics* 457.3 (2006), 899–915. ISSN: 1432-0746. DOI: 10.1051/0004-6361:20065351. URL: http://dx.doi.org/10.1051/0004-6361:20065351.

[11] A. M. Hillas. "Cerenkov light images of EAS produced by primary gamma rays and by nuclei". In: *International Cosmic Ray Conference* 3 (1995), p. 445.

[12] M.L. Ahnen et al. "Performance of the MAGIC telescopes under moonlight". In: *Astroparticle Physics* 94 (2017), 29–41. ISSN: 0927-6505. DOI: 10.1016/j.astropartphys.2017.08.001. URL: http://dx.doi.org/10.1016/j.astropartphys.2017.08.001.

[13] S. Preuß et al. “Study of the photon flux from the night sky at La Palma and Namibia, in the wavelength region relevant for imaging atmospheric Cherenkov telescopes”. In: *Nuclear Instruments and Methods in Physics Research Section A: Accelerators, Spectrometers, Detectors and Associated Equipment* 481.1-3 (2002), 229–240. ISSN: 0168-9002. DOI: 10.1016/s0168-9002(01)01264-5. URL: http://dx.doi.org/10.1016/S0168-9002(01)01264-5.

[14] Tomoyuki Nishita et al. “Display of the Earth Taking into Account Atmospheric Scattering”. In: *Proceedings of the 20th Annual Conference on Computer Graphics and Interactive Techniques*. SIGGRAPH ’93. Anaheim, CA: Association for Computing Machinery, 1993, 175–182. ISBN: 0897916018. DOI: 10.1145/166117.166140. URL: https://doi.org/10.1145/166117.166140.

[15] Alicja Wierzcholska et al. *Unraveling The Complex Nature Of The Very High-Energy γ-Ray Blazar PKS 2155-304*. 2019. arXiv: 1912.01880 [astro-ph.HE].

[16] Maximilian Shandri. “Investigation of Observation Quality Parameters for H.E.S.S.-II”. Master’s Thesis. 2018.

[17] F. Aharonian et al. “An Exceptional Very High Energy Gamma-Ray Flare of PKS 2155-304”. In: *The Astrophysical Journal* 664.2 (2007), L71–L74. ISSN: 1538-4357. DOI: 10.1086/520635. URL: http://dx.doi.org/10.1086/520635.

Danksagung

Ich möchte mich bei jedem bedanken, der mir bei der Erstellung dieser Bachelorarbeit weitergeholfen hat und mich während dieser Zeit in irgendeiner Weise unterstützt hat. Besonderer Dank geht an die folgenden Leute:

- Prof. Dr. Stefan Funk, der es mir ermöglicht hat, an einem so interessanten Thema zu arbeiten und allgemein Forschung in der Gammaastronomie zu betreiben
- Lenka Tomankova, die immer ein offenes Ohr hatte und mir meine Fragen beantwortet hat, aber ebenso meine Arbeit Korrektur gelesen hat
- Anke Yusafzai, die mir Daten und Informationen zukommen lassen hat, die ich für meine Arbeit gebraucht habe
- Die gesamte Gammagruppe im ECAP und die H.E.S.S. Kollaboration, durch die ich interessante Sachen aus der Gammaastronomie kennengelernt habe, die nicht mit meiner Arbeit zusammenhängen
- Meinen Freunden und meiner Familie, die mich in dieser Zeit unterstützt haben und auch mal abgelenkt haben, wenn es nötig war

Eigenständigkeitserklärung

Hiermit erkläre ich, dass ich die vorliegende Arbeit mit dem Titel „Analysis of moonlight data taken with H.E.S.S.“ selbstständig verfasst und keine anderen als die angegebenen Quellen und Hilfsmittel benutzt habe.

Sämtliche Ausführungen, die anderen Schriften wörtlich oder sinngemäß entnommen wurden, habe ich als solche kenntlich gemacht.

Erlangen, 09.04.2021

Christian Elflein